Charles University in Prague
Faculty of Mathematics and Physics

MASTER THESIS

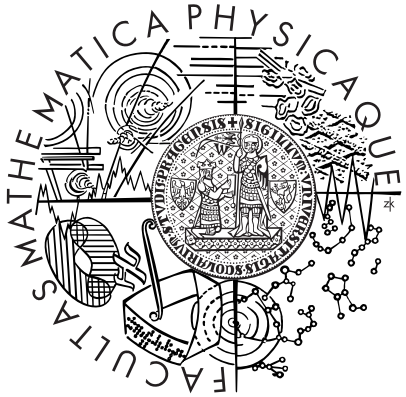

Zdeněk Kunický

The calculation of magnetic field distribution in nonlinear anisotropic media using the finite element method

Department of Numerical Mathematics

Master Thesis Supervisor: RNDr. Tomáš Vejchodský, Ph.D.,
Institute of Mathematics, Czech Academy of Sciences

Study branch: Mathematics, Numerical and Computational Mathematics

V prvé řadě bych rád poděkoval vedoucímu mé diplomové práce, panu Tomáši Vejchodskému, jehož připomínky a korekce pomohly ve značné míře ke zkvalitnění textu. Dále děkuji panu profesoru Michalovi Křížkovi za nápad na zajímavé téma diplomové práce. V neposlední řadě patří můj dík panu Bodo Heisemu za poskytnutí vlastních výsledků. Na závěr děkuji tvůrcům programů FreeFem++, Scilab, Inkscape a potažmo veškerého open-source softwaru za jejich práci, bez které by tento text nevznikl.

Declaration:
I confirm that I have prepared this master thesis independently by myself. All information taken from other sources and being reproduced in this thesis are clearly referenced.

Prohlášení:
Prohlašuji, že jsem svou diplomovou práci napsal samostatně a výhradně s použitím citovaných pramenů. Souhlasím se zapůjčováním práce a jejím zveřejňováním.

V Praze dne ..... Zdeněk Kunický

.....

Contents

1 Introduction **9**
- 1.1 The importance of the Subject . . . 9
- 1.2 Present state of anisotropic material modelling . . . 10
- 1.3 Thesis overview . . . 10

2 Brief overview of magnetic properties of matter **12**
- 2.1 Basic relations for magnetic fields . . . 12
  - 2.1.1 Maxwell's equations, stationary magnetic field . . . 12
  - 2.1.2 The engineering problem, regularity of fields on material interfaces 13
- 2.2 Constitutive relations, material classification . . . 14
  - 2.2.1 Constitutive material relations . . . 14
  - 2.2.2 Magnetically weak materials . . . 15
  - 2.2.3 Magnetically strong materials . . . 16

3 Modelling of B-H characteristics of anisotropic ferromagnets **20**
- 3.1 Analysis of general properties of a homogeneous, anhysteretic magnetic material . . . 20
  - 3.1.1 Irrotational and solenoidal vector fields . . . 21
  - 3.1.2 3D magnetic properties of a homogeneous, anhysteretic material 21
  - 3.1.3 2D magnetic properties of a homogeneous, anhysteretic material 26
- 3.2 2D models of an anisotropic steel sheet . . . 27
  - 3.2.1 Traditional measurement methods . . . 27
  - 3.2.2 Isotropic steel sheet modelling . . . 28
  - 3.2.3 Conventional model for anisotropic steel sheets . . . 30
  - 3.2.4 Elliptic model for anisotropic steel sheets . . . 30
  - 3.2.5 Multicurve models for anisotropic steel sheets . . . 31
  - 3.2.6 2D measurements of anisotropic steel sheets . . . 31
  - 3.2.7 Full 2D model of an anisotropic steel sheet . . . 32
- 3.3 3D modelling of magnetically anisotropic laminated structures . . . 37
  - 3.3.1 The problem of obtaining 3D B-H characteristics of a steel sheet from 2D measurements . . . 38
  - 3.3.2 3D model of steel-dielectric lamination . . . 39

4 The equations for scalar and vector magnetic potentials **43**
- 4.1 3D equations for magnetic potentials . . . 43
  - 4.1.1 Vector magnetic potential . . . 43
  - 4.1.2 Scalar magnetic potential . . . 44
  - 4.1.3 Global potentials and their properties . . . 44
  - 4.1.4 Definition of the engineering problem $\mathcal{P}$ . . . 45
  - 4.1.5 Comparision of 3D formulations . . . 46

4.2 2D equations for magnetic potentials 46
4.2.1 Obtaining 2D equations from 3D equations 46
4.2.2 Definition of an idealized engineering problem $\mathcal{Q}$ 50
4.2.3 Boundary conditions for idealized engineering problems 50
4.2.4 Comparision of 2D formulations 51

5 Weak formulations of 2D boundary value problems 53
5.1 Preliminary definitions and theorems 53
5.2 Weak formulations for scalar and vector magnetic potentials 57
5.2.1 Weak formulation of the boundary value problem $\mathcal{Q}^A$ 58
5.2.2 Weak formulation of the boundary value problem $\mathcal{Q}^\varphi$ 58
5.3 The existence and uniqueness theorems for 2D boundary value problems 59

6 The FEM modelling of the boundary value problem 69
6.1 Discretization of the boundary value problem 69
6.1.1 Formulation of the discrete problem 69
6.1.2 Convergence of the approximate solutions 70
6.2 Finding the discrete solution 72
6.2.1 Introducing the discrete functional 73
6.2.2 Adaptive Newton-Raphson method 73
6.2.3 Application of the iterative scheme 74
6.3 Application of the nonlinear scheme in practical computations 75
6.3.1 A benchmark problem for anisotropic models 76
6.3.2 The model of a three phase transformer core 76

7 Conclusion 78

A Figures of 2D model construction 79

B Results of the computations 83

Bibliography 90

Název práce: Výpočet magnetického pole v anizotropním a nelineárním prostředí metodou konečných prvků
Autor: Zdeněk Kunický
Katedra (ústav): Katedra numerické matematiky, Matematicko-fyzikální fakulta Univerzity Karlovy v Praze
Vedoucí diplomové práce: RNDr. Tomáš Vejchodský, Ph.D., Institute of Mathematics, Czech Academy of Sciences
e-mail vedoucho: vejchod@math.cas.cz

Abstrakt: V předložené práci studujeme modelování stacionárního magnetického pole v nelineárních, anizotropních prostředích metodou konečných prvků. Zkoumáme magnetické vlastnosti takovýchto materiálů a získané znalostni poté aplikujeme u konstrukce úplného 2D modelu anizotropního plechu, kde bylo dosaženo některých vylepšení s ohledem na již dříve publikované práce. Uvádíme také rozšíření 3D modelu plechových laminací pro případ anizotropních plechů. Poukazujeme na nedostatky standardních vět o existenci a jednoznačnosti okrajových úloh s tím, že tyto věty předpokládají materiálové vlastnosti jež neodpovídají fyzikální situaci. Místo nich uvádíme formulace nové, jež odrážejí skutečné fyzikální vlastnosti látek. Dokážeme obecné věty o existenci a jednoznačnosti pro získané okrajové úlohy, jakož i věty o konvergenci diskrétních řešení. Na závěr porovnáme konvenční a úplný 2D model anizotropního plechu ve dvou modelech jádra transformátoru. Diskrétní řešení hledáme adaptivní Newtonovou metodou. Získaná řešení pak předkládáme včetně komentáře.

Klíčová slova: anizotropní, magnetický, reluktivita, Newtonova metoda

Title: The calculation of magnetic field distribution in nonlinear anisotropic media
Author: Zdeněk Kunický
Department: Department of Numerical Mathematics, Faculty of Mathematics and Physics, Charles University in Prague
Supervisor: RNDr. Tomáš Vejchodský, Ph.D., Mathematical Institute of the Academy of Sciences of the Czech Republic
Supervisor's e-mail address: vejchod@math.cas.cz

Abstract: In the present work we study the modelling of stationary magnetic fields in nonlinear anisotropic media by FEM. The magnetic characteristics of such materials are thouroughly examined and eventually applied to the construction of a full 2D model of an anisotropic steel sheet. Some improvements in the construction in comparision with the ones previously published were achieved. We point out that the standard formulations and the subsequent theorems for the boundary value problems do not in fact correspond with the physical situation. Instead, we propose new formulations that reflect real physical properties of matter. General existence and uniqueness theorems for the obtained boundary value problems are proved as well as the convergence theorems for the discrete solutions. The conventional and full 2D model of an anisotropic steel sheet are compared in two transformer core models using the adaptive Newton-Raphson iterative scheme. The obtained results are then presented with commentary. This work also points out the steps needed for the construction of an accurate 3D model of steel-dielectric laminations that was not yet elaborated.

Keywords: anisotropic, magnetic, reluctivity, Newton-Raphson method

Chapter 1

Introduction

1.1 The importance of the Subject

The primary aim of an electrical equipment designer is to improve the properties of a device, such as material cost reduction or overall power efficiency. As a tool, a reliable numerical analysis software must be used, which provides accurate results of modelled electromagnetic quantities. The designers are highly regarded by industrial companies since their work can contribute to vast economic and energetic savings. In large-scale power transformers or generators, for instance, the energy rate flown through the device is enormously high and each efficiency improvement can considerably reduce power and cost expenses.

The high demand on effective machines is naturally accompanied by the deep study and dynamic improvements in material properties [16]. The most suitable materials for cores of high energy transfer devices are *ferromagnets* (Fe, Ni and their alloys, etc.), disposing of high relative permeability. To reduce the power losses, many improvements have been made for the materials such as subjecting the material to a process called *grain orienting* [18]. This yields a special process of cold-rolling and annealing the material, producing a 0.27–0.35 mm thin steel sheet with special orientation of crystal grains in a polycrystalline Fe-Si alloy (the so called *"Goss"* orientation) [36]. The cubic crystal itself has anisotropic properties and by aligning the crystals one produces a material anisotropic as a whole, i.e., *macroscopically*, with one direction of superior magnetic properties. This attribute is utilized in many devices where the direction of magnetic flow follows the material orientation such as high-efficiency transformers, generators or reactors.

However, anisotropy of magnetic properties probably appears even in the so called *isotropic sheets* when also considering other directions than that in the sheet plane, as is discussed in Section 3.3. Isotropic sheets find their applications in devices where the direction of magnetic flux is changing, in rotating machines such as electric motors or generators.

Finally, the material itself is not the only source of magnetic anisotropy. For the purpose of an enhanced prevention of *eddy currents*, the core parts of electrical machinery are made of *sheet laminations* with a dielectrical layer inserted between the sheets. The whole iron-dielectric block is then usually modelled as a single piece of anisotropic, homogeneous medium [20]. Moreover, besides the anisotropy all ferromagnets embody highly nonlinear behaviour and hysteresis, making numerical modelling of such materials even more difficult.

To sum up, anisotropic nonlinear ferromagnets are now standard in modern in-

dustry production such as motors, generators, power transformers, relays etc. [22]. A proper numerical modelling of these materials is demanded and utilized not only for the construction of more efficient devices, but also for better understanding of the processes that occur inside electromagnetic devices.

1.2 Present state of anisotropic material modelling

The nonlinear and anisotropic behaviour of magnetic media has been investigated by several groups of researchers [26, 32, 33] and more recently by [12, 31, 34].

During the finite element (FEM) computations, the performing program needs to access the magnetic characteristics of the materials involved. Those characteristics are obtained from the results of the measurements of material specimens. In fact, the continual development of new numerical models was strongly influenced by improvements in measurement techniques. Therefore, it is suitable to mention them along with the particular models. Until recently, for example, it was not possible to give exact "2D properties" of materials (i.e. taking into account different directions of the magnetic field and flux density). All measurements were limited to give just projections of the relevant quantities into particular directions, which lead to inaccurate representations [30]. Improvements in the testing unit (called a *single sheet tester, SST*), being able to give precise values for 2D characteristics up to high flux densities, were not introduced until 1999 [28]. Let us remark that even these measurements are not sufficient enough to reach the *saturation region*, where the material magnetic response is known to be linear and where we are able to give an exact expression of the material equations [21]. A detailed discussion and particular representations of different models together with some improvements and new thoughts will be covered in Chapter 3.

Although today's models and computing results are satisfactory, they lack a solid theoretical background. In fact, proper mathematical analysis only covers nonlinear and *perfectly isotropic* media [19] and nonlinear anisotropic media with assumptions on the material characteristics that are not met in real materials [7]. Traditionally, magnetic material properties are expressed in terms of *magnetic permeability* or *magnetic reluctivity*. As shown in this work, this representation is not convenient from the mathematical point of view when considering anisotropic media because of the non-monotonous nature of these nonlinear tensor quantities. Instead, a general mapping between magnetic fields and induction will be examined, restricted only by reasonable physical assumptions and the requirement to satisfy the Maxwell's equations.

1.3 Thesis overview

The proper understanding of the properties and limitations of various models of nonlinear anisotropic materials requires the knowledge of some results of the theory of magnetism. These results are briefly summarized in Chapter 2.

We will then apply these results in Chapter 3 in deducing the general mathematical properties of magnetic characteristics of a (generally anisotropic) material. The only restriction made upon the material is the assumption that the material is anhysteretic. Further, this chapter discusses the historical development of anisotropic material modelling up to the present state. Some improvements are suggested to the currently most accurate model of an anisotropic steel sheet as well as an extension of

the Bastos-Quichaud model for the steel and dielectric laminations to the case of a generally anisotropic steel [2] .

The equations for the FEM modelling are introduced in Chapter 4 including the exact steps for derivation of the 2D equations that are most commonly used for the magnetic modelling.

In Chapter 5 we introduce the weak formulations of the resulting 2D boundary value problems and we prove the existence and uniqueness of the solutions.

These boundary value problems are then discretized by FEM in Chapter 6. We present the convergence theorems for the discrete solutions and we suggest a scheme for obtaining the discrete solution. The scheme was then applied to a benchmark problem introduced in [31] and to a model of a three phase, three limb transformer core under full load. The results of the computations are then summarized in Appendix B.

Chapter 2

Brief overview of magnetic properties of matter

2.1 Basic relations for magnetic fields

2.1.1 Maxwell's equations, stationary magnetic field

Maxwell's equations represent a primary set of relations for electromagnetic field description. Let us introduce them in their differential form, i.e. as a system of partial differential equations (PDE):

$$\operatorname{rot} \mathcal{E} = -\frac{\partial \mathcal{B}}{\partial t}, \qquad \operatorname{div} \mathcal{D} = \rho, \tag{2.1}$$

$$\operatorname{rot} \mathcal{H} = \mathcal{J} + \frac{\partial \mathcal{D}}{\partial t}, \qquad \operatorname{div} \mathcal{B} = 0. \tag{2.2}$$

We recall that $\mathcal{H}$ is the *magnetic field strength* or *intensity*, $\mathcal{E}$ is the *electric field strength*, $\mathcal{B}$ denotes the *magnetic flux density*, also called the *magnetic induction*, $\mathcal{D}$ is the *electric flux density*, $\mathcal{J}$ the *electric current density* while ρ represents the *electric charge density*.

Calligraphic letters are used to emphasize that all above quantities have to be understood as functions of *four* variables, three spatial and one time variable, i.e. $\mathcal{H} = \mathcal{H}(x_1, x_2, x_3, t)$ with values in $\mathbb{R}^3$. The *divergence* and *rotation* operators are defined as usual

$$\operatorname{div} \mathbf{v} = \sum_{i=1}^{3} \partial_i v_i,$$
$$\operatorname{rot} \mathbf{v} = (\partial_2 v_3 - \partial_3 v_2, \partial_3 v_1 - \partial_1 v_3, \partial_1 v_2 - \partial_2 v_1)^{\mathrm{T}},$$

where $\mathbf{v} = (v_1, v_2, v_3)^T$ and $\partial_i v_j = \partial v_j / \partial x_i$.

In time independent, *stationary* case, Maxwell's equations decouple into two independent pairs, one pair for the stationary electric field, the other one for the stationary magnetic field. The latter one only is of interest in this work and will be examined in detail. Neglecting the time-derivative term in (2.2), we obtain

$$\operatorname{rot} \mathbf{H} = \mathbf{j}, \tag{2.3}$$

$$\operatorname{div} \mathbf{B} = 0. \tag{2.4}$$

Bold letters will be used for time independent vector variables. Here, for instance, $\mathbf{H}(x_1, x_2, x_3) = \mathcal{H}(x_1, x_2, x_3, t)$.

The integral form of equations (2.3)–(2.4) will be useful in deducing some general magnetic properties. They can be written as

$$\oint_l \mathbf{H} \cdot \mathrm{d}\mathbf{s} = I, \tag{2.5}$$

$$\oint_\Sigma \mathbf{B} \cdot \mathrm{d}\mathbf{s} = 0, \tag{2.6}$$

for any closed path l and any closed surface Σ. Here I denotes the *total free current* flowing through a surface P enclosed by the path l.[1]

As for now, equations (2.3)–(2.6) are just symbolic representations of generally accepted physical laws. The next subsection discusses in what mathematical sense are they fulfilled, i.e. what are their fields of validity.

There is still one more notable remark on how to comprehend the word *stationary*. Many engineering applications of magnetic materials make use of the *principle of electromagnetic induction*, that is, a time varying electric field creates an induced magnetic field and vice versa. A transformer, for example, could not in principle work at all without time-varying fields. From that reason it is essential to understand the word *stationary* properly; instead of *field not varying in time* rather *one snapshot of a generally time-variable field in a given instant of time*. A natural question arises - up to what point does that *snapshot* represent the correct physical solution of the non-stationary problem? Experiments show that, in case of *low frequency* applications (i.e. the *quasi-stationary problems*), this approximation is perfectly acceptable. This low-frequency condition is, however, very well fulfilled at the industry frequencies of 50–60 Hz, thus making our modelling meaningful [35].

2.1.2 The engineering problem, regularity of fields on material interfaces

This work studies the mathematical model of a common engineering problem that consists of finding the magnetic field distribution in a certain medium. The mathematical model of such an engineering problem will be denoted by $\mathcal{P}$ and will be simply called *an engineering problem* $\mathcal{P}$. Its exact definition will be given in Chapter 4. By that time, let us admit a vague definition of an engineering problem $\mathcal{P}$:

The aim of an engineering problem $\mathcal{P}$ is to find the distribution of $\mathbf{H}$ (or $\mathbf{B}$) in a domain of interest $\Omega \subset \mathbb{R}^3$ that satisfies certain interface and boundary conditions.

Let us have a domain $\Omega \subset \mathbb{R}^3$, i.e. an open connected subset of $\mathbb{R}^3$. The medium, represented by the domain Ω, can be inhomogeneous, i.e. it can represent e.g. an electrical device and the surrounding air. Nevertheless, the medium will always be supposed to be *piecewise homogeneous*, that is, just one homogeneous material occupies each domain $\mathcal{V}_i, i = 1, \ldots, N$. The whole *domain of interest* Ω is then divisible into sub-domains $\mathcal{V}_1, \ldots, \mathcal{V}_N : \bigcup_{i=1}^N \overline{\mathcal{V}}_i = \overline{\Omega}$, where $\mathcal{V}_i$ represent the individual homogeneous material sub-domains.

[1] One might ask whether such a definition is correct. Let P' be another surface enclosed by the same path l. Since the law of *continuity of electric charge* ensures the total flux of electric current through any closed surface being zero, the current I' flowing through P' must be equal to I.

The physical quantities, such as charge density or magnetic field strength, are known to be smooth and bounded on these sub-domains. Hence, we may suppose $\mathbf{B} \in \mathrm{C}^1(\overline{\mathcal{V}_i})$, $\mathbf{H} \in \mathrm{C}^1(\overline{\mathcal{V}_i})$, $i = 1, \ldots, N$, cf. also [35]. The equations (2.3) and (2.4) have then good meaning on $\mathcal{V}_i$, $i = 1, \ldots, N$, i.e. they are expected to be fulfilled in the classical sense.

Let us designate $\Omega^{mat} = \bigcup_{i=1}^{N} \mathcal{V}_i$. The set Ω^{mat} represents the *material part* of the domain Ω. The subset $\Omega^{int} = \Omega \backslash \Omega^{mat}$ contains the *material interfaces* S_j, $j = 1, \ldots M$. Obviously, it holds

$$\mathrm{meas}_3\, \Omega^{int} = 0, \tag{2.7}$$

where meas_n means the n-dimensional Lebesgue measure. If $S_j \subset \Omega^{int}$ is an interface between two different materials, e.g. iron and air, then $\mathbf{B}$ and $\mathbf{H}$ are known to be discontinuous on S, fulfilling the following relations [35]:

$$(\mathbf{B}_1 - \mathbf{B}_2) \cdot \mathbf{n} = 0, \tag{2.8}$$

$$\mathbf{n} \times (\mathbf{H}_1 - \mathbf{H}_2) = 0, \tag{2.9}$$

ensuring the continuity of the normal component of $\mathbf{B}$ and the tangential component of $\mathbf{H}$ only. [2] The vector $\mathbf{n}$ is a unit normal to the interface and the subscripts refer to the medium on the one and on the other side of S. The relations (2.8)–(2.9) are known as *the interface conditions*.

We see that the values of $\mathbf{B}(\mathbf{x})$ and $\mathbf{H}(\mathbf{x})$ are not defined for $\mathbf{x} \in \Omega^{int}$. Hence, the equations (2.3) and (2.4) are not valid in the classical sense on Ω^{int}. Similarly, the integral equations (2.5) and (2.6) are also valid only for Σ and l such that $\mathrm{meas}_2(\Sigma \cap \Omega^{int}) = 0$ and $\mathrm{meas}_1(l \cap \Omega^{int}) = 0$ respectively.

2.2 Constitutive relations, material classification

2.2.1 Constitutive material relations

The equations (2.3)–(2.4) do not give a full description for stationary magnetic fields and they have to be supplied by appropriate *constitutive (material) relations* which describe the various media involved. These relations are traditionally expressed as

$$\mathbf{B} = \mu(\mathbf{H})\, \mathbf{H}, \tag{2.10}$$

or, conversely, when the inverse variable dependence is demanded,

$$\mathbf{H} = \nu(\mathbf{B})\, \mathbf{B}. \tag{2.11}$$

Here μ is called the *magnetic permeability* while ν denotes the *magnetic reluctivity*. In the sequel, we discuss the forms these quantities can acquire for various materials.

To understand the fundamentals of magnetic anisotropy, we must present the concept of *magnetizing the material*. An important property of a material is its *magnetization* $\mathbf{M}$ defined as a volume density of elementary (atomic) magnetic moments. Using this quantity, equation (2.10) can be expressed as

$$\mathbf{B} = \mu_0(\mathbf{H} + \mathbf{M}), \tag{2.12}$$

[2] These equations say that the *surface divergence* and *surface rotation* vanish on S, i.e. $\mathrm{Div}\, \mathbf{B} = 0$ and $\mathrm{Rot}\, \mathbf{H} = 0$. Comparing these relations to (2.3) and (2.4) we notice the missing *surface current density* $\mathbf{j}_S$. In fact, the *surface* and *linear currents* and *charge densities*, widely used in theoretical electromagnetism, are inconvenient for numerical simulations and will be omitted from our considerations.

where $\mu_0 = 4\pi \cdot 10^{-7}\,\mathrm{H.m^{-1}}$ is the *permeability of vacuum* [35]. This relation is totally general, applicable to all materials at all conditions.

From (2.12) we also obtain the relation

$$\mathbf{H} = \nu_0 \mathbf{B} - \mathbf{M}, \tag{2.13}$$

where $\nu_0 = 1/\mu_0 = 7.96 \cdot 10^5\,\mathrm{A^2.N^{-1}}$ is the *reluctivity of vacuum*.

All materials can hereby be divided into two main groups, reflecting their response to applied magnetic fields: [3]

- *magnetically weak materials*, showing a weak response to the magnetic field,
- *magnetically strong materials* with strong response to the magnetic field.

2.2.2 Magnetically weak materials

For *magnetically weak materials*, the magnetizing process is usually described by a linear relationship between $\mathbf{H}$ and $\mathbf{M}$ which is very well fulfilled up to very high field intensities and wide range of temperatures [35]. It is commonly expressed as

$$\mathbf{M} = \chi_m \mathbf{H},$$

defining thus the *magnetic susceptibility* χ_m.

The relation (2.12) can then be reformulated as

$$\mathbf{B} = \mu_0(1 + \chi_m)\mathbf{H} = \mu_0 \mu_r \mathbf{H}. \tag{2.14}$$

Here $\mu_r = 1 + \chi_m$ is the *relative permeability* of a specific material. When comparing (2.14) to (2.10) we see that in case of the weak magnetic media the permeability $\mu = \mu_0 \mu_r$ is a constant for the specific material.

When the net atomic magnetic moment of a material is zero, the only reaction to the applied field is the *diamagnetic response*, which is a general property of matter. It results in an induced magnetic moment opposed to the applied magnetic field, hence in a decrease of magnetization. Such materials are called *diamagnets*. The magnetic susceptibility of diamagnets is negative and very small, normally of the order of 10^{-8} to 10^{-5} [41]. Several metals widely used in engineering are diamagnetic – copper, zinc, lead, gold, silver, etc. Further, most non-metallic solids, fluids, and gases are diamagnetic [35, 41].

When the atoms of a material have permanent magnetic moment, the diamagnetic effect only plays a minor role, being out-weighted by an alignment of the originally randomly pointing magnetic moments in order to minimize their magnetic energy. This describes the effect of *paramagnetism* and the corresponding materials are called *paramagnets*. The magnetic susceptibility of paramagnets is positive and, in general, much less than 1, usually of the order 10^{-6} to 10^{-3} [35]. Many metals are paramagnetic (aluminum, platinum, etc.), along with some crystalline salts and gases, such as oxygen [35].

Summarizing the properties of magnetically weak media, in most common engineering problems the linear dependence of $\mathbf{B}$ on $\mathbf{H}$ (the so called *linear B-H characteristics*) holds, with the respective relative permeability being a constant very close to 1, hence we may approximate the equation (2.14) by

$$\mathbf{B} = \mu_0 \mathbf{H}. \tag{2.15}$$

[3] The phenomenon of *superconductivity* brings new sights on this classification and will not be discussed here.

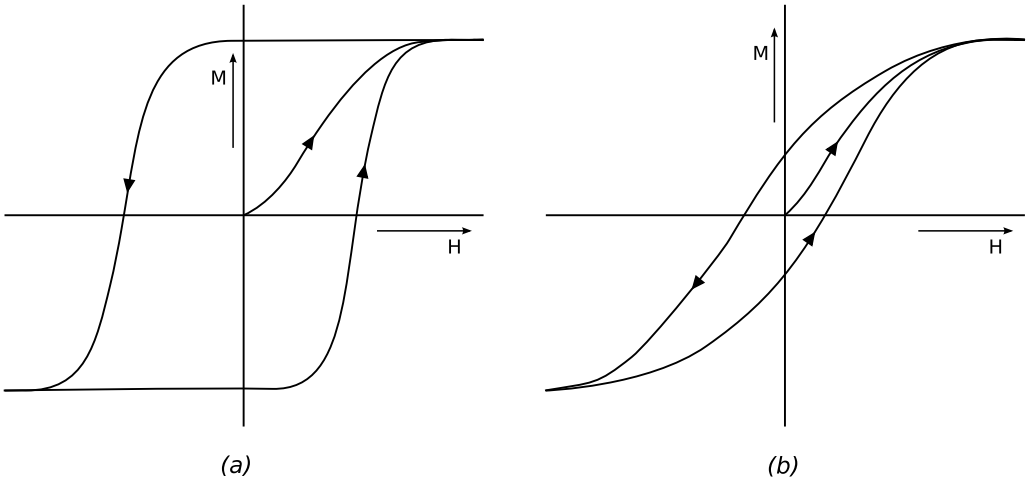

Figure 2.1: Hysteresis loops for (a) magnetically hard ferromagnets, (b) magnetically soft ferromagnets. The area of the loop gives a qualitative estimate of the material's hysteresis losses due to cyclic magnetization of the material

2.2.3 Magnetically strong materials

In certain materials, the application of a magnetic field may induce a very strong magnetization, commonly of the order of 10^6 A.m^{-1}, characterizing thus *magnetically strong materials* [41]. Although not numerous, counting e.g. iron, cobalt, nickel, or their alloys, *ferromagnets* are the most important materials among these for engineering applications. Typical property of ferromagnets, besides their very high permeability, is a complicated nonlinear dependency of magnetization values on the field strength, on the history of a specimen, and on many more factors [35]. The dependency of magnetization on the field strength during the cyclic magnetization process is given by the so called *hysteresis loop*. The hysteresis loops for two different types of ferromagnets are shown in Fig. 2.1.

The ferromagnets of type *(a)* are called *magnetically hard ferromagnets*. They find wide use in magnetic recording media or as permanent magnets (in electrical motors and generators, loudspeakers, etc.). Because of their nearly square-like hysteresis loop, they are inconvenient for alternating current (AC) applications; the *hysteresis losses*, qualitatively determined by the area of the loop, would then be too high. The material characteristics of hard ferromagnets differ from the other materials and they will not be studied in this work.

The ferromagnets of type *(b)* are used primarily for AC applications. These are called *magnetically soft ferromagnets*. In order to eliminate *eddy current losses* during their cyclic magnetization, they are usually distributed as thin *electrical steel sheets*, arranged into a laminated structure for use as magnetic cores of electric machines. In this case, magnetization is performed in parallel with the sheet surface.

During the manufacturing process of the sheets, there is a remarkable effect of crystal grain growth with a cubic structure. A single crystal exhibits excellent magnetic characteristics when magnetization is effected in the direction perpendicular to a face of the cube (the crystallographic $\langle 100 \rangle$ directions), while the worst being the directions of cube diagonal (the $\langle 111 \rangle$ directions) [16].

The properties of a *non-oriented electrical steel sheet*, with a more or less random orientation of grains, result in good magnetic characteristics in every direction in the

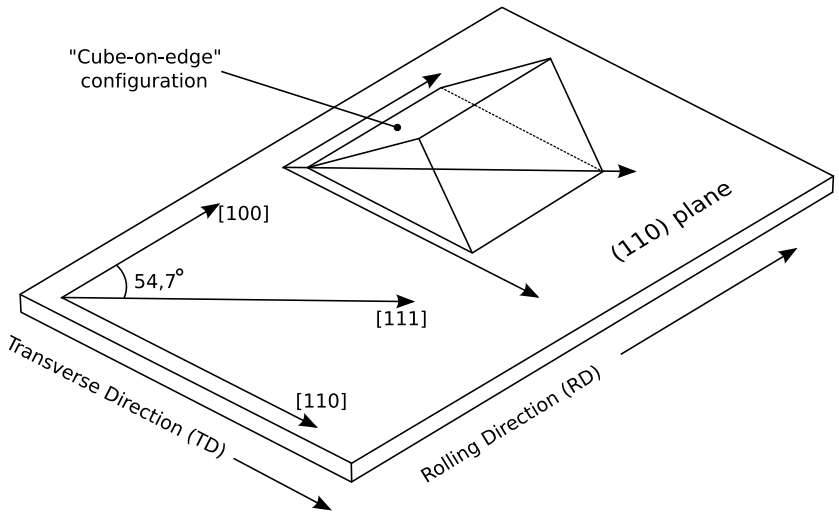

Figure 2.2: Detailed view of a Goss texture, with [100], [010] and [001] being the main crystallographic axes of a cubic grain

sheet plane. The major advantage of these sheets is their low manufacturing cost, making them attractive for use in small sized rotary machines, motors, etc. Nevertheless, even these so called *isotropic sheets* probably exhibit an anisotropy in the direction perpendicular to the sheet plane, as is discussed in Section 3.3.1. This leads to the definition of a *perfectly isotropic material*, whose magnetic properties are the same in all directions.

In the high-efficiency, large-scale electrical machinery, such as large-scale transformers or generators, there is a higher demand on *oriented electrical steel sheets*. These sheets have particularly excellent magnetic characteristics in one direction but when magnetized in other directions, they have magnetic characteristics inferior to those of non-oriented steel sheets. Accordingly, oriented electrical steel sheets are used in the form of combined laminated cores or wound cores, so that the rolling direction always corresponds to the direction of magnetization, thus enabling manufacture of transformers having smaller losses [40].

The grain-oriented (*anisotropic*) steel sheet was invented in 1934 by N.P. Goss, resulting in a *cube-on-edge*, also called *Goss orientation* of crystal grains. The configuration is shown in Fig. 2.2, having the crystallographic (110) plane parallel to the sheet plane [36]. The direction of material rolling (the *rolling direction*, i.e. RD, the crystallographic [100] direction) is the magnetically easiest one while the direction of worst magnetization being the "cube diagonal" at an angle about 54.7° to the RD [37] . The direction perpendicular to RD in the sheet plane, i.e. the crystallographic [110] direction, is usually referred to as the *transverse direction* (TD) and shows an intermediate level of magnetic material response to the applied field.

The properties of grain-oriented steels were continuously improved and today's finest quality sheets show a very small grain misorientation and almost ideal grain size, resulting in a substantial power loss reduction [16].

To understand the requirements on a numerical model of an oriented steel sheet, it is desirable to present the magnetization process in such a sheet in detail [22].

All ferromagnetic materials are characterized by the presence of *magnetic domains*, inside which the elementary (atomic) magnetic moments are aligned alike. The whole domain then exhibits a *macroscopic* magnetic moment, pointing to a direction of the

elementary moments. In the absence of an external magnetic field, these domains are randomly distributed with the magnetization vector along one of the preferred axes [100], [010] or [001] of the crystal grain. Since we are inspecting a thin sheet, the projections of magnetization vectors on the sheet plane will be considered only.

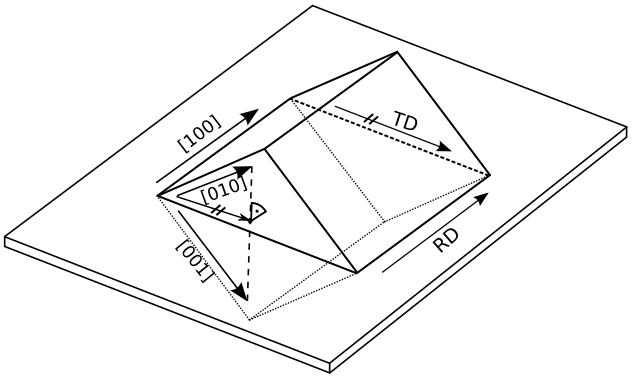

Figure 2.3: The projections of the principal directions of a Goss-oriented cubic crystal onto the sheet plane coincide with RD and TD.

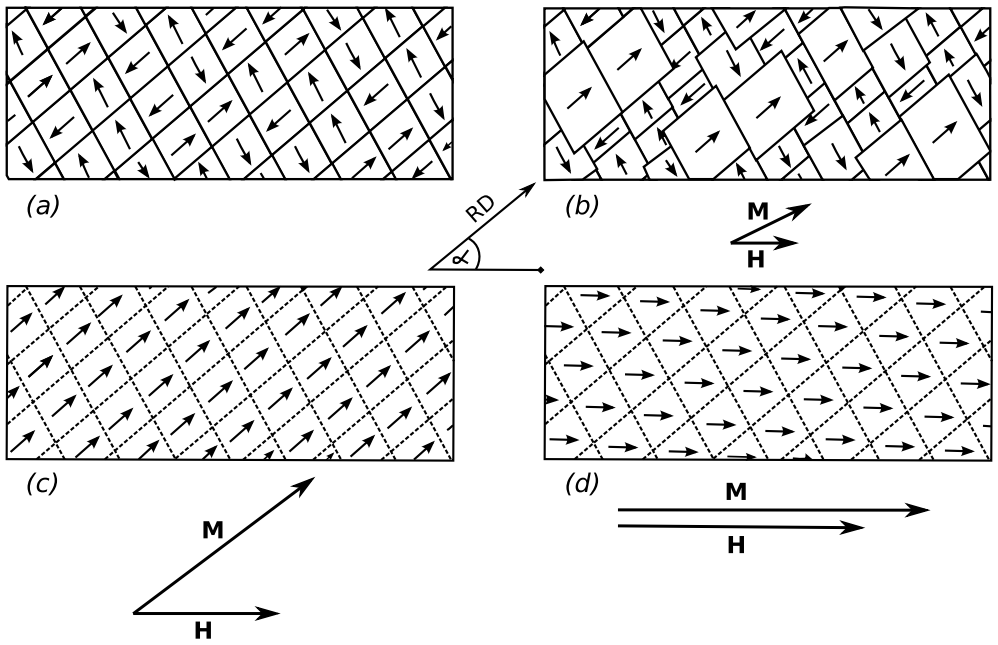

Figure 2.4: Domain processes occur if a material is subjected to an external field; (a) the demagnetized state, (b) the partial magnetization, (c) the irreversible rotation of domains and (d) the reversible rotation.

As seen in Fig. 2.3, the projections of the above mentioned principal crystallographic directions correspond to RD and TD. Thus, the magnetic moments are aligned with these directions in the initial, non-magnetized state, see Fig. 2.4 (a).

Let us suppose an external field applied in the sheet plane at a general angle α from the RD. When the field **H** increases slightly, the domains that are aligned in a direction close to that of **H** start growing (b). This process is known as the *domain wall movement*. At moderate levels, the domains suddenly and irreversibly rotate

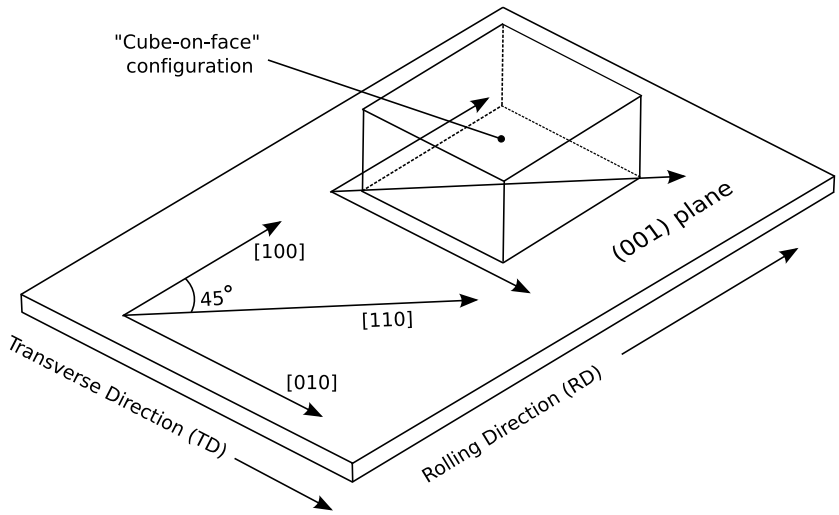

Figure 2.5: Detailed view of a cube-on-face texture, with [100], [010], and [001] being the main crystallographic axes of a cubic grain.

towards the easy axis that is closest to the applied field (c), showing *domain rotation* or *switching*. Once they are all parallel, forming one self-contained domain, they rotate reversibly towards the applied field up to the point of *magnetic saturation* (d), where the magnetization vector $\mathbf{M}$ is parallel to $\mathbf{H}$.

For iron, this happens at the macroscopic value of $M^{sat} = 1.71 \cdot 10^6\,\mathrm{A/m}$, which corresponds to the induction of $B^{sat} = \mu_0(H^{sat} + M^{sat}) \approx \mu_0 M^{sat} \doteq 2.15\,\mathrm{T}$ [22]. Any further increase of field strength creates negligible fluctuations in macroscopic magnetization. This allows us to suppose the linear B-H relationship, cf. (2.12). Another important observation shows that the magnetization vector $\mathbf{M}$, the induction vector $\mathbf{B}$, and the magnetic field strength vector $\mathbf{H}$, cf. (2.12), point the same direction only when the field applies to RD or TD, or $|\mathbf{H}| \geq H^{sat}$.

The release of $\mathbf{H}$ causes the imperfect release of magnetic domains to an energetically favourable state, given by the shape of the material's hysteresis loop. The narrower the loop the more perfect is the release and the smaller are the hysteresis losses.

In the future, an intense work on improvements of *doubly oriented* electrical steel sheets with a *cube-on-face* structure is expected [40]. Such a sheet is supposed to have excellent magnetic characteristics in *two* directions, the RD and TD, cf. Fig. 2.5. Although there are known methods for manufacturing such sheets, their magnetic characteristics are still poor for practical applications.

The permeability and reluctivity of ferromagnets, as defined by relations (2.10) and (2.11), are generally complicated nonlinear tensor functions $\mu = \mu(H_1, H_2, H_3, t)$, $\nu = \nu(B_1, B_2, B_3, t)$. In a stationary model, the time dependence has to be removed. However, as measurements show, these functions have poor properties such as non-monotonicity, as is seen in Fig. 3.3. These properties complicate the analysis of the resulting equations if the permeability or the reluctivity function is considered; from this point of view, it is more suitable to represent the material characteristics by direct mappings between $\mathbf{B}$ and $\mathbf{H}$. These mappings exhibit much better properties, as is shown in the following chapter.

Chapter 3

Modelling of B-H characteristics of anisotropic ferromagnets

During FEM computations of magnetic fields, the performing program needs to access the B-H characteristics of materials involved. Mathematically, the term *B-H characteristics* denotes a mapping that relates the vectors **B** and **H** for a given material. In this work, we will limit ourselves to study the properties of an idealized, *anhysteretic material*. Such a material is supposed to be energy loss-free when performing its cyclic magnetization. The general form of the mapping representing B-H characteristics of an anhysteretic material will be formally introduced and analysed in Section 3.1 . It covers isotropic as well as anisotropic materials.

Depending on the particular engineering problem, a model of an anisotropic material or structure may be required. These models can be classified as follows:

- full 3D model of an anisotropic steel sheet
- model of the laminated structure made up of steel sheets and dielectric layers; the sheets can be either isotropic or anisotropic
- simplified 2D model of an anisotropic steel sheet

Estimating a full 3D relation between **B** and **H** is difficult for anisotropic sheets, because all measurements are performed in the sheet plane. The values of **B** and **H** in other directions and the underlying relationship between them must then be guessed. Therefore, simplified 2D models are most commonly used and are examined in detail in Section 3.2.

Last years, when computing resources are becoming more powerful and available, new 3D models of laminated cores are appearing [2, 25]. A model for anisotropic sheets with laminations is proposed in Section 3.3, that is shown to be an extension of Bastos-Quichaud model which only covers perfectly isotropic sheets [2].

3.1 Analysis of general properties of a homogeneous, anhysteretic magnetic material

A model of a homogeneous magnetic medium should follow some restrictions made upon it as a consequence of physical and geometrical considerations. This section examines general mathematical properties of B-H characteristics of an anhysteretic material, both 3D and 2D.

3.1.1 Irrotational and solenoidal vector fields

This and the following chapters will make use of the properties of irrotational and solenoidal fields. For the two-dimensional case, we introduce the operators

$$\begin{aligned} \operatorname{rot} \mathbf{u} &= \partial_1 u_2 - \partial_2 u_1, \\ \operatorname{curl} v &= (\partial_2 v, -\partial_1 v), \end{aligned}$$

where $\mathbf{u} = (u_1, u_2)$.

Theorem 3.1 (Poincaré's lemma). *Let Ω be a simply connected domain in $\mathbb{R}^n$, $n = 2, 3$.*

(i) If $\mathbf{v} \in [C^1(\Omega)]^n$ is such that $\operatorname{rot} \mathbf{v} = 0$ on Ω, then there exists a function $p \in C^2(\Omega)$ such that $\mathbf{v} = \operatorname{grad} p$ on Ω. Moreover, the function p is unique to within a constant.

(ii) If $\mathbf{w} \in [C^1(\Omega)]^n$ is such that $\operatorname{div} \mathbf{w} = 0$ on Ω, then for $n = 3$ there exists a vector function $\mathbf{q} \in [C^1(\Omega)]^3$ such that $\mathbf{w} = \operatorname{rot} \mathbf{q}$ on Ω and for $n = 2$ there exists a scalar function $q \in C^1(\Omega)$ such that $\mathbf{w} = \operatorname{curl} q$ on Ω.

Proof. See [10]. □

In case *(i)*, the function $\mathbf{v}$ is called *irrotational*, while in case *(ii)* the function $\mathbf{w}$ is called *solenoidal*.

The problem of decomposition of an arbitrary vector field $\mathbf{u}$ on its irrotational and solenoidal parts is rather complex and depends on the regularity of $\mathbf{u}$ as well as the properties of $\partial\Omega$. We will limit ourselves to formulate the following theorem.

Theorem 3.2 (Helmholtz decomposition). *Let $n = 2, 3$ and let us denote*

$$B_r^n = \{x \in \mathbb{R}^n : |x| \leq r\}.$$

Then every vector field $\mathbf{u} \in [H^1(B_r^n)]^n$ has the unique decomposition

$$\begin{aligned} \mathbf{u} &= \operatorname{grad} p + \operatorname{rot} \mathbf{q} \quad \text{if } n = 3, \\ \mathbf{u} &= \operatorname{grad} p + \operatorname{curl} q \quad \text{if } n = 2, \end{aligned}$$

where $p \in H^2(B_r^n)$, $\mathbf{q} \in [H^2(B_r^3)]^3$ (resp. $q \in H^2(B_r^2)$ if $n = 2$), the function p is unique to within a constant and $\operatorname{rot} \mathbf{q} \cdot \mathbf{n}|_\Gamma = 0$ (resp. $\operatorname{curl} q \cdot \mathbf{n}|_\Gamma = 0$ if $n = 2$).

Proof. See [10]. □

3.1.2 3D magnetic properties of a homogeneous, anhysteretic material

In the following, $|\mathbf{v}|$ denotes the standard Euclidean norm of a vector $\mathbf{v} \in \mathbb{R}^n$. The B-H characteristics of a homogeneous, anhysteretic magnetic material can be represented by mappings $\mathcal{F}, \mathcal{G} : \mathbb{R}^3 \to \mathbb{R}^3$ such that

$$\mathcal{F}(\mathbf{H}) = \mathbf{B}, \tag{3.1}$$

$$\mathcal{G}(\mathbf{B}) = \mathbf{H}, \tag{3.2}$$

where $\mathcal{F} = (\mathcal{F}_1, \mathcal{F}_2, \mathcal{F}_3)$ and $\mathcal{G} = (\mathcal{G}_1, \mathcal{G}_2, \mathcal{G}_3)$. Measurements show that altering $\mathbf{H}$ causes a (macroscopically) smooth change of $\mathbf{B}$ with respect to $\mathbf{H}$ and vice versa ,[1] so we can suppose $\mathcal{F}, \mathcal{G} \in [C^1(\mathbb{R}^3)]^3$. We assume that every value of flux density corresponds to a unique value of field strength, so that $\mathcal{F}$ and $\mathcal{G}$ are bijective mappings from $\mathbb{R}^3$ onto $\mathbb{R}^3$ and $\mathcal{G} = \mathcal{F}^{-1}$.

The magnetically hard ferromagnets are excluded from our considerations. Hence, initially at zero fields, there is no induced magnetization. From (2.12) we have $\mathcal{F}(\mathbf{0}) = \mathcal{G}(\mathbf{0}) = \mathbf{0}$.

Let $\mathbf{H}_1, \mathbf{H}_2 \in \mathbb{R}^3$, $\mathbf{H}_1 \neq \mathbf{H}_2$. Equations (2.12) and (3.1) give

$$\begin{aligned}(\mathcal{F}(\mathbf{H}_2) - \mathcal{F}(\mathbf{H}_1))^T(\mathbf{H}_2 - \mathbf{H}_1) &= [\mu_0(\mathbf{H}_2 + \mathbf{M}_2) - \mu_0(\mathbf{H}_1 + \mathbf{M}_1)]^T(\mathbf{H}_2 - \mathbf{H}_1) = \\ &= \mu_0(\mathbf{H}_2 - \mathbf{H}_1)^T(\mathbf{H}_2 - \mathbf{H}_1) + \mu_0(\mathbf{M}_2 - \mathbf{M}_1)^T(\mathbf{H}_2 - \mathbf{H}_1) = \\ &= \mu_0|\Delta\mathbf{H}|^2 + \mu_0\Delta\mathbf{M}^T\Delta\mathbf{H}, \quad (3.3)\end{aligned}$$

where $\Delta\mathbf{H} = \mathbf{H}_2 - \mathbf{H}_1$ and $\Delta\mathbf{M} = \mathbf{M}_2 - \mathbf{M}_1$.

When the field changes from $\mathbf{H}_1$ to $\mathbf{H}_2$, the induced magnetization increment $\Delta\mathbf{M}$ naturally can not go "against" $\Delta\mathbf{H}$, i.e.

$$\Delta\mathbf{M}^T\Delta\mathbf{H} \geq 0. \quad (3.4)$$

Hence we obtain

$$(\mathcal{F}(\mathbf{H}_2) - \mathcal{F}(\mathbf{H}_1))^T(\mathbf{H}_2 - \mathbf{H}_1) = \mu_0|\Delta\mathbf{H}|^2 + \mu_0\Delta\mathbf{M}^T\Delta\mathbf{H} \geq \mu_0|\Delta\mathbf{H}|^2.$$

Thus, $\mathcal{F}$ is uniformly monotone [2] on $\mathbb{R}^3$.

Let $\mathbf{B}_1, \mathbf{B}_2 \in \mathbb{R}^3$, $\mathbf{B}_1 \neq \mathbf{B}_2$ and $\mathbf{H}_i = \mathcal{G}(\mathbf{B}_i)$, $i = 1, 2$. Similarly, from (2.13), (3.2) and (3.4) we have

$$\begin{aligned}&(\mathcal{G}(\mathbf{B}_2) - \mathcal{G}(\mathbf{B}_1))^T(\mathbf{B}_2 - \mathbf{B}_1) = \\ &\quad = [(\nu_0\mathbf{B}_2 - \mathbf{M}_2) - (\nu_0\mathbf{B}_1 - \mathbf{M}_1)]^T(\mathbf{B}_2 - \mathbf{B}_1) = \nu_0|\Delta\mathbf{B}|^2 + \nu_0\Delta\mathbf{M}^T\Delta\mathbf{B} = \\ &\quad\quad = \nu_0|\Delta\mathbf{B}|^2 + \nu_0\Delta\mathbf{M}^T(\mu_0\Delta\mathbf{H} + \Delta\mathbf{M}) \geq \nu_0|\Delta\mathbf{B}|^2,\end{aligned}$$

so $\mathcal{G}$ is also uniformly monotone on $\mathbb{R}^3$.

For being able to deduce further properties of $\mathcal{F}$ and $\mathcal{G}$, we need to introduce the term *magnetic energy density*. This physical quantity represents the volume density of the energy stored in the magnetic field. If the value of $\mathbf{B}$ at a given point $\mathbf{x} \in \mathbb{R}^3$ is $\mathbf{B}(\mathbf{x}) \equiv \tilde{\mathbf{B}}$, then the magnetic energy density w is only a function of $\tilde{\mathbf{B}}$ defined as

$$w(\mathbf{x}) = w(\tilde{\mathbf{B}}) = \int_{\mathbf{0}}^{\tilde{\mathbf{B}}} \mathcal{G}(\mathbf{s}) \cdot \mathrm{d}\mathbf{s}. \quad (3.5)$$

The integral symbol denotes the line integral over a curve in $\mathbb{R}^3$ with the end points $\mathbf{B} = \mathbf{0}$ and $\mathbf{B} = \tilde{\mathbf{B}}$. We have to show first that the definition is correct, i.e. path-independent. As it is described in [35] , the quantity $w_m = \oint_l \mathcal{G}(\mathbf{s}) \cdot \mathrm{d}\mathbf{s}$ represents the hysteretic energy loss when cyclically magnetizing the material so that $\mathbf{B}$ follows a closed curve l. Because the material is anhysteretic, $w_m = 0$ and we have

[1] The *domain switching phenomenon* mentioned in Chapter 2 causes the presence of measurable discontinuities in material's B-H characteristics [22]. Nevertheless, our approximation level allows us to neglect these discontinuities.

[2] We recall that a mapping $\mathcal{F} : \mathbb{R}^3 \to \mathbb{R}^3$ is *uniformly monotone* on $\mathbb{R}^3$ if there exists a constant $K > 0$ so that it holds $(\mathcal{F}(\mathbf{x}_2) - \mathcal{F}(\mathbf{x}_1))(\mathbf{x}_2 - \mathbf{x}_1) \geq K|\mathbf{x}_2 - \mathbf{x}_1|^2$ for every $\mathbf{x}_1, \mathbf{x}_2 \in \mathbb{R}^3$.

$$\oint_l \mathcal{G}(\mathbf{s}) \cdot \mathrm{d}\mathbf{s} = 0 \tag{3.6}$$

for any closed path l. In the following, the symbol used in (3.5) for a line integral will induce implicitly the path-independence of the integral.

Let m be another closed path. Let $\mathcal{G}'(\mathbf{B})$ denote the Jacobian matrix of $\mathcal{G}$ in $\mathbf{B} \in \mathbb{R}^3$. By using the substitution $\mathcal{F}(\mathbf{t}) = \mathbf{s}$, $\mathrm{d}\mathbf{t} = \mathrm{d}\mathcal{G}(\mathbf{s}) = \mathcal{G}'(\mathbf{s})\mathrm{d}\mathbf{s}$ and integration by parts, we obtain

$$\oint_m \mathcal{F}(\mathbf{t}) \cdot \mathrm{d}\mathbf{t} = \oint_{\mathcal{F}(m)} \mathbf{s}^T \mathcal{G}'(\mathbf{s}) \cdot \mathrm{d}\mathbf{s} = -\oint_{\mathcal{F}(m)} \mathcal{G}(\mathbf{s}) \cdot \mathrm{d}\mathbf{s} = 0. \tag{3.7}$$

With regard to the Green's theorem, we see from (3.6) and (3.7) that the functions $\mathcal{F}$ and $\mathcal{G}$ are irrotational on $\mathbb{R}^3$, i.e.

$$\partial_j \mathcal{F}_i = \partial_i \mathcal{F}_j, \quad i, j = 1, 2, 3, \tag{3.8}$$

$$\partial_j \mathcal{G}_i = \partial_i \mathcal{G}_j, \quad i, j = 1, 2, 3. \tag{3.9}$$

Hence, cf. Theorem 3.1, there exist functions $w, \tilde{w} : \mathbb{R}^3 \to \mathbb{R}$ such that

$$\operatorname{grad} w(\mathbf{B}) = \mathcal{G}(\mathbf{B}) \quad \forall \mathbf{B} \in \mathbb{R}^3, \tag{3.10}$$

$$\operatorname{grad} \tilde{w}(\mathbf{H}) = \mathcal{F}(\mathbf{H}) \quad \forall \mathbf{H} \in \mathbb{R}^3. \tag{3.11}$$

These functions are then given by relations

$$w(\mathbf{B}) = \int_{\mathbf{0}}^{\mathbf{B}} \mathcal{G}(\mathbf{s}) \cdot \mathrm{d}\mathbf{s}, \tag{3.12}$$

$$\tilde{w}(\mathbf{H}) = \int_{\mathbf{0}}^{\mathbf{H}} \mathcal{F}(\mathbf{t}) \cdot \mathrm{d}\mathbf{t}. \tag{3.13}$$

When we compare (3.12) to (3.5), we see that w is indeed the magnetic energy density, while $\tilde{w}$ is the so called *magnetic coenergy density.*[3]

Let us examine the Jacobian matrices $\mathcal{F}'$ and $\mathcal{G}'$. Let $\mathbf{H}$ be fixed and $\delta\mathbf{H}_\mathbf{d}$ be an arbitrary field increment of a fixed direction $\mathbf{d}$. Since $\mathcal{F} \in [C^1(\mathbb{R}^3)]^3$, we can write

$$\mathcal{F}(\mathbf{H} + \delta\mathbf{H}_\mathbf{d}) - \mathcal{F}(\mathbf{H}) = \mathcal{F}'(\mathbf{H})\, \delta\mathbf{H}_\mathbf{d} + \mathbf{o}(\delta H_\mathbf{d}), \tag{3.14}$$

where $\delta H_\mathbf{d} = |\delta\mathbf{H}_\mathbf{d}|$ and $\mathbf{o}(\delta H_\mathbf{d})$ is a vector whose components are $o(\delta H_\mathbf{d})$.

By multiplying (3.14) by $\delta\mathbf{H}_\mathbf{d}$ and comparing to (3.3), we get

$$\delta\mathbf{H}_\mathbf{d}^T\, \mathcal{F}'(\mathbf{H})\, \delta\mathbf{H}_\mathbf{d} = \mu_0 |\delta\mathbf{H}_\mathbf{d}|^2 + \mu_0 (\delta\mathbf{M}_\mathbf{d}^T \delta\mathbf{H}_\mathbf{d}) + \delta\mathbf{H}_\mathbf{d}^T \mathbf{o}(\delta H_\mathbf{d}),$$

where $\delta\mathbf{M}_\mathbf{d}$ is the magnetization increment when the field changes from $\mathbf{H}$ to $\mathbf{H} + \delta\mathbf{H}_\mathbf{d}$. Because, again, $\delta\mathbf{M}_\mathbf{d}^T \delta\mathbf{H}_\mathbf{d} \geq 0$, we have

$$\delta\mathbf{H}_\mathbf{d}^T\, \mathcal{F}'(\mathbf{H})\, \delta\mathbf{H}_\mathbf{d} \geq \mu_0 |\delta\mathbf{H}_\mathbf{d}|^2 + \delta\mathbf{H}_\mathbf{d}^T \mathbf{o}(\delta H_\mathbf{d}).$$

[3] There were attempts for a compact storage of B-H characteristics for numerical computations in terms of w or $\tilde{w}$, since only one scalar function was needed to store in this case. The value of $\mathcal{G}$ or $\mathcal{F}$ was then obtained by means of numerical differentiation from equations (3.10) or (3.11). Since the memory becomes cheaper and the capacity increases, there is no need for using these models anymore. The reference on these so called *energy* and *coenergy models* can be found in [33, 39].

If the field increment $\delta\mathbf{H_d}$ is small enough, we get

$$\delta\mathbf{H}_\mathbf{d}^T\,\mathcal{F}'(\mathbf{H})\,\delta\mathbf{H_d} \geq \frac{\mu_0}{2}|\delta\mathbf{H_d}|^2, \quad |\delta\mathbf{H_d}| \in (0, \varepsilon_\mathbf{d}).$$

Let us fix $\mathbf{v}_d = \delta\mathbf{H_d}$ to be such a small enough field increment. For $\alpha \in \mathbb{R}$ we have

$$(\alpha\mathbf{v_d})^T\mathcal{F}'(\mathbf{H})(\alpha\mathbf{v_d}) = \alpha^2\mathbf{v}_\mathbf{d}^T\mathcal{F}'(\mathbf{H})\mathbf{v_d} \geq \alpha^2\frac{\mu_0}{2}|\mathbf{v_d}|^2 = \frac{\mu_0}{2}|\alpha\mathbf{v_d}|^2 \stackrel{def}{=} C_1^{mat}|\alpha\mathbf{v_d}|^2.$$

Noting that C_1^{mat} is independent on $\mathbf{d}$ and $\mathbf{H}$, we obtain

$$\mathbf{u}^T\mathcal{F}'(\mathbf{H})\mathbf{u} \geq C_1^{mat}|\mathbf{u}|^2 \quad \forall\mathbf{H}\,, \forall\mathbf{u} \in \mathbb{R}^3, \tag{3.15}$$

or

$$|\mathcal{F}'(\mathbf{H})| \geq C_1^{mat} \quad \forall\mathbf{H} \in \mathbb{R}^3,$$

where $|\mathcal{F}'(\mathbf{H})|$ denotes the spectral norm of the matrix $\mathcal{F}'(\mathbf{H})$.

When a material reaches its magnetic saturation, the magnetization does not increase anymore. Thus we obtain from (2.12) the analytical expressions

$$\mathbf{B} = \mathcal{F}(\mathbf{H}) = \mu_0(\mathbf{H} + M^{sat}\mathbf{e_H}), \quad |\mathbf{H}| \geq H^{sat}, \tag{3.16}$$

$$\mathbf{H} = \mathcal{G}(\mathbf{B}) = \nu_0\mathbf{B} - M^{sat}\mathbf{e_B}, \qquad |\mathbf{B}| \geq B^{sat}, \tag{3.17}$$

where $\mathbf{e_H} = \mathbf{H}/|\mathbf{H}|$, $\mathbf{e_B} = \mathbf{B}/|\mathbf{B}|$, $\nu_0 = 1/\mu_0$ and $B^{sat}, H^{sat}, M^{sat}$ are constants characteristic for a given material satisfying the relation $B^{sat} = \mu_0(H^{sat} + M^{sat})$.

Differentiating (3.16) yields

$$\mathcal{F}'(\mathbf{H}) = \mu_0\mathbb{I} + \mu_0 M^{sat}\left[\frac{1}{H}\mathbb{I} - \frac{\mathbf{H}}{H^3}\mathbf{H}^T\right], \quad |\mathbf{H}| \geq H^{sat},$$

where $\mathbb{I}$ denotes the identity matrix. For $\mathbf{u} \in \mathbb{R}^3$ and $|\mathbf{H}| \geq H^{sat}$ we thus obtain

$$\begin{aligned} |\mathcal{F}'(\mathbf{H})\mathbf{u}| &= \left|\mu_0\mathbf{u} + \mu_0 M^{sat}\frac{\mathbf{u}}{H} - \mu_0\frac{\mathbf{H}}{H^3}\mathbf{H}^T\mathbf{u}\right| \leq \\ &\leq \mu_0|\mathbf{u}| + \mu_0\frac{M^{sat}}{H^{sat}}|\mathbf{u}| + \mu_0\frac{1}{H^{sat}}|\mathbf{u}| \stackrel{def}{=} K_1|\mathbf{u}|. \end{aligned} \tag{3.18}$$

Because $\mathcal{F} \in [C^1(\mathbb{R}^3)]^3$, we can set

$$K_2 = \max_{H \leq H^{sat}} |\mathcal{F}'(\mathbf{H})|, \tag{3.19}$$

and

$$C_2^{mat} = \max\{K_1, K_2\}.$$

Then it follows from (3.18) and (3.19) that

$$|\mathcal{F}'(\mathbf{H})| \leq C_2^{mat} \quad \forall\mathbf{H} \in \mathbb{R}^3. \tag{3.20}$$

From (3.8), (3.15), and (3.20) we see that the Jacobian matrix $\mathcal{F}'(\mathbf{H})$ is symmetric, uniformly positive definite, and uniformly bounded over $\mathbb{R}^3$. As a symmetric, positive

definite matrix, $\mathcal{F}'(\mathbf{H})$ is nonsingular. Using the inverse mapping theorem, we have for $\mathbf{B} \in \mathbb{R}^3$:

$$\mathcal{G}'(\mathbf{B}) = \Big[\mathcal{F}'\big(\mathcal{G}(\mathbf{B})\big)\Big]^{-1},$$

from where it follows that $\mathcal{G}'(\mathbf{B})$ is also symmetric, uniformly positive definite, and uniformly bounded over $\mathbb{R}^3$.

Further, the functions $\mathcal{F}$,$\mathcal{G}$ should reflect texture symmetries of the material. For example, when considering the Goss texture and the reference axes x as the RD, y as the TD and z the direction perpendicular to the sheet plane, then x-y , x-z and y-z planes are the planes of texture symmetry. For $\mathbf{H} = (H_1, H_2, H_3)$ and $\mathbf{B} = (B_1, B_2, B_3)$ this implies

$$\mathcal{F}(-H_1, H_2, H_3) = (-B_1, B_2, B_3) = (-\mathcal{F}_1(\mathbf{H}), \mathcal{F}_2(\mathbf{H}), \mathcal{F}_3(\mathbf{H})), \tag{3.21}$$
$$\mathcal{F}(H_1, -H_2, H_3) = (B_1, -B_2, B_3) = (\mathcal{F}_1(\mathbf{H}), -\mathcal{F}_2(\mathbf{H}), \mathcal{F}_3(\mathbf{H})), \tag{3.22}$$
$$\mathcal{F}(H_1, H_2, -H_3) = (B_1, B_2, -B_3) = (\mathcal{F}_1(\mathbf{H}), \mathcal{F}_2(\mathbf{H}), -\mathcal{F}_3(\mathbf{H})). \tag{3.23}$$

From here it follows that it is enough to define $\mathcal{F}$ for $H_i \geq 0$, $i = 1, 2, 3$. An analogue set of equation can be written for $\mathcal{G}$.

We can now summarize the above deductions into a theorem.

Theorem 3.3. *Let $\mathcal{F}, \mathcal{G} : \mathbb{R}^3 \to \mathbb{R}^3$ be vector functions that represent 3D magnetic characteristics of a homogeneous, anhysteretic material such that $\mathbf{B} = \mathcal{F}(\mathbf{H})$, $\mathbf{H} = \mathcal{G}(\mathbf{B})$.*

Then $\mathcal{F}, \mathcal{G} \in [C^1(\mathbb{R}^3)]^3$ are bijective mappings from $\mathbb{R}^3$ onto $\mathbb{R}^3$, $\mathcal{G} = \mathcal{F}^{-1}$, that fulfill:

1. *$\mathcal{F}(\mathbf{0}) = \mathbf{0}$, $\mathcal{G}(\mathbf{0}) = \mathbf{0}$.*
2. *$\mathcal{F}, \mathcal{G}$ are uniformly monotone on $\mathbb{R}^3$.*
3. *$\mathcal{F}, \mathcal{G}$ are irrotational vector fields, i.e.*

$$\partial_j \mathcal{F}_i = \partial_i \mathcal{F}_j, \quad i, j = 1, 2, 3,$$
$$\partial_j \mathcal{G}_i = \partial_i \mathcal{G}_j, \quad i, j = 1, 2, 3,$$

   and there exist functions $w, \tilde{w} : \mathbb{R}^3 \to \mathbb{R}$ such that $\operatorname{grad} w(\mathbf{B}) = \mathcal{G}(\mathbf{B})$ and $\operatorname{grad} \tilde{w}(\mathbf{H}) = \mathcal{F}(\mathbf{H})$, $\forall \mathbf{B}, \mathbf{H} \in \mathbb{R}^3$.

4. *The Jacobian matrices $\mathcal{F}'$ and $\mathcal{G}'$ are symmetric, uniformly positive definite, and uniformly bounded over $\mathbb{R}^3$. There exist material constants C_1^{mat}, C_2^{mat} such that*

$$C_1^{mat} \leq |\mathcal{F}'(\mathbf{H})| \leq C_2^{mat} \qquad \forall \mathbf{H} \in \mathbb{R}^3,$$
$$1/C_2^{mat} \leq |\mathcal{G}'(\mathbf{B})| \leq 1/C_1^{mat} \quad \forall \mathbf{B} \in \mathbb{R}^3.$$

5. *There exist material constants H^{sat}, B^{sat}, and M^{sat}, satisfying the relation*

$$B^{sat} = \mu_0(H^{sat} + M^{sat}),$$

   such that

$$\mathcal{F}(\mathbf{H}) = \mu_0(\mathbf{H} + M^{sat}\mathbf{e_H}), \ |\mathbf{H}| \geq H^{sat},$$
$$\mathcal{G}(\mathbf{B}) = \nu_0\mathbf{B} - M^{sat}\mathbf{e_B}, \ |\mathbf{B}| \geq B^{sat},$$

   where $\mathbf{e_H} = \mathbf{H}/|\mathbf{H}|$, $\mathbf{e_B} = \mathbf{B}/|\mathbf{B}|$ and $\nu_0 = 1/\mu_0$.

6. *The functions $\mathcal{F}$,$\mathcal{G}$ reflect texture symmetries of the material, see* (3.21)–(3.23).

3.1.3 2D magnetic properties of a homogeneous, anhysteretic material

Very often, only two-dimensional problems are studied. In this case, the magnetic field flow occurs only in the x-y plane. The 2D magnetic characteristics can thus be modelled by vector functions $\mathcal{F}, \mathcal{G} : \mathbb{R}^2 \to \mathbb{R}^2$. By repeating the thoughts from Section 3.1.2, we would achieve the following theorem.

Theorem 3.4. *Let $\mathcal{F}, \mathcal{G} : \mathbb{R}^2 \to \mathbb{R}^2$ be vector functions that represent 2D magnetic characteristics of a homogeneous, anhysteretic material such that $\mathbf{B} = \mathcal{F}(\mathbf{H})$, $\mathbf{H} = \mathcal{G}(\mathbf{B})$.*

Then $\mathcal{F}, \mathcal{G} \in [C^1(\mathbb{R}^2)]^2$ are bijective mappings from $\mathbb{R}^2$ onto $\mathbb{R}^2$, $\mathcal{G} = \mathcal{F}^{-1}$, that fulfill:

1. *$\mathcal{F}(\mathbf{0}) = \mathbf{0}$, $\mathcal{G}(\mathbf{0}) = \mathbf{0}$.*

2. *$\mathcal{F}, \mathcal{G}$ are uniformly monotone on $\mathbb{R}^2$.*

3. *$\mathcal{F}, \mathcal{G}$ are irrotational vector fields, i.e.*

$$\partial_1 \mathcal{F}_2 = \partial_2 \mathcal{F}_1, \tag{3.24}$$
$$\partial_1 \mathcal{G}_2 = \partial_2 \mathcal{G}_1, \tag{3.25}$$

   and there exist functions $w, \tilde{w} : \mathbb{R}^2 \to \mathbb{R}$ such that $\operatorname{grad} w(\mathbf{B}) = \mathcal{G}(\mathbf{B})$ and $\operatorname{grad} \tilde{w}(\mathbf{H}) = \mathcal{F}(\mathbf{H})$, $\forall \mathbf{B}, \mathbf{H} \in \mathbb{R}^2$.

4. *The Jacobian matrices $\mathcal{F}'$ and $\mathcal{G}'$ are symmetric, uniformly positive definite, and uniformly bounded over $\mathbb{R}^2$. There exist material constants C_1^{mat}, C_2^{mat} such that*

$$C_1^{mat} \le |\mathcal{F}'(\mathbf{H})| \le C_2^{mat} \qquad \forall \mathbf{H} \in \mathbb{R}^2, \tag{3.26}$$
$$1/C_2^{mat} \le |\mathcal{G}'(\mathbf{B})| \le 1/C_1^{mat} \quad \forall \mathbf{B} \in \mathbb{R}^2. \tag{3.27}$$

5. *There exist material constants H^{sat}, B^{sat}, and M^{sat}, satisfying the relation*

$$B^{sat} = \mu_0 (H^{sat} + M^{sat}), \tag{3.28}$$

   such that

$$\mathcal{F}(\mathbf{H}) = \mu_0 (\mathbf{H} + M^{sat} \mathbf{e}_{\mathbf{H}}), \ |\mathbf{H}| \ge H^{sat}, \tag{3.29}$$
$$\mathcal{G}(\mathbf{B}) = \nu_0 \mathbf{B} - M^{sat} \mathbf{e}_{\mathbf{B}}, \ |\mathbf{B}| \ge B^{sat}, \tag{3.30}$$

   where $\mathbf{e}_{\mathbf{H}} = \mathbf{H}/|\mathbf{H}|$, $\mathbf{e}_{\mathbf{B}} = \mathbf{B}/|\mathbf{B}|$ and $\nu_0 = 1/\mu_0$.

6. *The functions $\mathcal{F}$,$\mathcal{G}$ reflect texture symmetries of the material, see* (3.31)–(3.32) *below.*

When considering e.g. a horizontal 2D section of the Goss texture and the reference axes o_x as RD and o_y as TD, then o_x and o_y are the axes of the texture symmetry. For $\mathbf{H} = (H_1, H_2)$ and $\mathbf{B} = (B_1, B_2)$ this implies

$$\mathcal{F}(-H_1, H_2) = (-B_1, B_2) = (-\mathcal{F}_1(\mathbf{H}), \mathcal{F}_2(\mathbf{H})), \tag{3.31}$$
$$\mathcal{F}(H_1, -H_2) = (B_1, -B_2) = (\mathcal{F}_1(\mathbf{H}), -\mathcal{F}_2(\mathbf{H})), \tag{3.32}$$

from where we see that it is enough to define $\mathcal{F}$ on the first quadrant. We can obtain similar results for $\mathcal{G}$ as well.

3.2 2D models of an anisotropic steel sheet

In this section, an overview and historical development of 2D models of anisotropic, grain oriented steel sheet models is summarized. The values of $\mathbf{B}$ and $\mathbf{H}$ have only two components in this case. We will point out the conceptual differences between various models and indicate their numerical implementation. The construction of the models and the underlying accuracy was always influenced by the limitations of the measuring apparatus. From this reason, the measurement methods are briefly presented as well. Since many anisotropic model constructions are basically derived from the models for isotropic sheets, we will examine these isotropic models first.

3.2.1 Traditional measurement methods

The measurements for a sheet material are traditionally performed by means of an *Epstein frame* or a *Single sheet tester (SST)* [29]. A measured sheet sample is first cut in a direction deviated from the RD at an angle α and inserted into the tester. The symmetry of the sheet texture allows us to limit the range of $\alpha \in [0\,,\,90]$. For convenience, α is expressed in degrees.

The *exciting apparatus* is used to generate an alternating magnetic field inside the sample. The instant values of the magnetic field intensity and magnetic induction $\mathbf{h}(t)$ and $\mathbf{b}(t)$ form two vector periodic functions of time. The direction of one of these quantities can be controlled to be parallel to the cutting direction. Let, for instance, magnetic induction be the controlled quantity.

The *measuring apparatus*, consisting of *B-coils* or *probes* and *H-coils*, are used to capture the values of $\mathbf{h}_\alpha(t)$ and $\mathbf{b}_\alpha(t)$, which are the orthogonal projections of $\mathbf{h}(t)$ and $\mathbf{b}(t)$ onto the cutting direction. Their amplitudes $\mathbf{H}_\alpha$ and $\mathbf{B}_\alpha$ are then taken as the measured values. We note that the real value of $\mathbf{H}$, i.e. the amplitude of $\mathbf{h}(t)$, is equal to $\mathbf{H}_\alpha$ only when the sheet is isotropic or $\alpha = 0$ or $\alpha = 90$, i.e. the sample is cut in RD or TD. Generally, one can say that traditional measurement methods do not respect the direction difference between filed strength and flux density.

When repeating the measurements with different excitation strengths, one obtains a collection of measured values $\mathcal{S}_\alpha = \{B_i^\alpha, H_i^\alpha\}_{i=1}^{N_\alpha}$ for a particular direction α. For an isotropic sheet, one can obviously perform the measurements in just one, arbitrary direction and work with one collection of measured values $\mathcal{S}$ independent on α. Anisotropic sheets require more collections of measured values.

Although the measurement apparatus is being constantly improved, the measured values did not reach the saturation region so far, where the relation between $\mathbf{B}$ and $\mathbf{H}$ is known. Current methods can give reliable results up to $B_\alpha^{max} \equiv B_{N_\alpha}^\alpha \approx 1.8$–$2.0\,\mathrm{T}$.

We define the *measured region* as $\mathcal{K}_\alpha^m = \{B : 0 \leq B \leq B_\alpha^{max}\}$. At very high fields the measurements are affected by substantial flux leakage, thus giving inaccurate values. The *saturation region* is $\mathcal{K}^{sat} = \{B : B \geq B^{sat}\}$, where $B^{sat} \approx 2.15\,\mathrm{T}$, as stated in Section 2.2.3. The so called *transition region* $\mathcal{K}_\alpha^t = \{B : B_\alpha^{max} < B < B^{sat}\}$ is the one not covered by the measurements.

In real devices, the values of flux density seldom get over the measured region. However, in numerical computations, during first steps of an iterative scheme, the flux density may take extreme values. A good model is required to cover all regions to improve convergence results.

3.2.2 Isotropic steel sheet modelling

There are two different representations of an isotropic sheet model in use, both differ slightly in the model construction and are presented here.

The reluctivity (or permeability) function is the first representation. When the hysteresis effects are not taken into account, due to the symmetry of the material, $\mathbf{B}$ and $\mathbf{H}$ are parallel for all $\mathbf{B}, \mathbf{H} \in \mathbb{R}^2$, and the B-H characteristics must be direction-independent. Thus, μ and ν are then reduced to scalar functions of magnitude of $\mathbf{H}$ or $\mathbf{B}$ respectively. Equations (2.10) and (2.11) can hence be rewritten as

$$\mathbf{B} = \mu(H^2)\,\mathbf{H}, \tag{3.33}$$
$$\mathbf{H} = \nu(B^2)\,\mathbf{B}. \tag{3.34}$$

The problem is reduced to finding a scalar function of one real variable. Having a collection of measured values $\mathcal{S} = \{B_i, H_i\}_{i=1}^N$, the objective now is to define the reluctivity function $\nu(\tau), \tau \geq 0$.

The values of ν at $\tau_i = B_i^2$ can be calculated from (3.34) as $\nu_i \equiv \nu(\tau_i) = B_i/H_i$, $i = 1, \ldots, N$. On the saturation region, we have from (3.30) (omitting the vector directions):

$$H = \nu_0 B - M^{sat}, \quad B \in \mathcal{K}^{sat}. \tag{3.35}$$

Let us calculate the limit

$$\lim_{\tau\to\infty} \nu(\tau) = \lim_{\tau\to\infty} \frac{H}{B} = \lim_{\tau\to\infty} \frac{\nu_0 B - M^{sat}}{B} = \nu_0. \tag{3.36}$$

An analytical expression of the reluctivity function ν is then usually found such that it approximates the values ν_i at τ_i and fulfills (3.36). Examples of such functions may be found in [4] or [24], see also Figure 3.1(a).

The other representation is accomplished by defining a function g (or f) that directly relates $\mathbf{B}$ to $\mathbf{H}$. Again, because $\mathbf{B}$ is parallel to $\mathbf{H}$ and the vector relations are the same for all directions, it suffices to consider the magnitudes of $\mathbf{B}$ and $\mathbf{H}$ in an arbitrary direction,

$$B = f(H),$$
$$H = g(B).$$

We will now analyze the properties and construction of the function g, starting with the same collection of measured values $\mathcal{S} = \{B_i, H_i\}_{i=1}^N$.

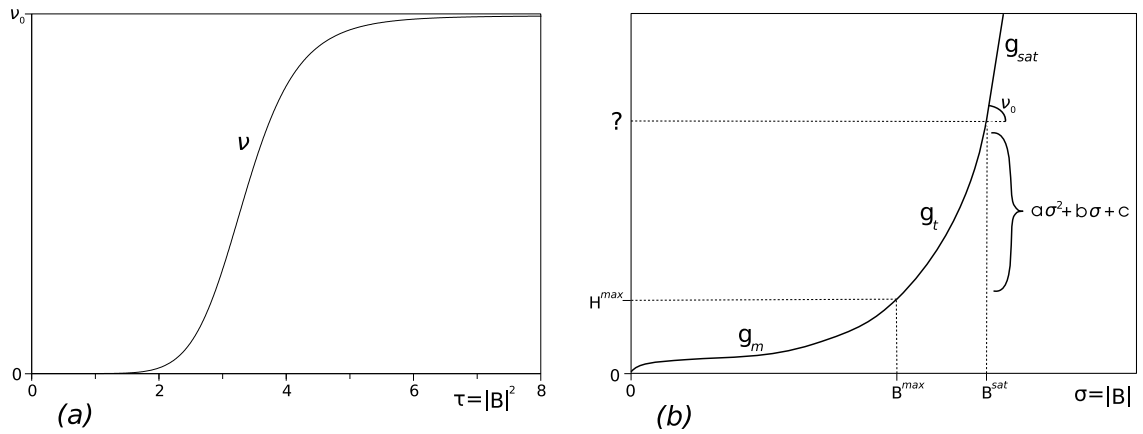

Figure 3.1: The model of an isotropic sheet represented by (a) the reluctivity function, (b) the function g.

Here, the values of g at $\sigma_i = B_i$ are directly $g_i \equiv g(\sigma_i) = H_i$. Because at zero fields there is no induced magnetization, $g_0 \equiv g(0) = 0$. We will deal with finding the function on each region separately; let us designate $g\,|_{\mathcal{K}^m} = g_m$, $g\,|_{\mathcal{K}^t} = g_t$, and $g|_{\mathcal{K}^{sat}} = g_{sat}$.

First, any (e.g. polynomial) approximation can be used to obtain g_m from the values g_i at σ_i. However, as stated in [39], the best convergence results are achieved when the material properties are modelled by a function at least C^1 continuous. Hence, cubic spline interpolations are more suitable for this purpose than a simple linear interpolation.

From (3.35) we see that g_{sat} is a linear function with derivative $g'_{sat} = \nu_0$, though we do not know the value of $H^{sat} = g\,(B^{sat})$.

The transition region $\mathcal{K}^t$ is not covered by the measured values. Nevertheless, if we assume g to be a quadratic function on $\mathcal{K}^t$, cf. Figure 3.1(b), then the function g_t can be expressed as

$$g_t = a\sigma^2 + b\sigma + c, \quad \sigma \in \mathcal{K}^t.$$

The unknown coefficients a, b, and c are then computed based on the following data:

$$\begin{aligned} g_t(B^{max}) &= g_m(B^{max}), \\ g'_t(B^{max}) &= g'_m(B^{max}), \\ g'_t(B^{sat}) &= \nu_0. \end{aligned}$$

g_{sat} is then defined as

$$g_{sat}(\sigma) = g_t(B^{sat}) + \nu_0(\sigma - B^{sat}), \quad \sigma \in \mathcal{K}^{sat}.$$

It can be easily seen that $g \in C^1[0, \infty)$.

The reluctivity representation is preferred for the model of an isotropic sheet because the resulting FEM equations are then solved faster than when the other representation is chosen. However, as we will see later in this chapter, the reluctivity representation is inconvenient when an accurate model of an anisotropic sheet is demanded. From this reason, the equations in terms of the reluctivity function are not introduced in this work.

3.2.3 Conventional model for anisotropic steel sheets

The *conventional model* for an anisotropic steel sheet consists of two B-H curves. A *B-H curve* is a representation of magnetic characteristics in a particular direction. The model uses two collections of measured values $\mathcal{S}_\alpha$, for $\alpha = 0$ and $\alpha = 90$. Two B-H curves for the rolling and transverse directions are first constructed analogously as in the isotropic case. The final model is then represented by a vector function $\mathcal{F} = (f_r, f_t)$ given by

$$B_r = f_r(H_r), \tag{3.37}$$
$$B_t = f_t(H_t), \tag{3.38}$$

where the subscripts r and t denote the coordinate systems designated by the rolling and transverse directions. Considering the sheet's texture symmetry, we can limit ourselves to define $\mathcal{F}$ for $H_r \geq 0$, $H_t \geq 0$.

Conversely, the H-B relation can be represented by a vector function $\mathcal{G} = (g_r, g_t)$ given by

$$H_r = g_r(B_r), \tag{3.39}$$
$$H_t = g_t(B_t). \tag{3.40}$$

Again, the texture symmetry allows us to define $\mathcal{G}$ only for $B_r \geq 0$, $B_t \geq 0$.

In terms of the permeability function, we obtain

$$\begin{pmatrix} B_r \\ B_t \end{pmatrix} = \begin{pmatrix} \mu_r(H_r^2) & 0 \\ 0 & \mu_t(H_t^2) \end{pmatrix} \begin{pmatrix} H_r \\ H_t \end{pmatrix},$$

and similarly for the reluctivity function

$$\begin{pmatrix} H_r \\ H_t \end{pmatrix} = \begin{pmatrix} \nu_r(B_r^2) & 0 \\ 0 & \nu_t(B_t^2) \end{pmatrix} \begin{pmatrix} B_r \\ B_t \end{pmatrix}.$$

This conventional model is commonly used in practical computations. However, measurements exhibit strong inaccuracies in this model. Fig. 3.2 (a) shows loci in the B-plane (the space of magnetic induction vectors) at constant field strength magnitudes in different cutting directions α. The values given by the conventional model are drawn by solid lines. As seen from the figure, the conventional model suggests the magnetically easiest direction at an angle $\beta \approx 30°$ from RD, which is incorrect.

Let us remark that the vector functions $\mathcal{F}$ and $\mathcal{G}$ defined by the conventional model are irrotational on $\mathbb{R}^2$, as is seen from (3.37)–(3.38) and (3.39)–(3.40), i.e.

$$\operatorname{rot} \mathcal{F} = 0, \quad \text{on } \mathbb{R}^2,$$
$$\operatorname{rot} \mathcal{G} = 0, \quad \text{on } \mathbb{R}^2.$$

3.2.4 Elliptic model for anisotropic steel sheets

At first glance, the measured B-loci in Fig. 3.2 (a) resemble by its shape an ellipse. This lead researchers to define an *elliptic model* [32]. It is commonly expressed in terms of the permeability function as

$$\begin{pmatrix} B_r \\ B_t \end{pmatrix} = \begin{pmatrix} \mu_r(H^2) & 0 \\ 0 & \mu_t(H^2) \end{pmatrix} \begin{pmatrix} H_r \\ H_t \end{pmatrix}, \tag{3.41}$$

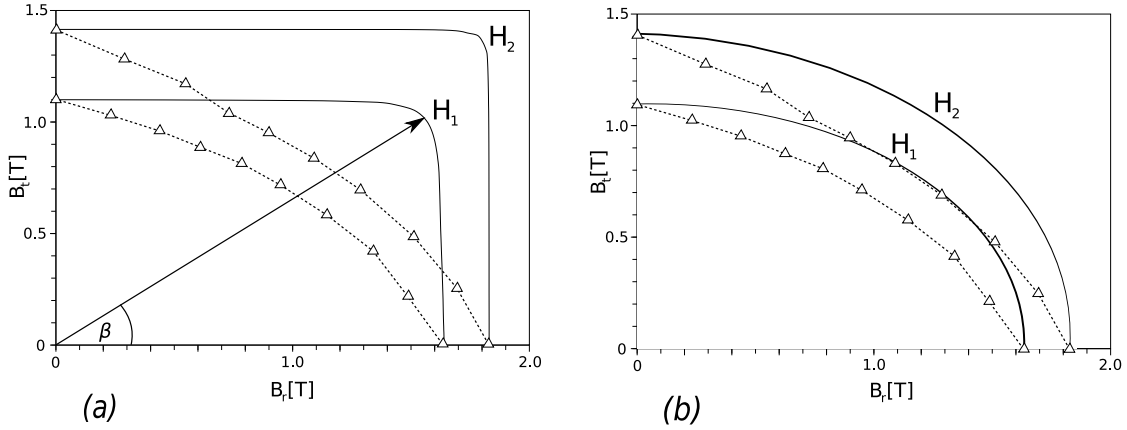

Figure 3.2: B-loci at constant field strength magnitudes; $H_1 = 200\,\mathrm{A.m^{-1}}, H_2 = 1000\,\mathrm{A.m^{-1}}$. Solid lines represent the values provided by (a) conventional model, (b) elliptic model. Dashed lines follow the measured values which are taken from [31] and [32].

where $H^2 = H_r^2 + H_t^2$. From (3.41) one gets easily

$$\frac{B_r^2}{\mu_r^2(H^2)} + \frac{B_t^2}{\mu_t^2(H^2)} = H^2. \tag{3.42}$$

Keeping the field strength magnitude constant, the values of magnetic flux density follow an ellipse in the B-plane, as seen from (3.42). Fig. 3.2(b) compares the values given by the elliptic model to the measured ones. It is worthwhile to note that, in the rolling and transverse directions, (3.41) will reduce to

$$\begin{aligned} B_r &= \mu_r(H_r^2)H_r \\ B_t &= \mu_t(H_t^2)H_t \ , \end{aligned}$$

being thus consistent with the conventional model and measured values.

3.2.5 Multicurve models for anisotropic steel sheets

In order to address the inaccuracies of the conventional and elliptic models depicted in Fig. 3.2, the so called *multicurve models* were invented. The main idea consists of using more B-H curves in different directions than just in RD and TD. Typically, 3 up to 10 curves are used. Shirkoohi and Liu [37], for instance, performed the measurements in 10 directions and constructed the reluctivity functions $\nu_r \equiv \nu_0\,,\ \nu_{10}\,, \ldots, \nu_{90} \equiv \nu_t$ from the measured collections $\mathcal{S}_\alpha\,, \alpha = 0, 10, \ldots, 90$, see Fig.3.3. They defined the reluctivity for the other intermediate angles by linear interpolation between the two nearest curves.

Even the multicurve models are not accurate though, since they do not respect the direction difference between **B** and **H**. A model that respects this phenomenon must follow 2D measurements of the material.

3.2.6 2D measurements of anisotropic steel sheets

The Nakata group first performed the measurements of magnetic properties of a sheet by means of an enhanced version of a single sheet tester (SST^2) [31]. The tester

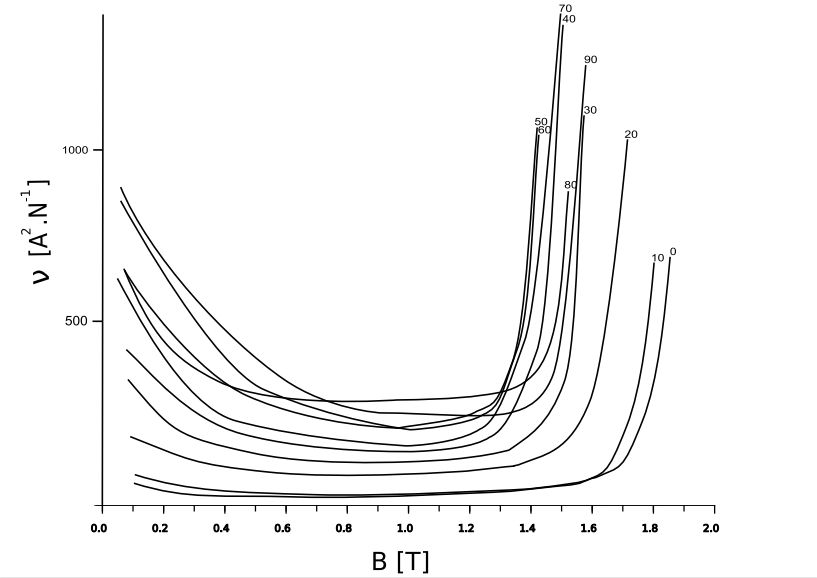

Figure 3.3: Ten-step reluctivities based on the measurements of CGO steel.

contains additional coils that measure 2D B-H relations. The tester's construction was even improved to give good results for high flux densities up to 2 T [28]. The values provided by SST^2 measurements are given in two representations, cartesian and polar.

The cartesian representation consists of $2m$ collections of measured values. We will associate the cartesian x-axis to RD and y-axis to TD. Each collection $\mathcal{S}^{car}_{x,j}, j = 1, \ldots, m$ contains N^j_x measured values of $\mathbf{B}$ and $\mathbf{H}$ in the x-direction, while $B^j_{y,i} \equiv B^j_y$ being a constant for $i = 1, \ldots, N^j_x$. Similarly, each collection $\mathcal{S}^{car}_{y,j}$ contains N^j_y measured values of $\mathbf{B}$ and $\mathbf{H}$ in the y-direction at constant $B^j_{x,i} \equiv B^j_x$, $i = 1, \ldots, N^j_y$. For instance, in [30] there are published measurements for $B^j_x, B^j_y = 0, 0.2, \ldots, 1.6, 1.8$. The individual collections contain the measured values

$$\mathcal{S}^{car}_{x,j} = \{B^j_{x,i}, H^j_{x,i}\}^{N^j_x}_{i=1}, \;\; \mathcal{S}^{car}_{y,j} = \{B^j_{y,i}, H^j_{y,i}\}^{N^j_y}_{i=1}, \;\; j = 1 \ldots m.$$

The supercollection of all $\mathcal{S}^{car}_{x,j}, j = 1, \ldots, m$ will be denoted by $\mathcal{M}^{car}_x$ and, analogously, the supercollection of all $\mathcal{S}^{car}_{y,j}, j = 1, \ldots, m$ will be denoted by $\mathcal{M}^{car}_y$.

The polar representation contains n collections of measured values. Let θ_H and θ_B be the angles between RD and $\mathbf{H}$ or $\mathbf{B}$ respectively. In this case, each collection $\mathcal{S}^{pol}_j, j = 1, \ldots, n$ consists of N_j measured data of $|\mathbf{B}|$, $|\mathbf{H}|$ and $\theta_{\mathbf{H}}$ at constant $\theta^j_{B,i} \equiv \theta^j_B, i = 1, \ldots, N_j$:

$$\mathcal{S}^{pol}_j = \; \{B^j_i, H^j_i, \theta^j_{H,i}\}^{N_j}_{i=1} \; , \;\; j = 1 \ldots n.$$

3.2.7 Full 2D model of an anisotropic steel sheet

In a general 2D magnetic modelling, we need to find a mapping

$$\mathcal{G} : \mathbb{R}^2 \to \mathbb{R}^2, \quad \mathcal{G} : \mathbf{B} \mapsto \mathbf{H}.$$

We describe in detail how the model was constructed with the aid of the mathematical software Scilab. The data that were measured for the material AISI:M-0H by Nakata [30] were obtained in the cartesian form from [21].

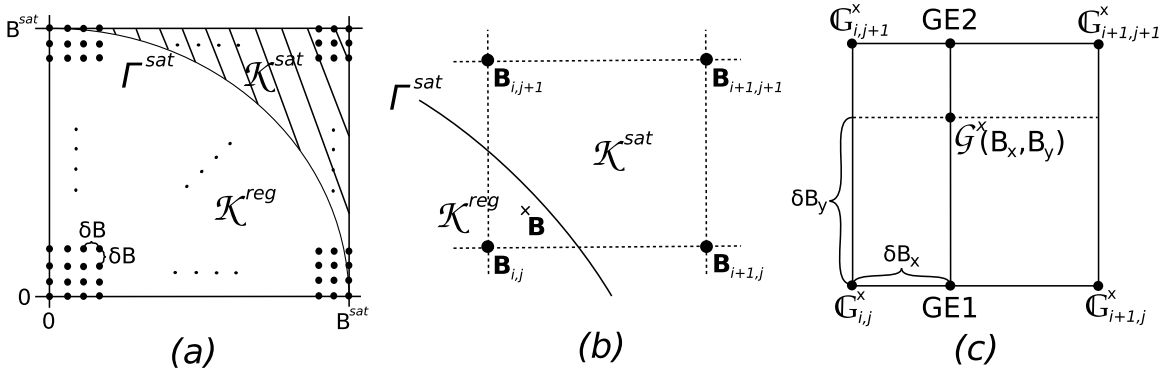

Figure 3.4: (a) The regular grid of induction vectors for which the value of $\mathcal{G}_x$ is stored, (b) a sketch that shows the necessity of storing the values of $\mathcal{G}_x$ in grid points near Γ^{sat}, (c) the calculation of the value of $\mathcal{G}_x$ at an arbitrary point $\mathbf{B} \in \mathcal{K}^{reg}$.

Let $\mathcal{G} = (\mathcal{G}_x, \mathcal{G}_y)$. The goal is to construct a function $\mathcal{G}_x(B_x, B_y)$ from the collection $\mathcal{M}_x^{car}$. Analogously, the function $\mathcal{G}_y(B_x, B_y)$ would be constructed from the collection $\mathcal{M}_y^{car}$. The texture symmetry of the sheet allows us to define these functions for $B_x, B_y \geq 0$.

In consistency with Section 3.2.1 we define the sets

$$\begin{aligned} Q &= \left\{\mathbf{B} \in \mathbb{R}^2 : B_x, B_y \geq 0\right\}, \\ \mathcal{K}^{reg} &= \left\{\mathbf{B} \in \mathbb{R}^2 : B < B^{sat}\right\} \cap Q, \\ \mathcal{K}^{sat} &= \left\{\mathbf{B} \in \mathbb{R}^2 : B \geq B^{sat}\right\} \cap Q, \\ \Gamma^{sat} &= \partial\mathcal{K}^{reg} \cap \partial\mathcal{K}^{sat}. \end{aligned}$$

For the subsequent application in the FEM computations, fast access to the function value $\mathcal{G}_x(B_x, B_y)$ for given $B_x, B_y \in Q$ is demanded. Our strategy is to define the function $\mathcal{G}_x$ on a coarse, regular grid with a very small step δB in both directions. The grid can end up at the values of $B_x = B_y = B^{sat}$, because the function will be defined analytically for $\mathbf{B} \in \mathcal{K}^{sat}$. The grid points will be denoted by $\mathbf{B}_{i,j} = (B^x_{i,j}, B^y_{i,j})$, $i, j = 0, \ldots, p$, where $p = B^{sat}/\delta B$. In our calculations, we used the values for $B^{sat} = 2.15$ and $\delta B = 0.01$. For convenience, the units are omitted.

The values of $\mathcal{G}_x$ at the grid points are saved in a square matrix $\mathbb{G}^x$. We notice from Fig. 3.4(a) that some of the grid points fall into $\mathcal{K}^{sat}$. These values will also be stored in the matrix $\mathbb{G}^x$. The values of $\mathcal{G}_x(\mathbf{B}_{i,j})$ for $\mathbf{B}_{i,j} \in \mathcal{K}^{sat}$ are necessary for the correct evaluation of $\mathcal{G}_x$ in $\mathbf{B} \in \mathcal{K}^{reg}$ near Γ^{sat}, see Fig. 3.4(b) and the next paragraph, and these values can be evaluated directly from the matrix $\mathbb{G}^x$.

During the FEM computation, the value of $\mathcal{G}_x$ at any point $\mathbf{B} = (B_x, B_y) \in \mathcal{K}^{reg}$ is then calculated as follows: we first find the indices i, j so that $\mathbf{B} \in \left[B^x_{i,j}, B^x_{i+1,j+1}\right) \times \left[B^y_{i,j}, B^y_{i+1,j+1}\right)$. A simple linear interpolation scheme is then used to compute $\mathcal{G}_x(B_x, B_y)$. The algorithm is then, cf. also Fig. 3.4(c):

$$
\begin{array}{|l|}
\hline
i = \lfloor B_x \ / \delta B \rfloor; \\
j = \lfloor B_y \ / \delta B \rfloor; \\
\delta B_x = B_x - B^x_{i,j}; \\
\delta B_y = B_y - B^y_{i,j}; \\
\mathrm{FALL1} = (\mathbb{G}^x_{i+1,j} - \mathbb{G}^x_{i,j})/\delta B; \\
\mathrm{GE1} = \mathbb{G}^x_{i,j} + \mathrm{FALL1} \cdot \delta B_x; \\
\mathrm{FALL2} = (\mathbb{G}^x_{i+1,j+1} - \mathbb{G}^x_{i,j+1})/\delta B; \\
\mathrm{GE2} = \mathbb{G}^x_{i,j+1} + \mathrm{FALL2} \cdot \delta B_x; \\
\mathrm{FALL3} = (\mathrm{GE2} - \mathrm{GE1})/\delta B; \\
\mathcal{G}_x(B_x, B_y) = \mathrm{GE1} + \mathrm{FALL3} \cdot \delta B_y. \\
\hline
\end{array}
$$

The operator $\lfloor \cdot \rfloor$ denotes the integer part of the division.

We find the analytical expression of $\mathcal{G}_x(B_x, B_y)$ for $\mathbf{B} = (B_x, B_y) \in \mathcal{K}^{sat}$. Let us chose a fixed value of H^{sat}. We used the value of $H^{sat} = 98000$. From (3.30) we obtain

$$
\begin{aligned}
\mathcal{G}_x(B_x, B_y) &= \nu_0 B_x - M^{sat} B_x / B = \\
&= \nu_0 B_x + (H^{sat} - \nu_0 B^{sat}) \frac{B_x}{\sqrt{B_x^2 + B_y^2}}, \quad \mathbf{B} \in \mathcal{K}^{sat}.
\end{aligned} \tag{3.43}
$$

We will also need the derivatives

$$
\frac{\partial \mathcal{G}_x}{\partial B_x}(B_x, B_y) = \nu_0 + (H^{sat} - \nu_0 B^{sat}) \frac{B_y^2}{(B_x^2 + B_y^2)^{3/2}}, \tag{3.44}
$$

$$
\frac{\partial \mathcal{G}_x}{\partial B_y}(B_x, B_y) = (\nu_0 B^{sat} - H^{sat}) \frac{B_x B_y}{(B_x^2 + B_y^2)^{3/2}}. \tag{3.45}
$$

We now approach the problem of obtaining the values of $\mathcal{G}_x$ at grid points from the measured collection $\mathcal{M}^{car}_x$. Let $j \in \{j = 1, \ldots, m\}$ be fixed. Each sub-collection $\mathcal{S}^{car}_{x,j}$ is first used to construct a function

$$
g_j : [0, \infty) \to \mathbb{R}, \quad g_j : B_x \mapsto H_x
$$

at constant $B^j_y \in \{0, 0.2, \ldots, 1.6, 1.8\}$. The construction is similar as in the isotropic case, cf. Section 3.2.2. Nevertheless, the construction of the function g did not work with a fixed value of H^{sat} as the input data that is necessary in the full 2D model for defining $\mathcal{G}_x$ by the analytical expression (3.43) on $\mathcal{K}^{sat}$.

The construction itself is performed as follows. We define

$$
B^{sat}_{x,j} = \sqrt{(B^{sat})^2 - \left(B^j_y\right)^2}, \quad H^{sat}_{x,j} = H^{sat} \frac{B^{sat}_{x,j}}{B^{sat}},
$$

see Fig. 3.5(a). Let $B^{max}_{x,j}$ denote the maximum induction value in the collection $S^{car}_{x,j}$. Again, we define the regions $\mathcal{K}^m_j = \left\{B : 0 \le B \le B^{max}_{x,j}\right\}$, $\mathcal{K}^t_j = \left\{B : B^{max}_{x,j} \le B \le B^{sat}_{x,j}\right\}$, $\mathcal{K}^{sat}_j = \left\{B : B \ge B^{sat}_{x,j}\right\}$ and the functions $g|_{\mathcal{K}^m_j} = g^m_j$, $g|_{\mathcal{K}^t_j} = g^t_j$, and $g|_{\mathcal{K}^{sat}_j} = g^{sat}_j$.

We first used Scilab's `splin(...),"monotone"` primitive to construct the function g^m_j on $\mathcal{K}^m_j$ from the measured values $S^{car}_{x,j}$. To preserve C^1 continuity of g_j over $[0, \infty)$, there are now four conditions on the function g^t_j:

$$
g^t_j(B^{max}_{x,j}) = g^m_j(B^{max}_{x,j}), \quad \left(g^t_j\right)'(B^{max}_{x,j}) = \left(g^m_j\right)'(B^{max}_{x,j}), \tag{3.46}
$$

$$
g^t_j(B^{sat}_{x,j}) = H^{sat}_{x,j}, \qquad \left(g^t_j\right)'(B^{sat}_{x,j}) = \frac{\partial \mathcal{G}_x}{\partial B_x}(B^{sat}_{x,j}, B^j_y). \tag{3.47}
$$

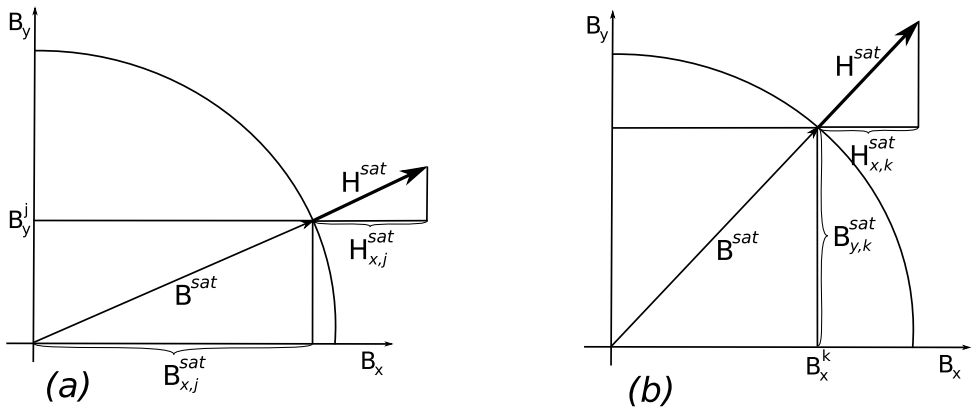

Figure 3.5: (a) Figures accompanying the explanation of how (a) the function g_j, (b) the function h_k is constructed.

The value of $\left(g_j^m\right)'(B_{x,j}^{max})$ was acquired by

$$\left(g_j^m\right)'(B_{x,j}^{max}) = \left(g_j^m(B_{x,j}^{max} + \delta x) - g_j^m(B_{x,j}^{max})\right)/\delta x,$$

where we put $\delta x = -10^{-10}$, while $\partial \mathcal{G}_x/\partial B_x(B_{x,j}^{sat}, B_y^j)$ is calculated from (3.44). Obviously, the quadratic interpolation is not anymore usable. At first glance, the cubic interpolation seems to be suitable. Unfortunately, as can be seen from Fig A.1 in Appendix A, the behaviour of the cubic function is unpredictable. However, much better results can be achieved when g_j^t is searched in the form

$$g_j^t(\sigma) = e^{A\sigma+B} + C\sigma + D, \quad A, B, C, D \in \mathbb{R}.$$

The application of the boundary conditions (3.46) and (3.47) leads to a system of four nonlinear equations for four unknowns A, B, C, D. This system is then solved by an iterative scheme. We utilized Scilab's `fsolve(...)` solver for that purpose. Finally, the function g_j^{sat} is defined as, cf. (3.43),

$$g_j^{sat}(\sigma) = \mathcal{G}_x(\sigma, B_y^j) = \nu_0\sigma + (H^{sat} - \nu_0 B^{sat})\frac{\sigma}{\sqrt{\sigma^2 + (B_y^j)^2}}, \quad \sigma \geq B_{x,j}^{sat}.$$

Further, we construct the functions $h_k, k = 0, \ldots, p$, in the crosswise direction. We recall that $p = B^{sat}/\delta B$. For a fixed $k \in \{0, \ldots, p\}$, the function h_k is

$$h_k : [0, \infty) \to \mathbb{R}, \quad h_k : B_y \mapsto H_x$$

at constant value of $B_x \equiv B_x^k$. Analogously, we define the values

$$B_{y,k}^{sat} = \sqrt{(B^{sat})^2 - (B_x^k)^2}, \quad H_{x,k}^{sat} = H^{sat}\frac{B_x^k}{B^{sat}},$$

cf. Fig. 3.5(b). Let M_k denote the last index j such that $B_y^j < B_{y,k}^{sat}$. The function h_k is then defined in $\tau_j = B_y^j$ as $h_k(\tau_j) = g_j(B_x^k)$, $j = 1, \ldots, M_k$. Further, we have for $\tau_{M_k+1} = B_{y,k}^{sat}$ the value $h_k(\tau_{M_k+1}) = H_{x,k}^{sat}$.

Because the symmetry considerations imply that the function h_k is even, cf. also (3.32), we get $(h_k)'(0) = 0$. We calculate from (3.45) the value of $(h_k)'(B_{y,k}^{sat}) =$

$\partial \mathcal{G}_x / \partial B_y(B_x^k, B_{y,k}^{sat})$. These relations may be taken into account by adding two more interpolation nodes $\tau_0 = -\delta y$, $\tau_{M_k+2} = B_{y,k}^{sat} + \delta y$ and by setting

$$h_k(\tau_0) = h_k(0),$$
$$h_k(\tau_{M_k+2}) = H_{x,k}^{sat} + (h_k)'(B_{y,k}^{sat}) \cdot \delta y.$$

In our calculation, we chose $\delta y = 0.1$.

The values of $h_k(\tau_j)$, $j = 0, \ldots, M_{k+2}$, are then interpolated similarly as the functions g_j^m. Again, we used Scilab's `splin(...),"monotone"` primitive. Finally, from (3.43) we obtain the expression of the function h_k on the saturation region as

$$h_k(\sigma) = \mathcal{G}_x(B_x^k, \sigma) = \nu_0 B_x^k + (H^{sat} - \nu_0 B^{sat}) \frac{B_x^k}{\sqrt{(B_x^k)^2 + \sigma^2}}, \quad \sigma \geq B_{y,k}^{sat}.$$

The figures of the functions h_k for different k may be seen in Appendix A.

The values of the functions $h_k, k = 0, \ldots, p$, at grid points $\mathbf{B}_{i,j}$, $i, j = 0, \ldots, p$, are then stored in a matrix $\tilde{\mathbb{G}}^x$. To optimize the properties of the function $\mathcal{G}_x$ and to improve the convergence of the iterative scheme that will be introduced in Chapter 6, some post-processing is suitable rather than working directly with these raw values.

First, the values $\tilde{\mathbb{G}}_{i,j}^x$ are not necessarily monotone.[4] In fact, in our calculations about 8 % of elements $\tilde{\mathbb{G}}_{i,j}^x$ of the matrix $\tilde{\mathbb{G}}^x$ did not satisfy the relation

$$(\tilde{\mathbb{G}}_{i,j}^x \leq \tilde{\mathbb{G}}_{i+1,j}^x) \text{ and } (\tilde{\mathbb{G}}_{i,j}^x \leq \tilde{\mathbb{G}}_{i,j+1}^x).$$

Therefore, we perform the *monotonization process* on the values of the matrix $\tilde{\mathbb{G}}^x$. The process is as follows: we order the elements of the matrix in the way demonstrated in Fig. 3.6 (a). Then we do for $m_1, \ldots, m_{(p+1)^2}$:

$$(\tilde{\mathbb{G}}_{i,j}^x > \tilde{\mathbb{G}}_{i+1,j}^x) \text{ or } (\tilde{\mathbb{G}}_{i,j}^x > \tilde{\mathbb{G}}_{i,j+1}^x) \;\Rightarrow\; \tilde{\mathbb{G}}_{i,j}^x \stackrel{def}{=} \min\{\tilde{\mathbb{G}}_{i+1,j}^x, \tilde{\mathbb{G}}_{i,j+1}^x\},$$

where $\tilde{\mathbb{G}}_{i,j}^x \equiv \tilde{\mathbb{G}}_{m_k}^x$, $k = 1, \ldots, (p+1)^2$. Certainly, the values with indices that are out of range are not tested. It is easily seen that the values $\tilde{\mathbb{G}}_{i,j}^x$ are monotone after the monotonization process is performed. The greatest relative change in the values of the matrix was not more than 2 % in our case.

The monotonized values are then smoothed by the *smoothing process* that involves (discrete) convolution with a 7×7 Gaussian convolution kernel G_σ given by the relations

$$G_\sigma(x_i, y_j) = \mathcal{N} e^{-\frac{x_i^2 + y_j^2}{2\sigma^2}}, \quad x_i, y_j = -3, -2, \ldots, 2, 3,$$

where $\mathcal{N}$ is the normalizing constant. The kernel is shown in Fig. 3.6 (b) with the value of $\sigma = 0.5$ that was used in our calculations. Performing twice the smoothing process caused the greatest relative change in the matrix values of 7 %. Then the monotonization process was reapplied to repair the minor monotonicity disruptions caused by the smoothing. After that, the values were stored in the final matrix $\mathbb{G}^x$.

However, the vector function $\mathcal{G}$ thus constructed is not, in general, irrotational, i.e. $\operatorname{rot} \mathcal{G} \neq 0$. We will see in Chapter 6 that the iteration scheme for solving the upcoming PDEs is also applicable for such a function, although this property leads to solving linear systems with non-symmetric matrices in every iteration step that considerably degrade the convergence rate of the iteration process.

[4] The monotonicity is naturally defined as $(i_1 \leq i_2 \text{ and } j_1 \leq j_2) \Rightarrow \tilde{\mathbb{G}}_{i_1,j_1}^x \leq \tilde{\mathbb{G}}_{i_2,j_2}^x$.

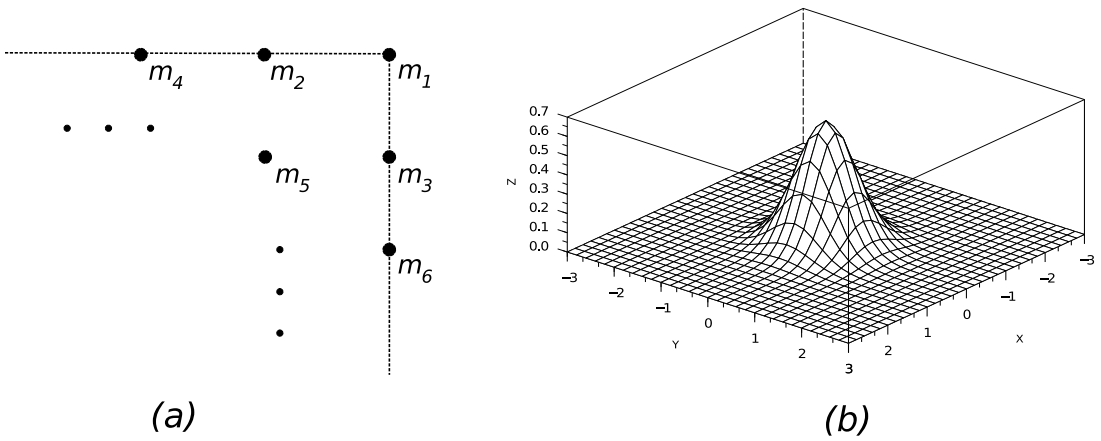

Figure 3.6: (a) The ordering of matrix elements for monotonization, (b) Gaussian convolution kernel G_σ with $\sigma = 0.5$.

We propose a possible way of working out this problem. From (3.45) we see that in the saturation region it holds

$$\operatorname{rot} \mathcal{G} = 0, \quad B \geq B^{sat}.$$

Let us define the set $B^{reg} = \{\mathbf{B} \in \mathbb{R}^2 : \mathbf{B} \leq B^{sat}\}$. Since the function $\tilde{\mathcal{G}} = \mathcal{G}|_{B^{reg}}$ fulfills $\tilde{\mathcal{G}} \in [H^1(B^{reg})]^2$, there exists its unique decomposition

$$\tilde{\mathcal{G}} = \operatorname{grad} p + \operatorname{curl} q \quad \text{on } B^{reg} \tag{3.48}$$

from Theorem 3.2. We are seeking the irrotational part of $\tilde{\mathcal{G}}$, i.e. the function $\operatorname{grad} p$. Performing the divergence operation on both sides of (3.48) yields

$$\Delta p = \operatorname{div} \tilde{\mathcal{G}}. \tag{3.49}$$

Let $\overline{p} = p|_{\partial B^{reg}}$ denote the trace (in the classical sense) of the function p on ∂B^{reg}. From (3.30) we see that $\tilde{\mathcal{G}}(\mathbf{x})$ is perpendicular to ∂B^{reg} for every $\mathbf{x} \in \partial B^{reg}$. Since $\operatorname{curl} q \cdot \mathbf{n}|_{\partial B^{reg}} = 0$, cf. Theorem 3.2, we deduce from (3.48) that $\tilde{\mathcal{G}} = \operatorname{grad} p$ on ∂B^{reg}. This implies that the trace $\overline{p}$ is constant on ∂B^{reg}, i.e. there exists $\overline{K} \in \mathbb{R}$ such that

$$p|_{\partial B^{reg}} = \overline{K}. \tag{3.50}$$

The relations (3.49)–(3.50) define a Dirichlet boundary value problem for the Poisson equation. By solving this problem we obtain the function p whose gradient is the irrotational part of $\tilde{\mathcal{G}}$. Since it is the gradient of p we are seeking, the constant $\overline{K}$ can be chosen arbitrarily. However, we did not implement the thoughts of this paragraph so their usefulness is not verified.

3.3 3D modelling of magnetically anisotropic laminated structures

The cores of electrical devices are usually made up of steel and dielectric laminations. A 3D model of such a laminated structure is proposed in Section 3.3.2. Any 3D model, however, needs to access the full 3D B-H characteristics of the steel. This bears some difficulties which are to be discussed first.

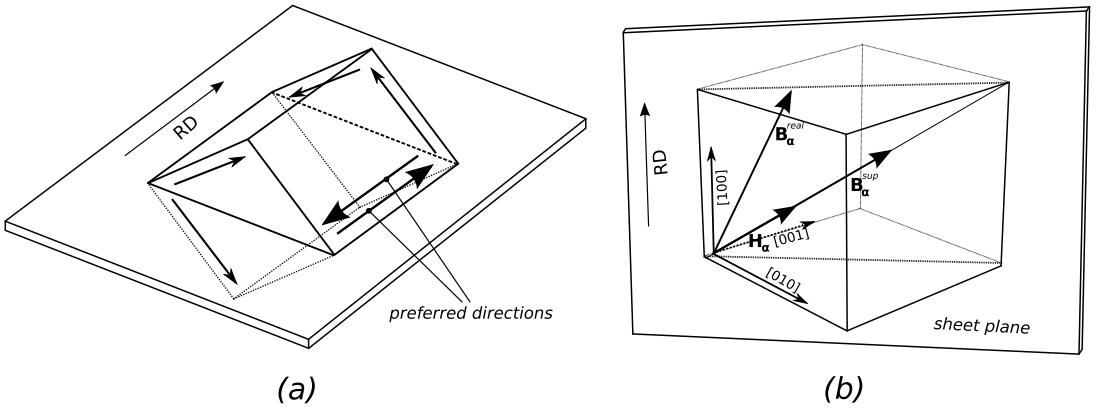

Figure 3.7: All possible directions of domain moments in the initial, non-magnetized state (a), illustration of supposed and measured directions of induction vectors when the field is applied in the magnetically hard direction in the sheet plane (b).

3.3.1 The problem of obtaining 3D B-H characteristics of a steel sheet from 2D measurements

We have discussed in Section 3.2 how to construct 2D B-H characteristics of a material represented by vector functions $\mathcal{F}, \mathcal{G} : \mathbb{R}^2 \to \mathbb{R}^2$. In order to get full 3D characteristics of the material, we need to extend $\mathcal{F}, \mathcal{G}$ on $\mathbb{R}^3$, i.e. to find mappings

$$\mathcal{F}^*, \mathcal{G}^* : \mathbb{R}^3 \to \mathbb{R}^3,$$
$$\mathcal{F}^*(x, y, 0)^T = \big(\mathcal{F}(x, y), 0\big)^T, \quad \mathcal{G}^*(x, y, 0)^T = \big(\mathcal{G}(x, y), 0\big)^T.$$

However, this bears some difficulties.

Let us consider a Goss-textured steel. Being aware of the cubic structure of the texture, an idea is to extend $\mathcal{F}$ in accordance to the texture symmetry, setting e.g. $\mathcal{F}^*(\mathbf{H}_{\langle 100\rangle}) = \mathcal{R}\mathcal{F}(\mathbf{H}_{RD})$, where $\mathbf{H}_{RD}$ is a vector in the rolling direction, $\mathbf{H}_{\langle 100\rangle}$ denotes a vector in one of the another magnetically easy directions (crystallographic $\langle 100\rangle$ directions, cube edges) with $|\mathbf{H}_{RD}| = |\mathbf{H}_{\langle 100\rangle}|$ and $\mathcal{R}$ is the rotation matrix that maps $\mathbf{H}_{RD}$ to $\mathbf{H}_{\langle 100\rangle}$.

This process would be correct if there were not any preferred directions of magnetic moments of the individual magnetic domains (we call them *domain moments* for the purpose of this section). We will give an argument that the domain moments lie preferably in the sheet plane.

Fig. 3.7 (a) shows all 6 possible directions of domain moments in the initial, non-magnetized state. We will recall the magnetization process described in Chapter 2. The field $\mathbf{H}_{\boldsymbol{\alpha}}$ will be applied in the direction $\boldsymbol{\alpha} = [111]$ (cube body diagonal, see Fig.2.2) . If all directions of domain moments were equally preferred, the supposed induction vector $\mathbf{B}^{sup}_{\boldsymbol{\alpha}}$ should be, due to the symmetry, parallel to $\mathbf{H}_{\boldsymbol{\alpha}}$, as shown on Fig. 3.7 (b) . Nevertheless, the real, measured value $\mathbf{B}^{real}_{\boldsymbol{\alpha}}$ is different. The direction of $\mathbf{B}^{real}_{\boldsymbol{\alpha}}$ indicates the superior influence of domain moments parallel to RD and leads us to a conclusion that they are relatively more numerous than the others.

Because the physical situation is similar for isotropic sheets, the domain moments may preferably lie in directions with lesser deviations from the sheet plane as well, although there is no grain orientation which would indicate this kind of anisotropy by measurements performed in the sheet plane. Hence we conclude that not even isotropic sheets are ideally isotropic.

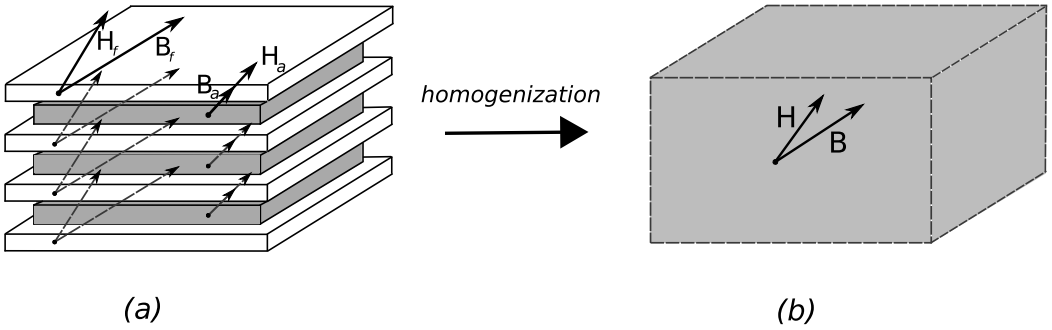

Figure 3.8: The process of *homogenization* consists in replacing the lamination (a) by a homogeneous block (b) with similar magnetic properties.

Any eventual accurate 3D model of a homogeneous steel sheet should be aware of the sheet's properties pointed out here. Since no one has dealt with the problem yet, it remains open.

3.3.2 3D model of steel-dielectric lamination

Bastos and Quichaud suggested a 3D model of laminated structures made up of thin steel and dielectric layers [2] . The steel was supposed to be perfectly isotropic. We are going to extend the model for an arbitrary anisotropic steel whose 3D magnetic properties are given by functions $\mathcal{F}, \mathcal{G}$.

Let ε and $1-\varepsilon$ be the relative amounts of volume occupied by the dielectric and the steel inside the lamination respectively. Let us consider a small region of the lamination, small enough so that the flux densities and field strengths are constant in both materials and large enough to cover several laminations. Such a region is depicted in Fig. 3.8 (a), where $\mathbf{B}_f$ and $\mathbf{H}_f$ are the values of the flux density and the field strength in the steel and $\mathbf{B}_a$ and $\mathbf{H}_a$ are the analogical values in the dielectric. As described in Secion 2.1.2 , $\mathbf{B}_a \neq \mathbf{B}_f$ and $\mathbf{H}_a \neq \mathbf{H}_f$. The model comes with an idea of *homogenization* , i.e. replacing the lamination by a homogeneous block with proper B-H characteristics. The final vector $\mathbf{H}$ (or $\mathbf{B}$) should be a weighted sum of $\mathbf{H}_f$ (or $\mathbf{B}_f$) and $\mathbf{H}_a$ (or $\mathbf{B}_a$) with weights being the relative quantities of steel and dielectric:

$$\mathbf{H} = \varepsilon \mathbf{H}_a + (1-\varepsilon)\mathbf{H}_f, \tag{3.51}$$

$$\mathbf{B} = \varepsilon \mathbf{B}_a + (1-\varepsilon)\mathbf{B}_f. \tag{3.52}$$

The aim is to give a method for computing $\mathbf{H}$ from $\mathbf{B}$ and vice versa.

We suppose that the material properties of the steel and the dielectric are given by equations

$$\mathbf{H}_f = \mathcal{G}(\mathbf{B}_f), \qquad \mathbf{H}_a = \nu_0 \mathbf{B}_a, \tag{3.53}$$

$$\mathbf{B}_f = \mathcal{F}(\mathbf{H}_f), \qquad \mathbf{B}_a = \mu_0 \mathbf{H}_a. \tag{3.54}$$

In this section, the subscript t will denote the tangential part of a vector in the plane of the sheets, similarly n the normal part. We have, for example, $\mathbf{H}_f = \mathbf{H}_{ft} + \mathbf{H}_{fn}$ etc.

The equations (2.8)–(2.9) guarantee the continuity of tangential part of the field strength and normal part of flux density through the lamination, so we have

$$\mathbf{H}_{at} = \mathbf{H}_{ft} \stackrel{def}{=} \mathbf{H}_t, \tag{3.55}$$

$$\mathbf{B}_{an} = \mathbf{B}_{fn} \stackrel{def}{=} \mathbf{B}_n. \tag{3.56}$$

From (3.51)–(3.52) we obtain

$$\begin{aligned} \mathbf{H}_n &= \varepsilon \mathbf{H}_{an} + (1-\varepsilon)\mathbf{H}_{fn}, \\ \mathbf{B}_t &= \varepsilon \mathbf{B}_{at} + (1-\varepsilon)\mathbf{B}_{ft}, \end{aligned}$$

and by expressing the dielectric quantities we have

$$\mathbf{H}_{an} = \frac{1}{\varepsilon}[\mathbf{H}_n - (1-\varepsilon)\mathbf{H}_{fn}], \tag{3.57}$$

$$\mathbf{B}_{at} = \frac{1}{\varepsilon}[\mathbf{B}_t - (1-\varepsilon)\mathbf{B}_{ft}]. \tag{3.58}$$

From (3.51), (3.53), and (3.56) we obtain

$$\begin{aligned} \mathbf{H} = \varepsilon \mathbf{H}_a + (1-\varepsilon)\mathbf{H}_f = \varepsilon \nu_0 \mathbf{B}_a + (1-\varepsilon)\mathcal{G}(\mathbf{B}_f) = \\ = \varepsilon \nu_0 (\mathbf{B}_{at} + \mathbf{B}_n) + (1-\varepsilon)\mathcal{G}(\mathbf{B}_{ft} + \mathbf{B}_n). \end{aligned} \tag{3.59}$$

Similarly, from (3.52), (3.54), and (3.55) we obtain

$$\begin{aligned} \mathbf{B} = \varepsilon \mathbf{B}_a + (1-\varepsilon)\mathbf{B}_f = \varepsilon \mu_0 \mathbf{H}_a + (1-\varepsilon)\mathcal{F}(\mathbf{H}_f) = \\ = \varepsilon \mu_0 (\mathbf{H}_t + \mathbf{H}_{an}) + (1-\varepsilon)\mathcal{F}(\mathbf{H}_t + \mathbf{H}_{fn}). \end{aligned} \tag{3.60}$$

By placing $\mathbf{B}_{at}$ from (3.58) and $\mathbf{H}_{an}$ from (3.57), the equations (3.59) and (3.60) can be rewritten into the form

$$\mathbf{H} = \nu_0[\varepsilon \mathbf{B}_n + \mathbf{B}_t - (1-\varepsilon)\mathbf{B}_{ft}] + (1-\varepsilon)\mathcal{G}(\mathbf{B}_{ft} + \mathbf{B}_n), \tag{3.61}$$

$$\mathbf{B} = \mu_0[\varepsilon \mathbf{H}_t + \mathbf{H}_n - (1-\varepsilon)\mathbf{H}_{fn}] + (1-\varepsilon)\mathcal{F}(\mathbf{H}_t + \mathbf{H}_{fn}). \tag{3.62}$$

In the cartesian system of coordinates with z direction being perpendicular to the laminations, (3.61)–(3.62) lead to a set of equations

$$\begin{aligned} H_1 &= \nu_0[B_1 - (1-\varepsilon)X] + (1-\varepsilon)\mathcal{G}_1(X, Y, B_3) \\ H_2 &= \nu_0[B_2 - (1-\varepsilon)Y] + (1-\varepsilon)\mathcal{G}_2(X, Y, B_3) \\ H_3 &= \nu_0\, \varepsilon B_3 + (1-\varepsilon)\, \mathcal{G}_3(X, Y, B_3) \\ B_1 &= \mu_0\, \varepsilon H_1 + (1-\varepsilon)\, \mathcal{F}_1(H_1, H_2, Z) \\ B_2 &= \mu_0\, \varepsilon H_2 + (1-\varepsilon)\, \mathcal{F}_2(H_1, H_2, Z) \\ B_3 &= \mu_0[H_3 - (1-\varepsilon)Z] + (1-\varepsilon)\mathcal{F}_3(H_1, H_2, Z), \end{aligned} \tag{3.63}$$

where $(X, Y, Z) = (B_{ft,1}, B_{ft,2}, H_{fn,3})$ may be regarded as a vector of dummy variables not needed as the output of the calculations.

For every fixed $\mathbf{H}$ or $\mathbf{B} \in \mathbb{R}^3$, (3.63) represents a system of 6 nonlinear equations for 6 unknowns. Solving the system gives the desired value of $\mathbf{B}$ or $\mathbf{H}$.

The model was previously studied for ideally isotropic steels. In this case, the steel characteristics are described by its relative permeability

$$\mathbf{B}_f = \mu_0 \mu_r(H_f^2)\, \mathbf{H}_f, \tag{3.64}$$

$$\mathbf{H}_f = \frac{1}{\mu_0 \mu_r(H_f^2)} \mathbf{B}_f. \tag{3.65}$$

Let us suppose a fixed value of field strength $\mathbf{H}$ and search for the corresponding flux density $\mathbf{B}$. Let $\mu_{f,\mathbf{H}}$ denote the value of the steel permeability corresponding to $\mathbf{H}$, i.e.

$$\mu_{f,\mathbf{H}} \stackrel{def}{=} \mu_0 \mu_r(H_f^2)|_{\mathbf{H}_f = \mathbf{H}_f(\mathbf{H})}\ . \tag{3.66}$$

Due to the symmetry of the steel properties the vectors $\mathbf{B}_t$ and $\mathbf{H}_t$ are parallel, and trivially, $\mathbf{B}_n$ and $\mathbf{H}_n$ are also parallel. So there exist constants μ_t, μ_n such that

$$\mathbf{B}_t = \mu_t \mathbf{H}_t, \tag{3.67}$$

$$\mathbf{B}_n = \mu_n \mathbf{H}_n. \tag{3.68}$$

In order to calculate $\mathbf{B}$, we have to find μ_t and μ_n.

By extracting the tangential part of (3.52) and with regard to (3.54), (3.55), (3.64), and (3.66) , we obtain

$$\mathbf{B}_t = \varepsilon \mathbf{B}_{at} + (1-\varepsilon)\mathbf{B}_{ft} = \varepsilon \mu_0 \mathbf{H}_t + (1-\varepsilon)\mu_{f,\mathbf{H}} \mathbf{H}_t. \tag{3.69}$$

Comparing (3.69) with (3.67) results in

$$\mu_t = \varepsilon \mu_0 + (1-\varepsilon)\mu_{f,\mathbf{H}}. \tag{3.70}$$

Similarly, by extracting the normal part of (3.51) and applying (3.53), (3.56), (3.65), and (3.66) we obtain

$$\mathbf{H}_n = \varepsilon \mathbf{H}_{an} + (1-\varepsilon)\mathbf{H}_{fn} = \varepsilon \nu_0 \mathbf{B}_n + (1-\varepsilon)\frac{1}{\mu_{f,\mathbf{H}}} \mathbf{B}_n. \tag{3.71}$$

Comparing (3.71) to (3.68) gives

$$\frac{1}{\mu_n} = \varepsilon \nu_0 + \frac{1-\varepsilon}{\mu_{f,\mathbf{H}}}. \tag{3.72}$$

We see from equations (3.70) and (3.72) that it is enough to compute $\mu_{f,\mathbf{H}} = \mu_0 \mu_r(H_f^2)$ to obtain μ_t and μ_n (the value of H_f^2 is unknown).

Because $\mathbf{B}_{fn} = \mathbf{B}_n$, we obtain from (3.64), (3.66), and (3.68)

$$\mathbf{H}_{fn} = \frac{\mu_n}{\mu_{f,\mathbf{H}}} \mathbf{H}_n.$$

Thus, we have

$$\frac{\mu_{f,\mathbf{H}}}{\mu_0} = \mu_r(H_f^2) = \mu_r(H_{ft}^2 + H_{fn}^2) = \mu_r\left(H_t^2 + \left(\frac{\mu_n}{\mu_{f,\mathbf{H}}}\right)^2 H_n^2\right). \tag{3.73}$$

From (3.72) we obtain

$$\frac{\mu_{f,\mathbf{H}}}{\mu_n} = \left(\frac{1-\varepsilon}{\mu_{f,\mathbf{H}}} + \varepsilon\nu_0\right)\mu_{f,\mathbf{H}} = \left(1 - \varepsilon + \varepsilon\nu_0\mu_{f,\mathbf{H}}\right)$$

and

$$\left(\frac{\mu_n}{\mu_{f,\mathbf{H}}}\right)^2 = \frac{1}{(1-\varepsilon+\varepsilon\nu_0\mu_{f,\mathbf{H}})^2}. \tag{3.74}$$

Placing (3.74) into (3.73) results in the final equation

$$\nu_0\mu_{f,\mathbf{H}} = \mu_r\left(H_t^2 + \frac{H_n^2}{(1-\varepsilon+\varepsilon\nu_0\mu_{f,\mathbf{H}})}\right).$$

We see that in the case of an ideally isotropic sheet, there is just one nonlinear equation to solve instead of the whole system (3.63) .

Chapter 4

The equations for scalar and vector magnetic potentials

The objective of the engineering problem $\mathcal{P}$ is to compute the distribution of the magnetic field strength $\mathbf{H}$ and magnetic induction $\mathbf{B}$ in a domain of interest Ω. We can limit ourselves to compute just one of these quantities because the other one can be calculated from the constitutive relations, cf. Section 2.2. The domain Ω commonly comprises more subdomains $\mathcal{V}_1, \ldots, \mathcal{V}_N$ that represent the domains of various materials. In this case, it would be difficult to work with equations (2.3)–(2.4) directly, because $\mathbf{H}$ and $\mathbf{B}$ exhibit discontinuities on the material interfaces. Hence, it is more suitable to reformulate these equations in terms of the *vector* and *scalar magnetic potential* for the FEM computations. We introduce the potentials and present their mathematical properties as deduced from particular problems, where the potentials are known.

Afterwards, the definition of an engineering problem $\mathcal{P}$ in terms of both potentials is given. Further, the physical situation is often idealized in a way that leads to the 2D formulations for the potentials. These 2D formulations then serve as the basis for defining an idealized engineering problem $\mathcal{Q}$. In this work, we will mostly deal with such an idealized 2D problem.

4.1 3D equations for magnetic potentials

4.1.1 Vector magnetic potential

Let $\mathcal{V}$ be a simply connected domain in $\mathbb{R}^3$ that is occupied by a homogeneous material. Let the material's constitutive relation is given by a function $\mathcal{G}$ such that

$$\mathbf{H} = \mathcal{G}(\mathbf{B}). \tag{4.1}$$

For convenience, we rewrite the equations (2.3)–(2.4):

$$\operatorname{rot} \mathbf{H} = \mathbf{j}, \tag{4.2}$$

$$\operatorname{div} \mathbf{B} = 0. \tag{4.3}$$

From (4.3) we see that the vector field $\mathbf{B}$ is solenoidal on $\mathcal{V}$. As a consequence, cf. Theorem 3.1, there exists a (vector) function $\mathbf{A} : \mathcal{V} \to \mathbb{R}^3$ such that

$$\operatorname{rot} \mathbf{A}(x) = \mathbf{B}(x) \ , \ x \in \mathcal{V}. \tag{4.4}$$

The function $\mathbf{A}$ is called the *vector magnetic potential*.

The above relation does not define the magnetic vector potential uniquely. There is a degree of freedom left for choosing a *gauge condition*. The *Coulomb gauge* is usually applied in case of a stationary magnetic field, that is,

$$\operatorname{div} \mathbf{A} = 0. \tag{4.5}$$

From (4.1), (4.2), and (4.4) we obtain

$$\operatorname{rot}(\mathcal{G}(\operatorname{rot} \mathbf{A}(x))) = \mathbf{j}\ ,\ x \in \mathcal{V}. \tag{4.6}$$

The above equation is the differential equation for the vector magnetic potential in the classical form when just one piece of homogeneous material is considered.

4.1.2 Scalar magnetic potential

Let $\mathcal{V}$ be as in Section 4.1.1. We now assume that the constitutive relation is given by a function $\mathcal{F}$ such that

$$\mathbf{B} = \mathcal{F}(\mathbf{H}). \tag{4.7}$$

Let us suppose that there is no macroscopic current flow through the material.[1] Then $\mathbf{j} = \mathbf{0}$ on $\mathcal{V}$ and the equations (4.2)–(4.3) change to

$$\operatorname{rot} \mathbf{H} = \mathbf{0}, \tag{4.8}$$

$$\operatorname{div} \mathbf{B} = 0. \tag{4.9}$$

From (4.8) we see that the vector field $\mathbf{H}$ is then irrotational on $\mathcal{V}$. With regards to Theorem 3.1, there exists a function $\varphi : \mathcal{V} \to \mathbb{R}$ such that

$$\operatorname{grad} \varphi(x) = \mathbf{H}(x),\ x \in \mathcal{V}. \tag{4.10}$$

The function φ is called the *scalar magnetic potential*.

From (4.7), (4.9), and (4.10) we obtain

$$-\operatorname{div}(\mathcal{F}(\operatorname{grad} \varphi(x))) = 0,\ x \in \mathcal{V}.$$

The above equation is the differential equation for the scalar magnetic potential in the classical form when just one piece of a homogeneous material is considered and when no current flow occurs inside that material.

4.1.3 Global potentials and their properties

Let $\Omega \subset \mathbb{R}^3$ be a simply connected domain, $\Omega = \Omega^{mat} \cup \Omega^{int}$ and $\Omega^{mat} = \bigcup_{i=1}^{N} \mathcal{V}_i$ are as in Section 2.1.2. Let the material constitutive relations are given by functions $\mathcal{F}_i, \mathcal{G}_i$, $i = 1, \ldots, N$.

The *global vector (magnetic) potential* $\mathbf{A} : \Omega \to \mathbb{R}^3$ is defined as a vector function that satisfies the equation

$$\operatorname{rot} \mathbf{A} = \mathbf{B} \quad \text{on } \Omega$$

in the sense of distributions. Let us suppose that the global vector potential exists.

Experiences indicate the following properties of $\mathbf{A}$ [35]:

[1] More accurately, we would say *no free macroscopic current flow*. The so called *bound currents* are hidden in the definition of $\mathbf{H}$ and are not included in the quantity $\mathbf{j}$.

(V1) $\mathbf{A} \in [C(\overline{\Omega})]^3$; $\mathbf{A}_i \equiv \mathbf{A}|_{\mathcal{V}_i}$ are smooth on $\mathcal{V}_i$, $i = 1, \ldots, N$.

(V2) The derivatives of $\mathbf{A}$ are discontinuous in Ω^{int}.

(V3) $\mathbf{A} \in H(\mathrm{rot}, \Omega) \cap H(\mathrm{div}, \Omega)$.

(V4) The functions $\mathbf{A}_i$ satisfy the equation

$$\mathrm{rot}(\mathcal{G}^i(\mathrm{rot}\, \mathbf{A}^i(x))) = \mathbf{j}\,,\ x \in \mathcal{V}_i.$$

The spaces $H(\mathrm{rot}, \Omega)$ and $H(\mathrm{div}, \Omega)$ are defined as

$$H(\mathrm{rot}, \Omega) = \{\mathbf{v} \in [L^2(\Omega)]^3 : \mathrm{rot}\, \mathbf{v} \in [L^2(\Omega)]^3\},$$
$$H(\mathrm{div}, \Omega) = \{\mathbf{v} \in [L^2(\Omega)]^3 : \mathrm{div}\, \mathbf{v} \in L^2(\Omega)\},$$

where the operators rot and div are understood in the sense of distributions. Generally, the derivatives $\partial_i A_j \notin L^2(\Omega)$. As experiments show, the derivatives of the potential can exhibit singularities at the corners of non-convex domains and material interfaces [9] .

Moreover, if $\mathbf{A}$ fulfills the gauge condition

$$\mathrm{div}\, \mathbf{A} = 0 \quad \text{on } \Omega \tag{4.11}$$

in the sense of distributions, then we say that the global vector potential fulfills the gauge condition (4.11) .

Similar properties are observed for the global scalar magnetic potential. When there is no macroscopic current flow through Ω, we can define the *global scalar (magnetic) potential* $\varphi : \Omega \to \mathbb{R}$ as a scalar function that fulfills

$$\mathrm{grad}\, \varphi = \mathbf{H} \quad \text{on } \Omega$$

in the sense of distributions.

The properties of the global scalar potential are analogous to that of the global vector potential:

(S1) $\varphi \in C(\overline{\Omega})$; $\varphi_i \equiv \varphi|_{\mathcal{V}_i}$ are smooth on $\mathcal{V}_i\,, i = 1, \ldots, N$.

(S2) The derivatives of φ are discontinuous on Ω^{int}.

(S3) $\varphi \in H^1(\Omega)$.

(S4) The functions φ_i satisfy the equation

$$-\,\mathrm{div}(\mathcal{F}^i(\mathrm{grad}\, \varphi_i(x))) = 0\,,\ x \in \mathcal{V}_i.$$

4.1.4 Definition of the engineering problem $\mathcal{P}$

Let $\Omega \subset \mathbb{R}^3$ be a simply connected domain, $\Omega = \Omega^{mat} \cup \Omega^{int}$ and $\Omega^{mat} = \bigcup_{i=1}^{N} \mathcal{V}_i$ are as in Section 2.1.2 and $\mathcal{F}_i, \mathcal{G}_i$ are the material characteristics of the homogeneous material that occupies $\mathcal{V}_i$, $i = 1, \ldots, N$.

The *engineering problem* $\mathcal{P}^A$ is defined as the boundary value problem that is given in its classical form as follows. Find a function $\mathbf{A} \in \left[C^2(\overline{\Omega})\right]^3$ such that

$$\operatorname{rot}(\mathcal{G}(\operatorname{rot}\mathbf{A})) = \mathbf{j} \quad \text{in } \Omega,$$

where $\mathcal{G}$ is defined as

$$\mathcal{G}(x;\mathbf{v}) = \mathcal{G}_i(\mathbf{v}), \quad x \in \mathcal{V}_i, \mathbf{v} \in \mathbb{R}^3.$$

Moreover, $\mathbf{A}$ satisfies prescribed boundary conditions on $\Gamma = \partial\Omega$. The boundary conditions for 3D problems are fairly different from that for 2D problems and their discussion is beyond the scope of this work. The engineering problem $\mathcal{P}^A$ will be also called the *boundary value problem* $\mathcal{P}^A$.

The *engineering problem* $\mathcal{P}^\varphi$ is defined as the boundary value problem that is given in its classical form as follows. Find a function $\varphi \in C^2(\overline{\Omega})$ such that

$$-\operatorname{div}(\mathcal{F}(\operatorname{grad}\varphi)) = 0 \quad \text{in } \Omega,$$

where $\mathcal{F}$ is defined as

$$\mathcal{F}(x;\mathbf{v}) = \mathcal{F}_i(\mathbf{v}), \quad x \in \mathcal{V}_i, \mathbf{v} \in \mathbb{R}^3.$$

Moreover, φ satisfies prescribed boundary conditions on $\Gamma = \partial\Omega$. The engineering problem $\mathcal{P}^\varphi$ will be also called the *boundary value problem* $\mathcal{P}^\varphi$.

The engineering problem $\mathcal{P}$ then may refer to one of the problems $\mathcal{P}^\varphi$ or $\mathcal{P}^A$.

4.1.5 Comparision of 3D formulations

We have seen so far that there are two possible boundary value problems to solve that lead to the computation of the respective potentials. The choice of the particular formulation depends on the physical situation. Both have their advantages that can be summarized as follows:

- The vector magnetic potential is defined generally without the limitation that imposes no current flow through the region Ω. Nevertheless, the computation of the vector potential is much more complicated and resource demanding than the scalar potential because a multidimensional FEM scheme must be used for the computation. Moreover, when Ω is a non-convex domain, we have generally $\mathbf{A} \notin [H^1(\Omega)]^3$. That requires a special choice of finite elements [9]. Further, the gauge condition must also be reflected in the choice of the FEM space.
- The scalar magnetic potential is generally much easier to compute because it is a scalar function and there are no further gauge conditions imposed to ensure the uniqueness of the potential. However, the scalar potential is applicable in regions with no current flow only.

4.2 2D equations for magnetic potentials

4.2.1 Obtaining 2D equations from 3D equations

In many practical problems, the magnetic flux occurs mainly in two dimensions. Let us associate a cartesian coordinate system $Oxyz$ with a physical situation where we can suppose

$$B_3 \equiv 0, \; H_3 \equiv 0, \tag{4.12}$$

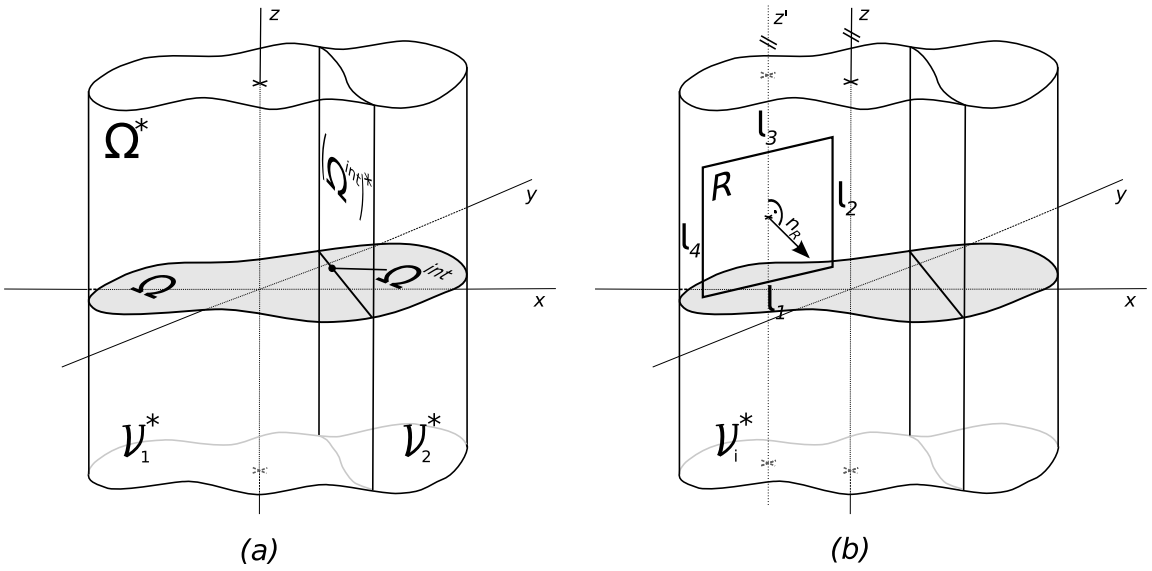

Figure 4.1: (a) The physical and mathematical domains of interest of an idealised engineering problem $\mathcal{Q}$. (b) A rectangle from Lemma 4.1.

where $\mathbf{B} = (B_1, B_2, B_3)$ and $\mathbf{H} = (H_1, H_2, H_3)$.

In this case, the (mathematical) domain of interest Ω may be reduced to a 2D section of that of the 3D problem. Accordingly, let $\Omega \subset \mathbb{R}^2$ be a simply connected domain, $\Omega = \Omega^{mat} \cup \Omega^{int}$ and $\Omega^{mat} = \bigcup_{i=1}^{N} \mathcal{V}_i$ are defined in analogy with in Section 2.1.2. Now we have, cf. also (2.7),

$$\operatorname{meas}_2 \Omega^{int} = 0. \tag{4.13}$$

With regard to (4.12), we can assume

$$\begin{aligned} \mathbf{B}, \mathbf{H} &: \Omega \to \mathbb{R}^2, \\ \mathbf{B} = \mathbf{B}(x, y), &\quad \mathbf{H} = \mathbf{H}(x, y). \end{aligned} \tag{4.14}$$

Physically, this corresponds to an idealized situation with a (physical) domain of interest $\Omega^* \subset \mathbb{R}^3$ being an infinite cylinder whose base is identical to Ω, i.e. $\Omega^* = \Omega \times \mathbb{R}$, cf. Fig. 4.1(a).[2] In this case, all physical quantities, defined on the (physical) domain Ω^*, are functions of first two variables only, e.g.

$$\begin{aligned} \mathbf{A}^*, \mathbf{j}^* &: \Omega^* \to \mathbb{R}^3, \\ \mathbf{A}^* = \mathbf{A}^*(x, y), &\quad \mathbf{j}^* = \mathbf{j}^*(x, y). \end{aligned}$$

Throughout this section, all corresponding *physical* domains and quantities are denoted by asterisks, i.e. $\mathcal{V}_i^* = \mathcal{V}_i \times \mathbb{R}$, $(\Omega^{int})^* = \Omega^{int} \times \mathbb{R}$ etc. Obviously, it holds

$$\operatorname{meas}_3 (\Omega^{int})^* = 0. \tag{4.15}$$

We will now examine the equation for the vector magnetic potential (4.6) for an idealized problem. We prove the following lemma first.

[2] This idealization is widely used in computations of the magnetic field in a steel sheet. The question is to what extent is this physical model that implies an infinite thickness accurate when applied to a 0.30 mm thin sheet.

Lemma 4.1. *Let us suppose an idealized physical situation described in this section. Let the global vector magnetic potential* $\mathbf{A}^*$ *exist in* Ω^* *and let it have the properties (V1)–(V2) from Section 4.1.3. Then*

(i) The electric current $\mathbf{j}^* = (j_1^*, j_2^*, j_3^*)$ *flows in the z-direction only, i.e.* $\mathbf{j}^* \equiv (0, 0, j_3^*)$ *a.e. in* Ω^*.

(ii) If $\mathbf{V}^* : \Omega^* \to \mathbb{R}^2$, $\mathbf{V}^* = (A_1^*, A_2^*)$ *denotes the first two components of the vector potential* $\mathbf{A}^*$, *then it holds* $\mathrm{rot}_2\, \mathbf{V}^* = 0$ *a.e. in* Ω^*, *where* $\mathrm{rot}_2\, \mathbf{V}^* = \partial_1 V_2^* - \partial_2 V_1^*$.

Proof. (i) Let $i \in \{1, \ldots, N\}$ be fixed. Let us choose an arbitrary rectangle $R \subset \mathcal{V}_i^*$ such that the unit normal $\mathbf{n}_R$ to its surface (that is determined uniquely from the orientation of ∂R) is perpendicular to the z-axis. One such rectangle is shown in Fig.4.1(b). Let $\partial R \equiv l = \bigcup_{i=1}^4 l_i$ be the (oriented) boundary curve of R, where l_i are line segments and l_2, l_4 are parallel to z. From (4.14) we have

$$\int_{l_1} \mathbf{H}^* \cdot \mathrm{d}\mathbf{s} = -\int_{l_3} \mathbf{H}^* \cdot \mathrm{d}\mathbf{s}, \tag{4.16}$$

and from (4.12) we obtain

$$\int_{l_2} \mathbf{H}^* \cdot \mathrm{d}\mathbf{s} = \int_{l_4} \mathbf{H}^* \cdot \mathrm{d}\mathbf{s} = 0. \tag{4.17}$$

The equations (4.16)–(4.17) lead to

$$\oint_l \mathbf{H}^* \cdot \mathrm{d}\mathbf{s} = 0.$$

With reference to Ampère's law (2.5) we obtain the net current $I = 0$ through the rectangle R.

Now, let us suppose that there exists $x \in \mathcal{V}_i^*$ such that $\mathbf{j}_0 \stackrel{def}{=} (j_1^*(x), j_2^*(x), 0) \neq 0$. Because $\mathbf{j}^*$ is continuous on $\mathcal{V}_i^*$, there exists a (small) rectangle $\tilde{R} \subset \mathcal{V}_i^*$ such that the unit normal to its surface $\mathbf{n}_{\tilde{R}}$ is parallel to $\mathbf{j}_0$ and

$$\mathbf{j}^* \cdot \mathbf{n}_{\tilde{R}} > 0 \quad \forall x \in \tilde{R}. \tag{4.18}$$

Obviously, $\mathbf{n}_{\tilde{R}}$ is perpendicular to the z-axis. From (4.18) we obtain that the net current $I_{\tilde{R}}$ through $\tilde{R}$ is

$$I_{\tilde{R}} = \int_{\tilde{R}} \mathbf{j} \cdot \mathrm{d}\mathbf{S} = \int_{\tilde{R}} \mathbf{j} \cdot \mathbf{n}_{\tilde{R}}\, \mathrm{d}S > 0.$$

That is a contradiction with $I_{\tilde{R}} = 0$. This implies $j_1^* = j_2^* \equiv 0$ on $\mathcal{V}_i^*$. Since this holds for every $i = 1, \ldots, N$, from (4.15) we conclude that $j_1^* = j_2^* \equiv 0$ a.e. in Ω^*

(ii) Let $i \in \{1, \ldots, N\}$ be fixed. Let us denote, consistently with the above formulations, $\mathbf{V} = \mathbf{V}^*|_\Omega$, $\mathbf{V}_i^* = \mathbf{V}^*|_{\mathcal{V}_i^*}$ and $\mathbf{V}_i = \mathbf{V}_i^*|_{\mathcal{V}_i}$. The condition (V1) from Section 4.1.3 gives $\mathbf{V}_i^* \in [C^1(\mathcal{V}_i^*)]^2$. This implies

$$\mathbf{V}_i \in [C^1(\mathcal{V}_i)]^2.$$

Let $l \subset \mathcal{V}_i$ be an arbitrary closed curve that embraces a surface $S \subset \mathcal{V}_i$. The *magnetic flow* Φ_m through S can be expressed as

$$\Phi_m \stackrel{def}{=} \int_S \mathbf{B}^* \cdot \mathrm{d}\mathbf{S} = \int_S \operatorname{rot} \mathbf{A}^* \cdot \mathrm{d}\mathbf{S} = \oint_l \mathbf{A}^* \cdot \mathrm{d}\mathbf{s} = \oint_l \mathbf{V}_i^* \cdot \mathrm{d}\mathbf{s} = \oint_l \mathbf{V}_i \cdot \mathrm{d}\mathbf{s}, \qquad (4.19)$$

where we used (4.4) and Stokes' theorem.

Because (4.12) holds, $\Phi_m = 0$ and we have

$$\oint_l \mathbf{V}_i \cdot \mathrm{d}\mathbf{s} = 0,$$

for any closed curve $l \subset \mathcal{V}_i$. With regard to Green's theorem we see that $\operatorname{rot} \mathbf{V}_i = 0$ in $\mathcal{V}_i$. Because $\mathbf{V}^* = \mathbf{V}^*(x, y)$, we obtain $\operatorname{rot}_2 \mathbf{V}_i^* = 0$ in $\mathcal{V}_i^*$. Again, since this holds for every $i = 1, \dots N$, with regard to (4.15) we conclude that $\operatorname{rot}_2 \mathbf{V}^* = 0$ a.e. in Ω^*. □

Because it is the rotation of the vector potential $\mathbf{A}^*$ that has the physical meaning, we can add any irrotational vector field $\mathbf{Z}^*$ to $\mathbf{A}^*$ and preserve its physical information. Let us choose

$$\mathbf{Z}^* = -(\mathbf{V}^*, 0) = -(A_1^*, A_2^*, 0).$$

It is easy to verify, with regard to Lemma 4.1, that $\operatorname{rot} \mathbf{Z}^* = 0$ a.e. in Ω^*. We then put

$$\tilde{\mathbf{A}}^* = \mathbf{A}^* + \mathbf{Z}^* = (A_1^*, A_2^*, A_3^*) - (A_1^*, A_2^*, 0) = (0, 0, A_3^*).$$

We emphasize, that the magnetic vector potential $\tilde{\mathbf{A}}^*$ describes *the same* physical situation as $\mathbf{A}^*$. Therefore, we may always consider the vector potential $\mathbf{A}^*$ to be of the form

$$\mathbf{A}^* = (0, 0, A^*).$$

Moreover, the potential in this form automatically fulfills the Coulomb gauge (4.5), because $A^* = A^*(x, y)$.

We see that it is obviously enough to compute $A = A^*|_\Omega$, where $\Omega \subset \mathbb{R}^2$. Hence, in case of this idealized physical situation, the magnetic vector potential is given by a real function $A = A(x, y)$ of two variables x, y.

If we put $j^* \equiv j_3^*$ and $j = j^*|_\Omega$, the equations (4.2) and (4.4) then take the form

$$\operatorname{rot} \mathbf{H} = j, \qquad (4.20)$$

$$\operatorname{curl} A = \mathbf{B}. \qquad (4.21)$$

The mathematical properties of the global function A are analogous to that of the vector potential $\mathbf{A}$, cf. (V1)–(V2) in Section 4.1.3.

Let the 2D material characteristics $\mathcal{G}_i : \mathbb{R}^2 \to \mathbb{R}^2$ are given, $i = 1, \dots, N$. The equations for $A_i = A|_{\mathcal{V}_i}$ can then be derived from (4.1), (4.20), and (4.21):

$$\operatorname{rot}(\mathcal{G}^i(\operatorname{curl} A_i(x))) = j, \ x \in \mathcal{V}_i, \ i = 1, \dots, N.$$

Since $\operatorname{rot} \mathbf{A}^* = (\partial_2 A^*, -\partial_1 A^*, 0)$, we see that the property (V3) reduces in 2D case to

$$A \in H^1(\Omega).$$

The situation is more straightforward for the scalar magnetic potential. Let us suppose our idealized physical situation with no current flow through Ω^*. Let $\varphi^* = \varphi^*(x, y)$ be the global scalar magnetic potential, $\varphi = \varphi^*|_\Omega$. The equations (4.9) and (4.10) remain the same, i.e.

$$\operatorname{div} \mathbf{B} = 0, \tag{4.22}$$

$$\operatorname{grad} \varphi = \mathbf{H}, \tag{4.23}$$

where $\operatorname{div} \mathbf{u} = \partial_1 u_1 + \partial_2 u_2$ and $\operatorname{grad} v = (\partial_1 v, \partial_2 v)$.

When the 2D magnetic characteristics $\mathcal{F}_i : \mathbb{R}^2 \to \mathbb{R}^2$ are given in $\mathcal{V}_i$, $i = 1, \dots, N$, the equations for $\varphi_i = \varphi|_{\mathcal{V}_i}$ can be derived from (4.7), (4.22), and (4.23):

$$-\operatorname{div}(\mathcal{F}^i(\operatorname{grad} \varphi_i(x))) = 0, \ x \in \mathcal{V}_i\,, \ i = 1, \dots, N. \tag{4.24}$$

Again, the mathematical properties of the global scalar potential φ are analogue to that in the 3D case, cf. (S1)–(S3) in Section 4.1.3 .

4.2.2 Definition of an idealized engineering problem $\mathcal{Q}$

Let $\Omega \subset \mathbb{R}^2$ be a simply connected domain, $\Omega = \Omega^{mat} \cup \Omega^{int}$ and $\Omega^{mat} = \bigcup_{i=1}^N \mathcal{V}_i$ are defined in analogy with Section 2.1.2 and $\mathcal{F}_i, \mathcal{G}_i$ are the material characteristics of the homogeneous material that occupies $\mathcal{V}_i$, $i = 1, \dots, N$.

The (idealized) *engineering problem* $\mathcal{Q}^A$ is defined as the boundary value problem that is given in its classical form as follows. Find a function $A \in C^2(\overline{\Omega})$ such that

$$\operatorname{rot}(\mathcal{G}(\operatorname{curl} A)) = j \quad \text{in } \Omega, \tag{4.25}$$

where $\mathcal{G}$ is defined as

$$\mathcal{G}(x; \mathbf{v}) = \mathcal{G}_i(\mathbf{v}), \quad x \in \mathcal{V}_i, \mathbf{v} \in \mathbb{R}^2.$$

Moreover, A satisfies prescribed boundary conditions on $\Gamma = \partial\Omega$, see Section 4.2.3 below. The engineering problem $\mathcal{Q}^A$ will be also called the *boundary value problem* $\mathcal{Q}^A$.

The (idealized) *engineering problem* $\mathcal{Q}^\varphi$ is defined as the boundary value problem that is given in its classical form as follows. Find a function $\varphi \in C^2(\overline{\Omega})$ such that

$$-\operatorname{div}(\mathcal{F}(\operatorname{grad} \varphi)) = 0 \quad \text{in } \Omega, \tag{4.26}$$

where $\mathcal{F}$ is defined as

$$\mathcal{F}(x; \mathbf{v}) = \mathcal{F}_i(\mathbf{v}), \quad x \in \mathcal{V}_i, \mathbf{v} \in \mathbb{R}^2.$$

Moreover, φ satisfies prescribed boundary conditions on $\Gamma = \partial\Omega$, see Section 4.2.3 below. The engineering problem $\mathcal{Q}^\varphi$ will be also called the *boundary value problem* $\mathcal{Q}^\varphi$.

The engineering problem $\mathcal{Q}$ then may refer to one of the problems $\mathcal{Q}^\varphi$ or $\mathcal{Q}^A$.

4.2.3 Boundary conditions for idealized engineering problems

The nature of magnetic fields suggests the field expands to infinity. Hence, the *infinite boundary conditions* are sometimes prescribed on $\partial\Omega$. Practically, these conditions are implemented by surrounding the device of interest by one layer of *infinite* or

open-boundary finite elements [5] . However, in many cases we may suppose that the magnetic flux is confined by a device's outer boundary and thus the problem can be restricted to a bounded domain of interest Ω. We will limit ourselves to consider such a bounded domain exclusively in this work.

By far the most common boundary conditions for both the vector and scalar magnetic potentials are the *piecewise constant Dirichlet* and *homogeneous Neumann boundary conditions*. We will briefly examine the practical situations where these conditions apply.

We see from equation (4.21) and from the definition of the curl operator that grad A is perpendicular to $\mathbf{B}$. Hence we deduce that the *magnetic flux line*, i.e. an oriented curve whose tangential vector direction at any point is the direction of the magnetic flux density vector $\mathbf{B}$, is in fact a line of constant magnetic vector potential A. The constant Dirichlet boundary condition imposed on A on a continuous curve $\tilde{\Gamma} \subset \Gamma_1 \subset \partial\Omega$ then actually corresponds to the fact that $\tilde{\Gamma}$ is a magnetic flux line. This condition can be used on the outer boundary of a magnetically closed device or when considering a symmetry of the problem.

Now we deduce the physical meaning of the homogeneous Neumann condition. We emphasize that we mean a generalized Neumann condition for nonlinear problems, as is introduced in [14]. In case of equation (4.25), the condition on $\Gamma_2 \subset \partial\Omega$ is

$$\mathcal{G}(\operatorname{curl} A) \cdot \mathbf{t} = 0 \quad \text{on } \Gamma_2, \tag{4.27}$$

where $\mathbf{t} = (t_1, t_2)$ is a unit tangent vector to Γ_2. Since from (4.21) and (3.2) we get $\mathcal{G}(\operatorname{curl} A) = \mathbf{H}$, we see from (4.27) that

$$\mathbf{H} \perp \mathbf{t} \quad \text{on } \Gamma_2,$$

where $\mathbf{t} = (t_1, t_2)$ is a unit tangent vector to Γ_2, i.e. the magnetic field vectors enter the boundary at right angles on Γ_2. This boundary condition can be used at the air side of the steel-air interface, where it is known that the magnetic field enters the steel under right angles [3], or, again, as a consequence of some symmetry considerations.

There is a duality in the boundary conditions for A and φ. The constant Dirichlet condition imposed on A corresponds to the same physical situation where we would set the homogeneous Neumann condition for φ and vice versa. Indeed, when considering the piecewise constant Dirichlet boundary condition for φ on $\Gamma_1 \subset \partial\Omega$, we obtain

$$\operatorname{grad} \varphi \perp \mathbf{t} \quad \text{on } \Gamma_1,$$

and from (4.23) we have $\mathbf{H} \perp \mathbf{t}$ on Γ_1.

Similarly, the homogeneous Neumann condition for equation (4.26) on $\Gamma_2 \subset \partial\Omega$ is

$$\mathcal{F}(\operatorname{grad} \varphi) \cdot \mathbf{n} = 0 \quad \text{on } \Gamma_2, \tag{4.28}$$

where $\mathbf{n} = (n_1, n_2)$ is a unit outer normal to Γ_2. Since from (4.23) and (3.1) we get $\mathcal{F}(\operatorname{grad} \varphi) = \mathbf{B}$, we see from (4.28) that $\mathbf{B}$ is parallel to $\mathbf{t}$, from where we conclude that each continuous curve $\tilde{\Gamma} \subset \Gamma_2$ is a magnetic flux line.

4.2.4 Comparision of 2D formulations

Again, there are two possible boundary value problems to solve in the case of the idealized physical problem. Being aware of the simplification of the equation for the magnetic vector potential, we can conclude:

- Since the solution of both boundary value problems is now equally difficult, the description of the idealized situation in terms of the magnetic vector potential is superior to that in terms of the scalar potential because no limits are imposed on the physical problems, i.e. the electric currents can flow through Ω.

There are two more advantages why to solve the boundary value problem $\mathcal{Q}^A$ rather than $\mathcal{Q}^\varphi$. First, as we have seen in the previous section, a contour of the constant potential A is a magnetic flux line. This facilitates the visualisation of the solution since, in fact, it is the flow of the flux lines that an engineer is interested in.

Further, let $C, D \in \mathbb{R}^2$. The magnetic flux Φ_m through a curve whose end points are C and D, cf. also (4.19), can in the 2D case be written as

$$\Phi_m = \int_{(C)}^{(D)} \mathbf{B} \cdot \mathrm{d}\mathbf{n_t} = \int_{(C)}^{(D)} \operatorname{grad} A \cdot \mathrm{d}\mathbf{t} = A(D) - A(C), \tag{4.29}$$

where $\mathbf{n_t} = (t_2, -t_1)$ is the vector perpendicular to $\mathbf{t}$ and $\mathbf{B} = \operatorname{curl} A = (\partial_2 A, -\partial_1 A)$. This fact is helpful in analyzing the visualized solution as well as in determining the correct boundary conditions when a prescribed magnetic flux is supposed to flow through a modelled device, see also Section 6.3.1.

From these reasons, we will primarily study the engineering problem $\mathcal{Q}^A$. However, because of the analogy of the equations for both problems, the proposed theorems for $\mathcal{Q}^A$ can easily be reformulated for $\mathcal{Q}^\varphi$. Thus, only the final results and theorems without detailed steps of the proofs will be proposed for $\mathcal{Q}^\varphi$ in Chapter 5 and finally, in Chapter 6, the problem $\mathcal{Q}^\varphi$ will be omitted from our considerations.

Chapter 5

Weak formulations of 2D boundary value problems

This chapter examines the weak formulation of the boundary value problem $\mathcal{Q}$. We first introduce the definitions and theorems used in this and next chapters in Section 5.1. The weak formulation of the boundary value problem $\mathcal{Q}$ in terms of both the vector and scalar magnetic potentials is presented in Section 5.2. The existence and uniqueness theorems for the weak solutions are provided in Section 5.3. We also prove that the problem of finding the weak solution of the boundary value problem $\mathcal{Q}$ is equivalent to finding the minimum of a certain uniformly convex functional. This functional will then be used in Chapter 6 in proving the convergence theorems for the discrete solutions and in building a scheme for the FEM analysis.

5.1 Preliminary definitions and theorems

Theorem 5.1. *Let $\mathcal{G} \in [C^1(\mathbb{R}^2)]^2$. For every $x, y \in \mathbb{R}^2$ the following equality holds*

$$\mathcal{G}(y) - \mathcal{G}(x) = \int_0^1 \mathcal{G}'(x + s(y - x))(y - x)\,\mathrm{d}s.$$

Proof. Let $\mathcal{G} = (\mathcal{G}_1, \mathcal{G}_2)$. The function

$$\alpha_i(s) = \mathcal{G}_i'(x + s(y - x))(y - x)$$

is continuous on $[0, 1]$ for $i = 1, 2$. Then we have

$$\int_0^1 \mathcal{G}_i'(x + s(y - x))(y - x)\mathrm{d}s = \Big[\mathcal{G}_i(x + s(y - x))\Big]_0^1 = \mathcal{G}_i(y) - \mathcal{G}_i(x).$$

□

In the following, Λ^n denotes the set of Lebesgue measurable subsets of $\mathbb{R}^n$.

Theorem 5.2. *Let $\Omega \in \Lambda^n$ and $I \in \Lambda^k$. Let f be a measurable function on $\Omega \times I$ and let there exist a constant $K > 0$ such that*

$$\int_{\Omega \times I} |f(x, t)|\,\mathrm{d}x\mathrm{d}t \leq K.$$

Then the function $F(x)$ defined by

$$F(x) = \int_I f(x,t)\,\mathrm{d}t\,, \quad x \in \Omega,$$

is measurable on Ω, $F \in L^1(\Omega)$, *and*

$$\|F\|_{L^1(\Omega)} \leq K.$$

Proof. The statement of the lemma is an easy consequence of the Fubini theorem, whose proof can be found in [27]. □

The symbol $\mathcal{L}^n$ will denote the set of bounded domains in $\mathbb{R}^n$ with Lipschitz continuous boundary.

Definition 5.3. Let $\Omega \in \mathcal{L}^n$, $m \geq 1$ and

$$h = h(x;\xi)$$

be a function defined for almost all $x \in \Omega$ and for all $\xi \in \mathbb{R}^m$. The function h is said to be a *Carathéodory function* if

(i) for all $\xi \in \mathbb{R}^m$ the function

$$h_\xi(x) = h(x;\xi)$$

(regarded as a function of the variable x) is measurable on Ω.

(ii) for almost all $x \in \Omega$ the function

$$h_x(\xi) = h(x;\xi)$$

(regarded as a function of the variable ξ) is continuous on $\mathbb{R}^m$.

The fact that h is a Carathéodory function will be designated by $h \in \mathrm{CAR}$.

Theorem 5.4. *Let* $\Omega \in \mathcal{L}^n$, $m \geq 1$ *and* $h(x,\xi) \in \mathrm{CAR}$. *Let* $u_i(x)\,, i = 1,\ldots,m$ *are measurable functions on* Ω. *Then the compound function*

$$g(x) = h(x; u_1(x), \ldots, u_m(x))$$

is also measurable on Ω.

Proof. See [15]. □

Definition 5.5. Let $\Omega \in \mathcal{L}^n$ and $h \in \mathrm{CAR}$. The operator χ defined for m-tuples of functions u_i, $i = 1,\ldots,m$, that are measurable on Ω by the formula

$$\chi(u_1,\ldots,u_m)(x) = h(x; u_1(x),\ldots,u_m(x))\,, \quad x \in \Omega$$

is called the *Nemickiĭ operator* given by the function h.

In the following, we will deal with a special subclass of the Carathéodory functions.

Definition 5.6. Let $\Omega \in \mathcal{L}^n$, $p > 1$, $q = p/(p-1)$. Then $h \in \mathrm{CAR}(p)$ if $h \in \mathrm{CAR}$ and h fulfills the following condition; there exist $c \geq 0$ and $g \in L^q(\Omega)$ such that for almost all $x \in \Omega$ and for all $\xi \in \mathbb{R}^m$

$$|h(x;\xi)| \leq g(x) + c\sum_{i=1}^{m} |\xi_i|^{p-1}. \tag{5.1}$$

Theorem 5.7. *Let $\Omega \in \mathcal{L}^n$, $p > 1$, $q = p/(p-1)$. Let $h \in \mathrm{CAR}(p)$. Then the Nemickiĭ operator χ given by the function h is a continuous operator $\chi : [L^p(\Omega)]^m \to L^q(\Omega)$.*

Proof. See [15]. □

Let X be a Banach space. Its norm will be designated as $\|\cdot\|_X$. Particularly, for $\Omega \in \mathcal{L}^n$ the symbols $\|\cdot\|_0$ and $\|\cdot\|_1$ denote the standard norms in $L^2(\Omega)$ and $H^1(\Omega)$, respectively. The seminorm $|\cdot|_1$ on $H^1(\Omega)$ is defined by

$$|u|_1 = \left[\sum_{i=1}^{n} \int_\Omega |\partial_i u|^2 \,\mathrm{d}x \right]^{\frac{1}{2}}.$$

Theorem 5.8. *Let $\Omega \in \mathcal{L}^n$ and Γ_1 is a relatively open subset of $\partial\Omega$, $\Gamma_1 \neq \emptyset$. Let*

$$V = \{v \in H^1(\Omega) \,|\, v = 0 \text{ on } \Gamma_1\}.$$

in the sense of traces. Then the form

$$g(u, v) = \sum_{i=1}^{n} \int_\Omega \partial_i u \, \partial_i v \,\mathrm{d}x$$

is a scalar product on V, the couple (V, g) is a Hilbert space and the induced norm $|\cdot|_1$ is equivalent to $\|\cdot\|_1$.

Proof. The statement of the theorem is a consequence of the Friedrichs' inequality whose proof can be found in [42]. □

Definition 5.9. Let X be a Banach space and $F : X \to \mathbb{R}$. The functional F is said to be

- *coercive*, if

$$\lim_{\|u\|_X \to \infty} F(u) = \infty.$$

- *strictly convex*, if for all $u, v \in X$, $u \neq v$ and $t \in (0, 1)$ it holds

$$F(tu + (1-t)v) < tF(u) + (1-t)F(v).$$

Definition 5.10. Let X be a Banach space, $F : X \to \mathbb{R}$ and $u, v \in X$. If there exists a finite limit

$$\mathrm{d}F(u; v) = \lim_{t \to 0} \frac{F(u + tv) - F(u)}{t},$$

then $\mathrm{d}F(u; v)$ is called the *differential of F in $u \in X$ in the direction v*. Moreover, if for $u \in X$ the differential $\mathrm{d}F(u; v)$ exists for all $v \in X$, and if the mapping

$$\mathrm{d}F(u)(v) = \mathrm{d}F(u; v)$$

is linear and continuous, i.e. $\mathrm{d}F(u) \in X^*$, then F is said to have the *Gâteaux derivative* $F'(u) = \mathrm{d}F(u)$ in $u \in X$. If the derivative exists for all $u \in X$, then F is said to be *differentiable in the Gâteaux sense on X.*

Let $F'(u)$ exist for all $u \in X$. Let $u, v_1, v_2 \in X$. If there exists a finite limit

$$\mathrm{d}^2F(u;v_1,v_2)=\lim_{t\to 0}\frac{\mathrm{d}F(u+tv_2;v_1)-\mathrm{d}F(u;v_1)}{t},$$

then $\mathrm{d}^2F(u;v_1,v_2)$ is called the *second differential of F in $u\in X$ in the directions v_1,v_2*. Moreover, if for $u\in X$ the second differential $\mathrm{d}^2F(u;v_1,v_2)$ exists for all $v_1,v_2\in X$ and, if the mapping

$$\mathrm{d}^2F(u)\colon X\to X^*,$$
$$\big[\mathrm{d}^2F(u)(v_2)\big](v_1)=\mathrm{d}^2F(u;v_1,v_2)$$

is linear and continuous, then F is said to have the *second Gâteaux derivative* $F''(u)=\mathrm{d}^2F(u)$ in $u\in X$. If the second derivative exists for all $u\in X$, then F is said to be *twice differentiable in the Gâteaux sense on X.*

Definition 5.11. Let X be a Banach space, $F:X\to\mathbb{R}$ and $u\in X$. If there exists a functional $\mathrm{d}F(u)\in X^*$ such that

$$\lim_{\|v\|_X\to 0}\frac{|F(u+v)-F(u)-\mathrm{d}F(u)(v)|}{\|v\|_X}=0, \tag{5.2}$$

then the functional $\mathrm{d}F(u)$ is called the *Fréchet differential of F in $u\in X$*. If the differential exists for all $u\in X$, then F is said to be *differentiable in the Fréchet sense on X.*

Theorem 5.12. *Let X be a Banach space. Let the functional $F:X\to\mathbb{R}$ be twice differentiable in Gâteaux sense on X. Then for every $u,v\in X$ exists $\theta\in(0,1)$ such that*

$$F(v)=F(u)+F'(u;v-u)+\frac{1}{2}F''(u+\theta(v-u);v-u,v-u).$$

Proof. See [6]. □

Theorem 5.13. *Let X be a Banach space, $F:X\to\mathbb{R}$ be a functional that is differentiable on X in the Gâteaux sense. Moreover, if $\mathrm{d}^2F(u;v_1,v_2)$ exists for all $u,v_1,v_2\in X$ and if*

$$\mathrm{d}^2F(u;v,v)>0\,,\quad \forall u,v\in X\,,v\neq 0,$$

then F is strictly convex on X.

Proof. See [14]. □

Definition 5.14. Let X be a Banach space. Let the function F fulfill the assumptions from Theorem 5.13. Additionally, if there exists a constant $C>0$ such that it holds

$$\mathrm{d}^2F(u;v,v)\geq C\|v\|_X^2\quad\forall u,v\in X,$$

then F is said to be *uniformly convex* on X.

Definition 5.15. Let X be a Banach space and X^* its dual. Then the operator $T:X\to X^*$ is said to be

- *bounded*, if the image of every bounded subset of X is a bounded subset in X^*.

- *strictly monotone*, if for all $u, v \in X$, $u \neq v$ is

$$\langle Tu - Tv, u - v \rangle > 0.$$

- *strongly monotone*, if there exists a constant $\underline{K}$ such that

$$\langle Tu - Tv, u - v \rangle \geq \underline{K} \|u - v\|_X^2 \quad \forall u, v \in X.$$

- *coercive*, if

$$\lim_{\|u\|_X \to \infty} \frac{\langle Tu, u \rangle}{\|u\|_X} = \infty.$$

- *potential*, if there exists a functional Π differentiable in the Gâteaux sense on X such that

$$\langle \Pi'(u), v \rangle = \langle T(u), v \rangle$$

for all $u, v \in X$, i.e. $\Pi'(u) = T(u)$ on X.

Theorem 5.16. *Let X be a reflexive Banach space. Let the operator $T : X \to X^*$ be bounded, strictly monotone, coercive, and potential.*

Then the problem of finding $u \in X$ such that

$$\langle Tu, v \rangle = 0 \quad \forall v \in X$$

has a unique solution. Moreover, the solution $u \in X$ is the only one that minimizes the potential Π of the operator T, i.e.

$$u = \arg\min_{v \in X} \Pi(v),$$

and

$$\Pi(v) > \Pi(u), \quad u \neq v.$$

Proof. See [14]. □

5.2 Weak formulations for scalar and vector magnetic potentials

Let us consider an engineering problem $\mathcal{Q}$. We recall that $\Omega \subset \mathbb{R}^2$ is a simply connected domain, $\Omega = \Omega^{mat} \cup \Omega^{int}$, $\Omega^{mat} = \bigcup_{i=1}^{N} \mathcal{V}_i$, where $\mathrm{meas}_2\, \Omega^{int} = 0$. In the following we will suppose just one kind of the ferromagnetic material involved in $\mathcal{Q}$. This assumption is for the sake of making the upcoming definitions and theorem proofs more simple and clearer and the generalization to an arbitrary number of ferromagnets is easy. If $\mathcal{V}_i$, $i = 1, \ldots, m$ are the domains of the ferromagnetic material, then $\Omega_1 = \bigcup_{i=1}^{m} \mathcal{V}_i$ denotes the subset of Ω that corresponds to that ferromagnet. Similarly, $\Omega_0 = \bigcup_{i=m+1}^{N} \mathcal{V}_i$ is the subset of Ω that includes the domains of paramagnets and diamagnets. Their constitutive relations can be modelled accurately by a single linear function, cf. (2.15).

5.2.1 Weak formulation of the boundary value problem $\mathcal{Q}^A$

Let $\Omega \in \mathcal{L}^2$ be a simply connected domain, Γ_1 and Γ_2 are disjoint relatively open subsets of $\partial\Omega$ such that $\overline{\Gamma}_1 \cup \overline{\Gamma}_2 = \partial\Omega$, $\Gamma_1 \neq \emptyset$ and both Γ_1 and Γ_2 have a finite number of components. If we set $\hat{u} \equiv A$, we can rewrite the boundary value problem $\mathcal{Q}^A$ in the classical form:

Find a function $\hat{u} \in C^2(\overline{\Omega})$ such that

$$\operatorname{rot}(\mathcal{G}(\operatorname{curl}\hat{u})) = j \ \text{ in } \Omega, \tag{5.3}$$
$$\hat{u} = \overline{u} \ \text{ on } \Gamma_1, \tag{5.4}$$
$$\mathcal{G}(\operatorname{curl}\hat{u}) \cdot \mathbf{t} = 0 \ \text{ on } \Gamma_2, \tag{5.5}$$

where $\mathbf{t}$ is a unit tangent vector to Γ_2, $j, \overline{u} \in C(\overline{\Omega})$, and $\mathcal{G}$ is defined as follows:

$$\mathcal{G}(x, \mathbf{v}) = \begin{cases} \nu_0 \mathbf{v} & \text{for } x \in \Omega_0, \mathbf{v} \in \mathbb{R}^2, \\ \mathcal{G}_f(\mathbf{v}) & \text{for } x \in \Omega_1, \mathbf{v} \in \mathbb{R}^2, \end{cases} \tag{5.6}$$

where Ω_0 and Ω_1 are disjoint measurable subsets of Ω, $\overline{\Omega} = \overline{\Omega}_0 \cup \overline{\Omega}_1$, and $\mathcal{G}_f$ is a model of the material characteristics of the ferromagnet involved. Let the function $\mathcal{G}_f$ has the properties outlined by Theorem 3.4.

The weak formulation of the boundary value problem $\mathcal{Q}^A$ consists of finding a function $\hat{u} \in H^1(\Omega)$ such that

$$\hat{u} - \overline{u} \in V, \tag{5.7}$$
$$\int_\Omega \mathcal{G}(\operatorname{curl}\hat{u}) \cdot \operatorname{curl} v \, \mathrm{d}x = \int_\Omega j \, v \, \mathrm{d}x \quad \forall v \in V, \tag{5.8}$$

where

$$V = \{v \in H^1(\Omega) \,|\, v = 0 \text{ on } \Gamma_1\} \tag{5.9}$$

is the space of the test functions, $\overline{u} \in H^1(\Omega)$ and $j \in L^2(\Omega)$.

So far, we do not know whether the integral in (5.8) exists at all for $\hat{u}, v \in V$. This and other issues are addressed in Section 5.3.

5.2.2 Weak formulation of the boundary value problem $\mathcal{Q}^\varphi$

Let Ω, Γ_1, and Γ_2 are as in Section 5.2.1. If we set $\hat{\varphi} \equiv \varphi$, we can rewrite the boundary value problem $\mathcal{Q}^\varphi$ in the classical form:

Find the function $\hat{\varphi} \in C^2(\overline{\Omega})$ such that

$$-\operatorname{div}(\mathcal{F}(\operatorname{grad}\hat{\varphi})) = 0 \ \text{ in } \Omega,$$
$$\hat{\varphi} = \overline{\varphi} \ \text{ on } \Gamma_1,$$
$$\mathcal{F}(\operatorname{grad}\hat{\varphi}) \cdot \mathbf{n} = 0 \ \text{ on } \Gamma_2,$$

where $\mathbf{n}$ is the unit outer normal to Γ_2, $\overline{\varphi} \in C(\overline{\Omega})$, and $\mathcal{F}$ is defined as follows:

$$\mathcal{F}(x, \mathbf{v}) = \begin{cases} \mu_0 \mathbf{v} & \text{for } x \in \Omega_0, \mathbf{v} \in \mathbb{R}^2, \\ \mathcal{F}_f(\mathbf{v}) & \text{for } x \in \Omega_1, \mathbf{v} \in \mathbb{R}^2, \end{cases} \tag{5.10}$$

where Ω_0 and Ω_1 are as in Section 5.2.1 and $\mathcal{F}_f = \mathcal{G}_f^{-1}$.

The weak formulation of the boundary value problem $\mathcal{Q}^\varphi$ consists of finding a function $\hat{\varphi} \in H^1(\Omega)$ such that

$$\hat{\varphi} - \overline{\varphi} \in V, \tag{5.11}$$

$$\int_\Omega \mathcal{F}(\operatorname{grad}\hat{\varphi}) \cdot \operatorname{grad} v \,\mathrm{d}x = 0 \quad \forall v \in V, \tag{5.12}$$

where V is given by (5.9) and $\overline{\varphi} \in H^1(\Omega)$.

5.3 The existence and uniqueness theorems for 2D boundary value problems

We slightly revise the standard weak formulation of the boundary value problem $\mathcal{Q}^A$. We will find the function $u \in V$ such that

$$\int_\Omega \mathcal{G}(\operatorname{curl}(u + \overline{u})) \cdot \operatorname{curl} v \,\mathrm{d}x - \int_\Omega j\, v \,\mathrm{d}x = 0 \quad \forall v \in V. \tag{5.13}$$

For $v \in V$ we define the operator T as follows:

$$\langle Tv, w\rangle = \int_\Omega \mathcal{G}(\operatorname{curl}(v + \overline{u})) \cdot \operatorname{curl} w \,\mathrm{d}x - \int_\Omega j\, w \,\mathrm{d}x \quad \forall w \in V. \tag{5.14}$$

Then the solution $u \in V$ fulfills

$$\langle Tu, v\rangle = 0 \quad \forall v \in V.$$

The aim is to verify the assumptions of Theorem 5.16, where $X \equiv V$. Therefore, we need to analyze the properties of the operator T.

First, it follows from Theorem 5.8 that $\|\cdot\|_1$ and $|\cdot|_1$ are equivalent norms on V. This fact will be utilized in the following without further explanations.

Lemma 5.17. *Let*

$$h_i(x; \xi_1, \xi_2) = \mathcal{G}_i(\xi_2, -\xi_1)\,, \quad i = 1, 2,$$

where $\mathcal{G} = (\mathcal{G}_1, \mathcal{G}_2)$ is a function defined by (5.6). *Then $h_i \in \mathrm{CAR}(2)$, $i = 1, 2$.*

Proof. Let $\xi = (\xi_1, \xi_2)$ and let us perform the proof for $i = 1$.

Let $\tilde{\xi} \in \mathbb{R}^2$ be fixed. We see that $h_1(x, \tilde{\xi})$ is a constant function on Ω_0 and Ω_1. Because Ω_0 and Ω_1 are measurable subsets of Ω and $\overline{\Omega} = \overline{\Omega}_0 \cup \overline{\Omega}_1$, we conclude that $h_1(x; \tilde{\xi})$ as a function of x is measurable on Ω.

In the following, we will refer to the properties of the function $\mathcal{G}_f$ from Theorem 3.4. From (5.6) we see that $h_1(\tilde{x}, \xi)$ is continuous on $\mathbb{R}^2$ for $\tilde{x} \in \Omega_0$. Because $\mathcal{G}_f$ is continuous on $\mathbb{R}^2$, we have that $h_1(\tilde{x}, \xi)$ is continuous on $\mathbb{R}^2$ for $\tilde{x} \in \Omega_1$. Since $\Omega_0 \cup \Omega_1 = \Omega^{mat}$ and $\mathrm{meas}_2(\Omega \setminus \Omega^{mat}) = 0$ we conclude that $h_1 \in \mathrm{CAR}$.

To show that $h_1 \in \mathrm{CAR}(2)$ we need to find the constant $c \geq 0$ and the function $g \in L^2(\Omega)$ from Theorem 5.8. From (5.6) and (3.30) we obtain the analytical expression of h_1 for $|\xi| \geq B^{sat}$,

$$h_1(x, \xi) = \begin{cases} \nu_0 \xi_2\,, & x \in \Omega_0, \\ \nu_0 \xi_2 - M^{sat} e(\xi_2)\,, & x \in \Omega_1, \end{cases}$$

where $\xi = (\xi_1, \xi_2)$ and $|e(\xi_2)| \leq 1$.

Because the magnitude of magnetization satisfies $|\mathbf{M}_\xi| \leq M^{sat}$ for $|\xi| \leq B^{sat}$, cf. Section 3.1, we can choose $c = \nu_0$ and $g \equiv M^{sat}$ on Ω, and then the relation (5.1) will be fulfilled for $p = 2$, $\xi \in \mathbb{R}^2$ and $x \in \Omega^{mat}$, hence $h_1 \in \mathrm{CAR}(2)$. □

Theorem 5.18. *The operator T defined by* (5.14) *is a bounded operator $T : V \to V^*$.*

Proof. Let $u \in V$ be fixed, $|u|_1 \leq K_1$. Let $|\overline{u}|_1 = K_2$. We have

$$|\langle Tu, v\rangle| \leq \int_\Omega \Big[\Big|\mathcal{G}_2(\mathrm{curl}(u+\overline{u}))\Big|\big|\partial_1 v\big| + \Big|\mathcal{G}_1(\mathrm{curl}(u+\overline{u}))\Big|\big|\partial_2 v\big|\Big]\,\mathrm{d}x + \int_\Omega |jv|\mathrm{d}x.$$

Because $\mathrm{curl}(u+\overline{u}) \in \big[L^2(\Omega)\big]^2$, it follows from Lemma 5.17 and Theorem 5.7 that

$$h_i = \mathcal{G}_i(\mathrm{curl}(u+\overline{u})) \in L^2(\Omega), \quad i = 1, 2.$$

By using the Hölder inequality and Theorem 5.8 we obtain

$$|\langle Tu, v\rangle| \leq \Big(\sum_{i=1}^{2} \|\mathcal{G}_i(\mathrm{curl}(u+\overline{u}))\|_0\Big)|v|_1 + K_3|v|_1,$$

for a positive constant K_3. Since the Nemickiĭ operator given by the function h_i is continuous and because

$$\|\mathrm{curl}(u+\overline{u})\|_{[L^2(\Omega)]^2} = |u+\overline{u}|_1,$$

we finally obtain

$$|\langle Tu, v\rangle| \leq K_4|u+\overline{u}|_1|v|_1 + K_3|v|_1 \leq [K_4(K_1+K_2)+K_3]|v|_1 = K_5|v_1|,$$

where K_4 and K_5 are positive constants.

Since Tu is obviously linear, we observe that $Tu \in V^*$. Moreover,

$$\|Tu\|_{V^*} \leq K_5,$$

when $|u|_1 \leq K_1$. We conclude that T is a bounded operator on V.

□

Theorem 5.19. *The operator T defined by* (5.14) *is strongly monotone.*

Proof. We have

$$\langle Tu - Tv, u - v\rangle = \int_\Omega \Big[\mathcal{G}(\mathrm{curl}(u+\overline{u})) - \mathcal{G}(\mathrm{curl}(v+\overline{u}))\Big]\,\mathrm{curl}(u-v)\,\mathrm{d}x.$$

Let us define

$$I_i(u, v) = \int_{\Omega_i} \Big[\mathcal{G}(\mathrm{curl}(u+\overline{u})) - \mathcal{G}(\mathrm{curl}(v+\overline{u}))\Big]\,\mathrm{curl}(u-v)\,\mathrm{d}x\,,\ i = 0, 1.$$

From (5.6) we obtain

$$I_0(u,v) = \int_{\Omega_0} \nu_0\big[\partial_1(u+\overline{u}) - \partial_1(v+\overline{u})\big]\partial_1(u-v) + \\ + \nu_0\big[\partial_2(u+\overline{u}) - \partial_2(v+\overline{u})\big]\partial_2(u-v)\,\mathrm{d}x = \int_{\Omega_0} \nu_0[\mathrm{grad}(u-v)]^2\,\mathrm{d}x,$$

and

$$I_1(u,v) = \int_{\Omega_1} \big[-\mathcal{G}_{f,2}(U_1,U_2) + \mathcal{G}_{f,2}(V_1,V_2)\big](-U_2+V_2) + \\ + \big[\mathcal{G}_{f,1}(U_1,U_2) - \mathcal{G}_{f,1}(V_1,V_2)\big](U_1-V_1)\,\mathrm{d}x = \int_{\Omega_1} \big[\mathcal{G}_f(U) - \mathcal{G}_f(V)\big](U-V)\,\mathrm{d}x,$$

where $U = (U_1,U_2) = \mathrm{curl}(u+\overline{u})$ and $V = (V_1,V_2) = \mathrm{curl}(v+\overline{u})$.

Let K be the constant of uniform monotonicity of $\mathcal{G}_f$. Then

$$I_1(u,v) \geq \int_{\Omega_1} K|U-V|^2\,\mathrm{d}x = \\ = K\int_{\Omega_1} [\mathrm{curl}(u-v)]^2\,\mathrm{d}x = K\int_{\Omega_1} [\mathrm{grad}(u-v)]^2\,\mathrm{d}x.$$

If we set $\underline{K} = \min\{\nu_0, K\}$, we then get

$$\langle Tu - Tv, u-v\rangle \geq \underline{K}\int_{\Omega_1} [\mathrm{grad}(u-v)]^2\,\mathrm{d}x = \underline{K}|u-v|^2.$$

□

Theorem 5.20. *Let the function $\overline{u}$ have bounded derivatives, i.e. there exists a constant $K>0$ such that $\partial_i\overline{u}(x) \leq K$ a.e. in Ω, $i=1,2$. Then the operator T defined by* (5.14) *is coercive.*

Proof. Without the loss of generality, we may assume $\partial_i\overline{u}(x) \leq K$ for all $x \in \Omega$.

In the following we will use the notation

$$I_1(u) = -\mathcal{G}_2(\mathrm{curl}(u+\overline{u}))\,\partial_1 u,$$
$$I_2(u) = \mathcal{G}_1(\mathrm{curl}(u+\overline{u}))\,\partial_2 u,$$

Let us set $\tilde{K} = 2(B^{sat}+K)$ and define for $u \in V$

$$\Omega_x = \Omega_x(u) = \{x \in \Omega : |\partial_1 u(x)| \geq \tilde{K}\}, \tag{5.15}$$
$$\Omega_y = \Omega_y(u) = \{x \in \Omega : |\partial_2 u(x)| \geq \tilde{K}\}, \tag{5.16}$$
$$\Omega_2 = \Omega_2(u) = \Omega_x(u) \cup \Omega_y(u), \tag{5.17}$$
$$\Omega_3 = \Omega_3(u) = \Omega \setminus \Omega_2(u). \tag{5.18}$$

Our aim is to find the estimates of $I_1(u)$ and $I_2(u)$ on Ω. Fig.5.1 shows a sketch of how the domain Ω will be divided in order to find the estimates in different parts of Ω that are denoted by *(i)–(v)*. All cases will be treated separately.

(i) Let $x \in \Omega_1 \cap \Omega_x$. Let us examine the argument of the function $\mathcal{G}$. We have

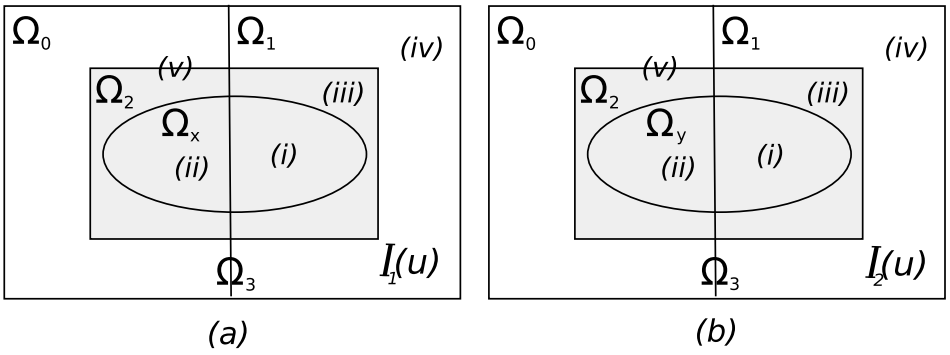

Figure 5.1: The divisions of the domain Ω for estimates (a) of $I_1(u)$ and (b) of $I_2(u)$.

$$(\mathrm{curl}(u+\overline{u}))^2 = \big(\partial_1 u(x) + \partial_1\overline{u}(x)\big)^2 + \big(\partial_2 u(x) + \partial_2\overline{u}(x)\big)^2 \geq \big(B^{sat}\big)^2,$$

because $x \in \Omega_x$. We see that the argument reached the saturation region. Hence

$$\begin{aligned} I_1(u) = -\mathcal{G}_{f,2}\big(\partial_2 u + \partial_2\overline{u}, -\partial_1 u - \partial_1\overline{u}\big)\partial_1 u = \\ = \big[\nu_0(\partial_1 u + \partial_1\overline{u}) - M^{sat}e_1(u)\big]\partial_1 u, \end{aligned}$$

where $|e_1(u)| \leq 1$. Since

$$\begin{aligned} |\nu_0\partial_1 u| - |\nu_0\partial_2\overline{u}| - |M^{sat}e_2(u)| \geq \\ \geq \nu_0\big[|\partial_1 u| - (K + \mu_0 M^{sat})\big] \geq \nu_0\big[|\partial_1 u| - (K + B^{sat})\big], \end{aligned}$$

we see that $I_1(u) \geq 0$. Then we obtain

$$\begin{aligned} I_1(u) = |I_1(u)| = \nu_0\big|\partial_1 u + \partial_1\overline{u} - \mu_0 M^{sat}e_1(u)\big||\partial_1 u| \geq \\ \geq \nu_0\Big(|\partial_1 u| - |\partial_1\overline{u}| - |\mu_0 M^{sat}e_1(u)|\Big)|\partial_1 u| \geq \\ \geq \nu_0\Big(|\partial_1 u| - (K + B^{sat})\Big)|\partial_1 u| \geq \frac{\nu_0}{2}\big|\partial_1 u\big|^2, \end{aligned}$$

where the last inequality follows from (5.15), because for $x \in \Omega_x$ it holds

$$|\partial_1 u| \geq 2(K + B^{sat}),$$

hence

$$(K + B^{sat}) \leq \frac{1}{2}|\partial_1 u|.$$

Analogously, for $x \in \Omega_1 \cap \Omega_y$ we obtain

$$I_2(u) \geq \frac{\nu_0}{2}\big|\partial_2 u\big|^2.$$

(ii) Let $x \in \Omega_0 \cap \Omega_x$. Then

$$I_1(u) = \nu_0\big(\partial_1 u + \partial_1\overline{u}\big)\partial_1 u.$$

Since $x \in \Omega_x$, we see that $I_1(u) \geq 0$. We can write

$$I_1(u) = \nu_0\big|\partial_1 u + \partial_1\overline{u}\big||\partial_1 u| \geq \frac{\nu_0}{2}\big|\partial_1 u\big|^2,$$

where the last inequality is obtained similarly as for $x \in \Omega_1 \cap \Omega_x$.

Analogously, we have for $x \in \Omega_0 \cap \Omega_y$

$$I_2(u) \geq \frac{\nu_0}{2}\big|\partial_2 u\big|^2.$$

(iii) If $x \in \Omega_1 \cap (\Omega_2 \setminus \Omega_x)$, then

$$|I_1(u)| = \big|\nu_0(\partial_1 u + \partial_1 \overline{u}) - M^{sat} e_1(u)\big||\partial_1 u| \leq \\ \leq \big[\nu_0(\tilde{K} + K) + M^{sat}\big]\tilde{K} = M_1.$$

Analogously, for $x \in \Omega_1 \cap (\Omega_2 \setminus \Omega_y)$ we obtain

$$|I_2(u)| \leq M_1.$$

(iv) For $x \in \Omega_1 \cap \Omega_3$ we have

$$\big|I_1(u)\big| = \big|-\mathcal{G}_{f,2}(\partial_2 u + \partial_2 \overline{u}, -\partial_1 u - \partial_1 \overline{u})\big||\partial_1 u| \leq M_3,$$

where

$$M_3 = \tilde{K} \cdot \sup_{\substack{|\alpha_i| \leq \tilde{K}+K, \\ i=1,2}} \big|\mathcal{G}_{f,2}(\alpha_1, \alpha_2)\big|.$$

Notice that $M_3 < \infty$ because $\mathcal{G}_{f,2}$ is continuous on $\mathbb{R}^2$.

Analogously, for x from the same set $x \in \Omega_1 \cap \Omega_3$ we obtain

$$|I_2(u)| \leq M_3.$$

(v) Finally, for $x \in \Omega_0 \cap (\Omega \setminus \Omega_x)$ we have

$$|I_1(u)| = \big|\nu_0(\partial_1 u + \partial_1 \overline{u})\big||\partial_1 u| \leq \nu_0(\tilde{K} + K)\tilde{K} = M_2,$$

and similarly for $x \in \Omega_0 \cap (\Omega \setminus \Omega_y)$

$$|I_2(u)| \leq M_2.$$

Now, we obtain from Theorem 5.8 that there exists $C > 0$ such that

$$\left| \int_\Omega ju \,\mathrm{d}x \right| \leq C|u|_1.$$

Let us examine the norm $|u|_1$. We have

$$\begin{aligned} |u|_1^2 &= \int_\Omega (\partial_1 u)^2 + (\partial_2 u)^2 \mathrm{d}x = \\ &= \int_{\Omega_x} (\partial_1 u)^2 \mathrm{d}x + \int_{\Omega \setminus \Omega_x} (\partial_1 u)^2 \mathrm{d}x + \int_{\Omega_y} (\partial_2 u)^2 \mathrm{d}x + \int_{\Omega \setminus \Omega_y} (\partial_2 u)^2 \mathrm{d}x \leq \\ &\leq \int_{\Omega_x} (\partial_1 u)^2 \mathrm{d}x + \int_{\Omega_y} (\partial_2 u)^2 \mathrm{d}x + 2\tilde{K} \operatorname{meas}_2 \Omega \overset{def}{=} R(u) + 2\tilde{K} \operatorname{meas}_2 \Omega, \end{aligned} \tag{5.19}$$

where we set

$$R(u) = \int_{\Omega_x} (\partial_1 u)^2 \mathrm{d}x + \int_{\Omega_y} (\partial_2 u)^2 \mathrm{d}x.$$

From (5.19) we see that

$$|u|_1 \to \infty \;\Leftrightarrow\; R(u) \to \infty.$$

From the above results we obtain

$$\begin{aligned}\int_\Omega \sum_{i=1}^{2} I_i(u)\,\mathrm{d}x &= \int_{\Omega_x} I_1(u)\,\mathrm{d}x + \\ &+ \int_{\Omega_y} I_2(u)\,\mathrm{d}x + \int_{\Omega\setminus\Omega_x} I_1(u)\,\mathrm{d}x + \int_{\Omega\setminus\Omega_y} I_2(u)\,\mathrm{d}x \geq \\ \geq \frac{\nu_0}{2}\Big[\int_{\Omega_x} (\partial_1 u)^2\,\mathrm{d}x + \int_{\Omega_y} (\partial_2 u)^2\,\mathrm{d}x\Big] - M\,\mathrm{meas}_2\,\Omega &= \frac{\nu_0}{2} R(u) - M\,\mathrm{meas}_2\,\Omega,\end{aligned} \tag{5.20}$$

where

$$M = \max_{i=1,2,3} M_i.$$

Since we need (5.20) to be non-negative, we will consider only such $u \in V$ that fulfill

$$R(u) \geq \frac{2}{\nu_0} M\,\mathrm{meas}_2\,\Omega.$$

From (5.19) and (5.20) we finally obtain

$$\begin{aligned}\frac{\langle Tu, u\rangle}{|u|_1} = \frac{1}{|u|_1}\Big[\int_\Omega \sum_{i=1}^{2} I_i(u)\,\mathrm{d}x + \int_\Omega ju\,\mathrm{d}x\Big] \geq \\ \geq \frac{\frac{\nu_0}{2} R(u) - M\,\mathrm{meas}_2\,\Omega}{\sqrt{R(u) + 2\tilde{K}\,\mathrm{meas}_2\,\Omega}} - C \xrightarrow{R(u)\to\infty} \infty\,.\end{aligned}$$

□

Lemma 5.21. *Let $\mathcal{G}$ be defined by* (5.6) *and $\mathbf{h} = (h_1, h_2) \in [L^2(\Omega)]^2$. Then the function*

$$F(x) = \int_{\mathbf{0}}^{\mathbf{h}(x)} \mathcal{G}(\mathbf{s})\,\mathrm{d}\mathbf{s}$$

is measurable on Ω and $F(x) \in L^1(\Omega)$.

Proof. By selecting a line segment as the integration curve, whose parametrization is

$$\gamma(x;t) = t\mathbf{h}(x)\,, \quad t \in (0,1),\, x \in \Omega,$$

we obtain

$$F(x) = \int_{\mathbf{0}}^{\mathbf{h}(x)} \mathcal{G}(\mathbf{s})\,\mathrm{d}\mathbf{s} = \int_0^1 \mathcal{G}(t\mathbf{h}(x))\mathbf{h}(x)\,\mathrm{d}t.$$

The aim is to verify the assumptions of Theorem 5.2 for the function

$$f(x,t) = \mathcal{G}(t\mathbf{h}(x))\mathbf{h}(x)\,, \quad (x,t) \in \Omega \times [0,1].$$

The function f is measurable on $\Omega \times [0,1]$, cf. Lemma 5.17 and Theorem 5.4.

We shall find the upper bound of the functions

$$g_i(x,t) = \mathcal{G}_i(t\mathbf{h}(x))\,, \quad i = 1,2.$$

that is independent of t. For $x \in \Omega_0$ we have

$$|g_i(x,t)| = |\nu_0 t h_i(x)| \le \nu_0 |h_i(x)|.$$

Let $x \in \Omega_1$. If $|t\mathbf{h}(x)| \le B^{sat}$, then the field magnitude

$$|\mathcal{G}_f(t\mathbf{h}(x))| \le H^{sat},$$

cf. Section 3.1. We obtain

$$|g_i(x,t)| = |\mathcal{G}_{f,i}(t\mathbf{h}(x))| \le H^{sat} = \nu_0 B^{sat} - M^{sat} \le \nu_0 B^{sat}.$$

If $|t\mathbf{h}(x)| \ge B^{sat}$, then we have from (3.30)

$$|g_i(x,t)| = |\nu_0 t h_i(x) - M^{sat} e_i| \le \nu_0(|h_i(x)| + \mu_0 M^{sat}) \le \nu_0(|h_i(x)| + B^{sat}).$$

From the above relations we see that

$$|g_i(x,t)| \le \nu_0(|h_i(x)| + B^{sat})\,, \quad x \in \Omega^{mat},\, t \in [0,1].$$

Finally, by using the Fubini theorem and the Hölder inequality, we obtain

$$\int_{\Omega\times[0,1]} |f(x,t)|\,\mathrm{d}x\mathrm{d}t \le \sum_{i=1}^{2} \int_{\Omega\times[0,1]} \nu_0(|h_i(x)| + B^{sat})|h_i(x)|\,\mathrm{d}x\mathrm{d}t =$$

$$= \sum_{i=1}^{2} \int_{\Omega} \nu_0(|h_i(x)| + B^{sat})|h_i(x)|\,\mathrm{d}x \le \sum_{i=1}^{2} \nu_0 \|h_i + B^{sat}\|_0 \|h_i\|_0 = K,$$

where $K > 0$ is a constant.

□

Theorem 5.22. *The operator T defined by* (5.14) *is potential. The potential Π of the operator T is differentiable in the Fréchet sense and twice differentiable in the Gâteaux sense on V. The potential is given by the formula*

$$\Pi(v) = \int_\Omega \left(\int_{\mathbf{0}}^{\mathrm{curl}(v+\overline{u})} \mathcal{G}(\mathbf{s})\,\mathrm{d}\mathbf{s} \right) \mathrm{d}x - \int_\Omega j(v+\overline{u})\,\mathrm{d}x\,, \quad v \in V.$$

Moreover, Π is coercive and uniformly convex on V.

Proof. With regard to Lemma 5.21 we see that the functional is defined correctly for $v \in V$, since $\mathrm{curl}(v+\overline{u}) \in [L^2(\Omega)]^2$.

In order to prove the potentiality of T, we need to show, cf. (5.14), that the functional $\mathrm{d}\Pi(u)$, defined for every $u \in V$ by the equation

$$\langle \mathrm{d}\Pi(u), v\rangle = \int_\Omega \mathcal{G}(\mathrm{curl}(u+\overline{u})) \cdot \mathrm{curl}\, v\,\mathrm{d}x - \int_\Omega j\, v\,\mathrm{d}x, \quad \forall v \in V, \tag{5.21}$$

is the differential of Π in $u \in V$.

Let $u \in V$ be fixed. First, $\mathrm{d}\Pi(u) \in V^*$. The linearity is obvious and continuity follows from Theorem 5.7. For $v \in V$ we have

$$\begin{aligned}\left|\Pi(u+v)-\Pi(u)-\langle \mathrm{d}\Pi(u), v\rangle\right| = \Bigg| \int_\Omega \Bigg(\int_{\mathbf{0}}^{\mathrm{curl}(u+v+\overline{u})} \mathcal{G}(\mathbf{s})\,\mathrm{d}\mathbf{s}\Bigg)\mathrm{d}x - \\ - \int_\Omega \Bigg(\int_{\mathbf{0}}^{\mathrm{curl}(u+\overline{u})} \mathcal{G}(\mathbf{s})\,\mathrm{d}\mathbf{s}\Bigg)\mathrm{d}x - \int_\Omega \mathcal{G}(\mathrm{curl}(u+\overline{u}))\cdot \mathrm{curl}\, v\,\mathrm{d}x\Bigg|.\end{aligned}$$

Because $\oint_l \mathcal{G}(\mathbf{s})\,\mathrm{d}\mathbf{s} = 0$ for every closed curve l, we obtain

$$\begin{aligned}\left|\Pi(u+v)-\Pi(u)-\langle \mathrm{d}\Pi(u), v\rangle\right| = \\ \Bigg| \int_\Omega \Bigg(\int_{\mathrm{curl}(u+\overline{u})}^{\mathrm{curl}(u+v+\overline{u})} \mathcal{G}(\mathbf{s})\,\mathrm{d}\mathbf{s}\Bigg)\mathrm{d}x - \int_\Omega \mathcal{G}(\mathrm{curl}(u+\overline{u}))\cdot \mathrm{curl}\, v\,\mathrm{d}x\Bigg|.\end{aligned}$$

The linear parametrization

$$\gamma(x;t) = \mathrm{curl}(u(x)+\overline{u}(x)) + t\,\mathrm{curl}(v(x))$$

yields

$$\int_{\mathrm{curl}(u+\overline{u})}^{\mathrm{curl}(u+v+\overline{u})} \mathcal{G}(\mathbf{s})\,\mathrm{d}\mathbf{s} = \int_0^1 \mathcal{G}(\mathrm{curl}(u+\overline{u}) + t\,\mathrm{curl}\, v)\,\mathrm{curl}\, v\,\mathrm{d}t.$$

Since $\mathcal{G}(x,\cdot) \in [C^1(\mathbb{R}^2)]^2$ a.e. in Ω, we then get, with regard to Theorem 5.1,

$$\begin{aligned}\left|\Pi(u+v)-\Pi(u)-\langle \mathrm{d}\Pi(u), v\rangle\right| = \\ \left| \int_\Omega \int_0^1 \left[\mathcal{G}(\mathrm{curl}(u+\overline{u}) + t\,\mathrm{curl}\, v) - \mathcal{G}(\mathrm{curl}(u+\overline{u}))\right]\mathrm{d}t\,\mathrm{curl}\, v\,\mathrm{d}x\right| = \\ \left| \int_\Omega \left[\int_0^1 \int_0^1 (t\,\mathrm{curl}\, v)^T \mathcal{G}'(\mathrm{curl}(u+\overline{u}) + st\,\mathrm{curl}\, v)\,\mathrm{curl}\, v\,\mathrm{d}s\mathrm{d}t\right]\mathrm{d}x\right|.\end{aligned}$$

Let us estimate the norm $|\mathcal{G}'(x,\cdot)|$. It follows from (5.6) and (3.27) that

$$|\mathcal{G}'(x,\mathbf{s})| \le \begin{cases} \nu_0, & \forall \mathbf{s} \in \mathbb{R}^2, x \in \Omega_0, \\ 1/C_1^{mat}, & \forall \mathbf{s} \in \mathbb{R}^2, x \in \Omega_1. \end{cases} \tag{5.22}$$

If we then put

$$\overline{M} = \max\{\nu_0, 1/C_1^{mat}\}, \tag{5.23}$$

we obtain

$$\begin{aligned}\left|\Pi(u+v)-\Pi(u)-\langle \mathrm{d}\Pi(u), v\rangle\right| \le \overline{M} \int_\Omega \left[\int_0^1 \int_0^1 |t| (\mathrm{curl}\, v)^2 \mathrm{d}s\mathrm{d}t\right]\mathrm{d}x \le \\ \le \overline{M} \int_\Omega (\mathrm{curl}\, v)^2\,\mathrm{d}x = \overline{M} \int_\Omega (\mathrm{grad}\, v)^2\,\mathrm{d}x = \overline{M}|v|_1^2 \le \overline{M}\|v\|_1^2.\end{aligned} \tag{5.24}$$

The division of the last equation by $\|v\|_1$ affirms, cf. relation (5.2), that $\mathrm{d}\Pi(u)$ is indeed the Fréchet differential of Π in u. Then, trivially, $\mathrm{d}\Pi(u)$ is also the Gâteaux derivative of Π in u.

The coercivity of Π follows from the coercivity of T and it is proved in [14]. Let us calculate the second Gâteaux differential of Π. Let $u, v_1, v_2 \in V$ be fixed. The formal differentiation of (5.21) yields

$$\begin{aligned} \mathrm{d}^2\Pi(u; v_1, v_2) &= \frac{\mathrm{d}}{\mathrm{d}t}\Big[\mathrm{d}\Pi(u+tv_2; v_1)\Big]\Big|_{t=0} = \\ &= \int_\Omega (\operatorname{curl} v_1)^T \mathcal{G}'(\operatorname{curl}(u+\overline{u}+tv_2)) \operatorname{curl} v_2 \,\mathrm{d}x\Big|_{t=0} = \\ &= \int_\Omega (\operatorname{curl} v_1)^T \mathcal{G}'(\operatorname{curl}(u+\overline{u})) \operatorname{curl} v_2 \,\mathrm{d}x\,. \end{aligned} \tag{5.25}$$

We still need to justify the change of the order of integration and differentiation. The assumptions of the standard theorem from the theory of Lebesgue integral need to be verified. Particularly, we must find the integrable majorant $\tilde{g}$ of the function

$$\tilde{F}(x,t) = (\operatorname{curl} v_1)^T \mathcal{G}'(\operatorname{curl}(u+\overline{u}+tv_2)) \operatorname{curl} v_2.$$

If we define

$$\tilde{g}(x) = \overline{M} |\operatorname{curl} v_1||\operatorname{curl} v_2|,$$

then, with regard to (5.22) and (5.23), we see that

$$|\tilde{F}(x,t)| \le \tilde{g}(x) \quad \forall t \in \mathbb{R}, \text{a.e. in } \Omega.$$

Moreover, it is seen easily that $\tilde{g} \in L^1(\Omega)$. The other assumptions needed to justify the interchange of the integration and differentiation can be verified easily as well.

Now we show that the operator $\mathrm{d}^2F(u)$ is linear and continuous. The linearity is obvious from (5.25). Let $\tilde{v}_2 \in V$ be fixed, $|\tilde{v}_2| \le K$. Then

$$\begin{aligned} \big[\mathrm{d}^2\Pi(u)(\tilde{v}_2)\big](v_1) &= \mathrm{d}^2\Pi(u; v_1, \tilde{v}_2) \le \\ &\le \overline{M} \int_\Omega |\operatorname{curl} v_1||\operatorname{curl} \tilde{v}_2| \,\mathrm{d}x \le \overline{M}|v_1|_1|\tilde{v}_2|_1 \le K\overline{M}|v_1|_1, \end{aligned}$$

hence

$$\big\|\mathrm{d}^2\Pi(u)(\tilde{v}_2)\big\|_{V^*} \le K\overline{M}$$

and $\mathrm{d}^2\Pi(u)$ is continuous.

For $v_1 = v_2 = v$ we obtain

$$\mathrm{d}^2\Pi(u; v, v) = \int_\Omega (\operatorname{curl} v)^T \mathcal{G}'(\operatorname{curl}(u+\overline{u})) \operatorname{curl} v \,\mathrm{d}x =: \int_\Omega \beta(x) \,\mathrm{d}x. \tag{5.26}$$

From (3.27) we have

$$\beta(x) \ge \begin{cases} \nu_0 (\operatorname{curl} v)^2, & x \in \Omega_0, \\ 1/C_2^{mat} (\operatorname{curl} v)^2. & x \in \Omega_1. \end{cases}$$

If we put $\underline{M} = \min\{\nu_0, 1/C_2^{mat}\}$, we get

$$\mathrm{d}^2\Pi(u; v, v) \ge \underline{M} \int_\Omega (\operatorname{curl} v)^2 \mathrm{d}x = \underline{M} \int_\Omega (\operatorname{grad} v)^2 \mathrm{d}x = \underline{M}|v|_1^2, \tag{5.27}$$

hence Π is uniformly convex on V. □

Theorem 5.23. *Let $\Omega \in \mathcal{L}^2$ be a simply connected domain. Let Γ_1 and Γ_2 be disjoint relatively open subsets of $\partial\Omega$ such that $\overline{\Gamma}_1 \cup \overline{\Gamma}_2 = \partial\Omega$, $\Gamma_1 \neq \emptyset$ and both Γ_1 and Γ_2 have a finite number of components. Let the function $\mathcal{G}$ be defined by (5.6), where $\mathcal{G}_f$ has the properties outlined by Theorem 3.4. Let the function $\overline{u}$ have bounded derivatives.*

Then the boundary value problem $\mathcal{Q}^A$ defined by relations (5.7)–(5.8) has a unique weak solution $\hat{u} \in H^1(\Omega)$. Moreover, the function $u \in V$, $u = \hat{u} - \overline{u}$ minimizes the functional Π, defined as

$$\Pi(v) = \int_\Omega \left(\int_{\mathbf{0}}^{\operatorname{curl}(v+\overline{u})} \mathcal{G}(\mathbf{s})\,\mathrm{d}\mathbf{s} \right) \mathrm{d}x - \int_\Omega j(v+\overline{u})\,\mathrm{d}x$$

on V. The functional Π is differentiable in the Fréchet sense, twice differentiable in the Gâteaux sense and uniformly convex on V.

Proof. The assumptions of Theorem 5.16 are fulfilled by the operator T, as it is shown in Theorems 5.18, 5.19, 5.20 and 5.22. Because T is strongly monotone, it is also strictly monotone. The reflexivity of V follows from the reflexivity of $H^1(\Omega)$ and the fact that V is a closed subspace of $H^1(\Omega)$. Hence there exists a unique solution $u \in V$ of the problem defined in (5.13) that implies the existence of the unique weak solution $\hat{u} \in H^1(\Omega)$ of the boundary vlaue problem $\mathcal{Q}^A$. The minimization property of Π and its mathematical properties are shown in Theorem 5.22. □

Remark 5.24. The assumption of bounded derivatives of the function $\overline{u}$ is not limiting at all. As we have seen in Section 4.2.3, the constant values of the potential u are usually prescribed on different parts of $\partial\Omega$ that make such a choice of $\overline{u}$ possible.

In an analogous manner, we could prove the following theorem for the scalar magnetic potential.

Theorem 5.25. *Let $\Omega \in \mathcal{L}^2$ be a simply connected domain, Γ_1 and Γ_2 are disjoint relatively open subsets of $\partial\Omega$ such that $\overline{\Gamma}_1 \cup \overline{\Gamma}_2 = \partial\Omega$, $\Gamma_1 \neq \emptyset$ and both Γ_1 and Γ_2 have a finite number of components. Let the function $\mathcal{F}$ be defined by (5.10), where $\mathcal{F}_f$ has the properties outlined by Theorem 3.4. Let the function $\overline{\varphi}$ have bounded derivatives.*

Then the boundary value problem $\mathcal{Q}^\varphi$ defined by relations (5.11)–(5.12) has a unique weak solution $\hat{\varphi} \in H^1(\Omega)$. Moreover, the function $\varphi \in V$, $\varphi = \hat{\varphi} - \overline{\varphi}$ minimizes the functional Φ, defined as

$$\Phi(v) = \int_\Omega \left(\int_{\mathbf{0}}^{\operatorname{grad}(v+\overline{\varphi})} \mathcal{F}(\mathbf{s})\,\mathrm{d}\mathbf{s} \right) \mathrm{d}x$$

on V. The functional Π is differentiable in the Fréchet sense, twice differentiable in the Gâteaux sense and uniformly convex on V.

Remark 5.26. Realizing that $\operatorname{curl}(u+\overline{u}) = \operatorname{curl}\hat{u} = \mathbf{B}$ and $\operatorname{grad}(\varphi+\overline{\varphi}) = \operatorname{grad}\hat{\varphi} = \mathbf{H}$, we can write the potentials Π and Φ in the forms that are well known in the engineering community,

$$\Pi(v) = \int_\Omega \left(\int_{\mathbf{0}}^{\mathbf{B}} \mathcal{G}(\mathbf{b})\,\mathrm{d}\mathbf{b} \right) \mathrm{d}x - \int_\Omega jv\,\mathrm{d}x = \int_\Omega w(x)\,\mathrm{d}x - \int_\Omega jv\,\mathrm{d}x,$$
$$\Phi(v) = \int_\Omega \left(\int_{\mathbf{0}}^{\mathbf{H}} \mathcal{F}(\mathbf{h})\,\mathrm{d}\mathbf{h} \right) \mathrm{d}x = \int_\Omega w'(x)\,\mathrm{d}x,$$

where $w(x)$ and $w'(x)$ are the magnetic energy and coenergy densities, cf. relations (3.12) and (3.13).

Chapter 6

The FEM modelling of the boundary value problem

6.1 Discretization of the boundary value problem

Throughout this chapter, Ω will be a polygonal domain. We will study the most common piecewise linear approximation of the weak solution of the boundary value problem $\mathcal{Q}^A$. We first formulate the discrete problem and show the existence and uniqueness of the discrete solution in Section 6.1.1. Two convergence theorems are then proved in Section 6.1.2.

6.1.1 Formulation of the discrete problem

Let us suppose an engineering problem $\mathcal{Q}^A$. Let $\mathcal{T}_h$ be a triangulation of Ω that consists of standard first order triangular finite elements. Let the triangulation is consistent with boundary conditions, i.e. the interior of each edge of a triangle $K \in \mathcal{T}_h$ is disjoint with $\overline{\Gamma}_1 \cap \overline{\Gamma}_2$. We define the function spaces

$$X_h = \left\{ v_h \in C(\overline{\Omega}) |\ v_h|_K \in P_1(K)\ \ \forall K \in \mathcal{T}(K) \right\}, \tag{6.1}$$

$$V_h = \left\{ v_h \in X_h |\ v_h = 0 \ \text{ on } \Gamma_1 \right\}, \tag{6.2}$$

where $P_1(K)$ denotes the space of linear functions on K.

The discrete formulation $\mathcal{Q}_h^A$ of the boundary value problem $\mathcal{Q}^A$ can be formulated as finding the function $\hat{u}_h \in X_h$ such that

$$\hat{u}_h - \overline{u}_h \in V_h, \tag{6.3}$$

$$\int_\Omega \mathcal{G}(\operatorname{curl} \hat{u}_h) \cdot \operatorname{curl} v_h \, \mathrm{d}x = \int_\Omega j \, v_h \, \mathrm{d}x \,, \quad \forall v_h \in V_h, \tag{6.4}$$

where $\overline{u}_h \in X_h$ is an approximation of the Dirichlet boundary data $\overline{u}$.

The same procedure as when proving the existence and uniqueness of the weak solution of the boundary value problem $\mathcal{Q}^A$ results in the existence and uniqueness theorem for the discrete problem $\mathcal{Q}_h^A$.

Theorem 6.1. *Let Ω be a polygonal domain, Γ_1 and Γ_2 be disjoint relatively open subsets of $\partial\Omega$ such that $\overline{\Gamma}_1 \cup \overline{\Gamma}_2 = \partial\Omega$, $\Gamma_1 \neq \emptyset$. Let the function $\mathcal{G}$ be defined by* (5.6),

where $\mathcal{G}_f$ has the properties outlined by Theorem 3.4. Let $\mathcal{T}_h$ be a triangulation of Ω introduced above.

Then the discrete boundary value problem $\mathcal{Q}_h^A$ defined by relations (6.3)–(6.4) has a unique solution $\hat{u}_h \in X_h$. Moreover, the function $u_h \in V$, $u_h = \hat{u}_h - \overline{u}_h$ minimizes the functional Π, defined as

$$\Pi(v_h) = \int_\Omega \left(\int_{\mathbf{0}}^{\operatorname{curl}(v_h+\overline{u}_h)} \mathcal{G}(\mathbf{s})\,\mathrm{d}\mathbf{s} \right) \mathrm{d}x - \int_\Omega j(v_h + \overline{u}_h)\,\mathrm{d}x$$

on V_h. The functional Π is differentiable in the Fréchet sense, twice differentiable in the Gâteaux sense and uniformly convex on V_h.

Proof. V_h and X_h are finite dimensional subspaces of V and $H^1(\Omega)$ respectively, hence these are reflexive Banach spaces. The function $\overline{u}_h$ has bounded derivatives since $\overline{u}_h \in X_h$. For the rest of the proof, see the proof of Theorem 5.23. □

6.1.2 Convergence of the approximate solutions

Let $\chi = \{\mathcal{T}_h\}_{h>0}$ be a regular system of triangulations of Ω, where each $\mathcal{T}_h \in \chi$ is consistent with boundary conditions. We recall that a system of triangulations is *regular*, if there exists a constant $\kappa > 0$ such that for every $\mathcal{T}_h \in \chi$ and every $K \in \mathcal{T}_h$ the inequality

$$\kappa h_K^2 \leq \operatorname{meas}_2 K,$$

holds, where $h_K = \operatorname{diam}(K)$.

In the following we will assume that the function $\overline{u} \in H^1(\Omega)$, cf. (5.4), fulfills

$$\overline{u} \in X_h \quad \forall h > 0.$$

As we have seen in Section 4.2.3, we usually prescribe a piecewise constant value of $\overline{u}$ on Γ_1, hence this assumption is reasonable. Then, obviously, we have

$$\overline{u} \equiv \overline{u}_h \quad \forall h > 0. \tag{6.5}$$

We are going to study the convergence of the discrete solution $\hat{u}_h$ to the exact solution $\hat{u}$ in the $\|\cdot\|_1$ norm when h approaches zero and prove an estimate of the error when the solution $\hat{u}$ is regular. Because (6.5) holds, we have

$$\|\hat{u}_h - \hat{u}\|_1 = \|(u_h + \overline{u}_h) - (u + \overline{u})\|_1 = \|u_h - u\|_1, \tag{6.6}$$

thus we can study the convergence of u_h to u instead. We first formulate the standard interpolation theorem. We recall that the interpolation operator π_h is defined for every function $v \in C(\overline{\Omega})$ as

$$\pi_h : C(\overline{\Omega}) \to X_h,$$
$$(\pi_h v)(B) = v(B), \quad B \text{ node of } \mathcal{T}_h.$$

Theorem 6.2. *Let $\chi = \{\mathcal{T}_h\}$ be a regular system of triangulations of a polygonal domain Ω, where each $\mathcal{T}_h \in \chi$ has the properties from Section 6.1.1. Let $v \in H^{k+1}(\Omega)$, where $k \in \mathbb{N}$. Then there exist constants $h_0, C > 0$ such that for every triangulation $\mathcal{T}_h \in \chi$ with $h \in (0, h_0)$ the inequality*

$$\|v - \pi_h v\|_1 \leq Ch^k |v|_{k+1}.$$

holds.

Proof. It follows from the Sobolev embedding theorem that $\pi_h v \in C(\overline{\Omega})$, hence the interpolation is well defined. The proof can be found in [8]. □

Lemma 6.3. *Let Ω be a polygonal domain. Let V and V_h are the function spaces defined by (5.9) and (6.2). Then for every $u \in V$ and $\delta > 0$ exists $h_\delta > 0$ such that*

$$h \in (0, h_\delta) \;\Rightarrow\; \exists w_h \in V_h : \|u - w_h\|_1 < \delta. \tag{6.7}$$

Proof. Let $u \in V$ and $\delta > 0$. Since $C^\infty(\overline{\Omega}) \cap V$ is dense in V, there exists $u^\delta \in C^\infty(\overline{\Omega}) \cap V$ such that

$$\|u^\delta - u\|_1 < \frac{\delta}{2}.$$

We obtain from Theorem 6.2 (for $k = 1$), that

$$\|u^\delta - \pi_h u^\delta\|_1 \leq Ch|u^\delta|_2.$$

If we then choose

$$h_\delta = \min\Big\{h_0, \frac{\delta}{2C|u^\delta|_2}\Big\},$$

we have

$$\|u - \pi_h u^\delta\|_1 \leq \|u - u^\delta\|_1 + \|u^\delta - \pi_h u^\delta\|_1 < \frac{\delta}{2} + \frac{\delta}{2} = \delta$$

for $h \in (0, h_\delta)$. Because each triangulation $\mathcal{T}_h \in \chi$ fulfills the consistency condition, it holds $\pi_h u^\delta \in V_h \; \forall h \in (0, h_\delta)$. Then we can take $w_h = intro\pi_h u^\delta$. □

Theorem 6.4. *Let Ω be a polygonal domain. Let Γ_1, Γ_2 and the function $\mathcal{G}$ fulfill the conditions from Theorem 6.1. Let $\chi = \{\mathcal{T}_h\}_{h>0}$ be a regular system of triangulations of Ω that satisfies the conditions from Theorem 6.2. Let $\overline{u} \in X_h$ for all $h > 0$.*

If $\hat{u}$ is the (unique) solution of the boundary value problem $\mathcal{Q}^A$ and $\hat{u}_h$ are the (unique) solutions of the discretized problems $\mathcal{Q}_h^A$, $h > 0$, then

$$\lim_{h \to 0} \|\hat{u} - \hat{u}_h\|_1 = 0.$$

Proof. We have seen in this section, cf. (6.6), that we can find the estimate for the norm $\|u - u_h\|_1$ instead. As was stated in Theorems 5.23 and 6.1, the functions u and u_h minimize the functional Π on V and V_h respectively.

Let $\varepsilon > 0$. Because Π has the Fréchet differential in u, it is continuous in u. Then there exists $\delta > 0$ such that for every $v \in V$ it holds

$$\|u - v\|_1 < \delta \;\Rightarrow\; |\Pi(u) - \Pi(v)| < \varepsilon. \tag{6.8}$$

Lemma 6.3 ensures the existence of $h_\delta > 0$ such that (6.7) holds. We get from (6.7) and (6.8) that

$$|\Pi(u) - \Pi(w_h)| < \varepsilon \quad \forall h \in (0, h_\delta)\,.$$

From here and from the fact that

$$\Pi(u) \leq \Pi(u_h) \leq \Pi(w_h),$$

we obtain

$$\lim_{h\to 0} \Pi(u_h) = \Pi(u). \tag{6.9}$$

The Euler extremal condition $\Pi'(u) = 0$ implies

$$\Pi'(u; v-u) = 0 \quad \forall v \in V. \tag{6.10}$$

Because Π is uniformly convex on V, there exists a constant $M > 0$ such that

$$M\|w\|_1^2 \leq \frac{1}{2}\Pi''(v; w, w) \quad \forall w, v \in V. \tag{6.11}$$

From (6.10), (6.11), and from Theorem 5.12 we get

$$\begin{aligned} M\|u-u_h\|_1^2 = M\|u-u_h\|_1^2 + \Pi'(u; u_h - u) \leq \\ \leq \frac{1}{2}\Pi''(u+\theta_h(u_h-u); u_h-u, u_h-u) + \Pi'(u; u_h-u) = \\ = \Pi(u_h) - \Pi(u). \end{aligned} \tag{6.12}$$

We see from (6.9) and (6.12) that $\|u-u_h\|_1^2 \to 0$ when $h \to 0$. □

Theorem 6.5. *Let the assumptions of Theorem 6.4 are fulfilled. Additionally, if the function $u \in H^2(\Omega)$, then there exist constants $h_0, K > 0$ such that*

$$\|\hat{u} - \hat{u}_h\|_1 \leq Kh \quad \forall h \in (0, h_0)\,.$$

Proof. Theorem 6.2 ensures the existence of constants $h_0, C > 0$ so that

$$\|u - \pi_h u\|_1 \leq Ch|u|_2 \quad \forall h \in (0, h_0)\,. \tag{6.13}$$

Again, because each triangulation $\mathcal{T}_h \in \chi$ fulfills the consistency condition, we have $\pi_h u \in V_h$ for all $h \in (0, h_0)$. If we put in (5.24) $v \overset{def}{=} \pi_h u - u$, then we obtain from (5.24), (6.10), (6.12), and (6.13)

$$\begin{aligned} M\|u-u_h\|_1^2 \leq \Pi(u_h) - \Pi(u) \leq \Pi(\pi_h u) - \Pi(u) = \\ = \Pi(\pi_h u) - \Pi(u) - \Pi'(u; \pi_h u - u) \leq \\ \leq \overline{M}\|u - \pi_h u\|_1^2 \leq \overline{M}C^2h^2|u|_2^2. \end{aligned}$$

Finally, the choice of

$$K = \sqrt{\frac{\overline{M}}{M}}C|u|_2$$

completes the proof.

□

6.2 Finding the discrete solution

Let $h > 0$ be fixed. We now approach the problem of finding the discrete solution $\hat{u}_h$ of the discrete problem $\mathcal{Q}_h^A$, resp. the shifted function $u_h = \hat{u}_h - \overline{u}_h$.

6.2.1 Introducing the discrete functional

Let

$$u_h(x,y) = \sum_{k=1}^{N} u_k \psi_k(x,y),$$

where $\psi_k(x,y)$, $k = 1, \ldots, N$ are the (global) basis functions of V_h.

We define the functional Π_h as

$$\Pi_h : \mathbb{R}^N \to \mathbb{R},$$
$$\Pi_h(v_1, \ldots, v_N) \equiv \Pi\Big(\sum_{k=1}^{N} v_k \psi_k(x,y)\Big)$$

for $(v_1, \ldots, v_N)^T \in \mathbb{R}^N$. The functional Π_h retains the properties from Theorem 6.1, while the vector $(u_1, \ldots, u_N)^T$ minimizes the functional on $\mathbb{R}^N$. A nonlinear iterative scheme for finding the minimum of a functional thus may be used to find the vector $(u_1, \ldots, u_N)^T$.

6.2.2 Adaptive Newton-Raphson method

Let J be a twice differentiable functional with nonsingular Hessian matrix on $\mathbb{R}^N$. Let there exist a vector $u_{ex} \in \mathbb{R}^n$ that minimizes the functional J on $\mathbb{R}^n$, i.e.

$$u_{ex} = \arg\min_{v \in \mathbb{R}^n} J(v), \ v \in \mathbb{R}^n.$$

and let the vector u_{ex} be unique. The *adaptive Newton-Raphson* iterative scheme for finding the vector u_{ex} is defined as follows. If $u^{(n)} \in \mathbb{R}^N$ is the vector obtained by the scheme at the n-th iteration step, then $u^{(n+1)}$ is obtained by

$$u^{(n+1)} = u^{(n)} - \alpha^{(n)} \big[J''(u^{(n)})\big]^{-1} J'(u^{(n)}),$$

where $\alpha^{(n)}$ is the *relaxation factor* at the n-th step of the iteration. The vector $u^{(0)}$ can be chosen arbitrarily, in our computations we used $u^{(0)} = 0$. We set

$$w^{(n)} = \big[J''(u^{(n)})\big]^{-1} J'(u^{(n)}). \tag{6.14}$$

The vector $w^{(n)}$ can be calculated by solving the linear system

$$\big[J''(u^{(n)})\big] w^{(n)} = J'(u^{(n)}).$$

The distance of a vector $v \in \mathbb{R}^N$ from u_{ex} is measured by the *residual function* $R(v)$. The Euler extremal condition implies

$$J'(u_{ex}) = 0.$$

We define the residual function as

$$R(v) = |J'(v)|^2, \quad v \in \mathbb{R}^N.$$

The iteration process is stopped when for some $n \geq 0$ and $\varepsilon > 0$ is

$$R(u^{(n)}) < \varepsilon.$$

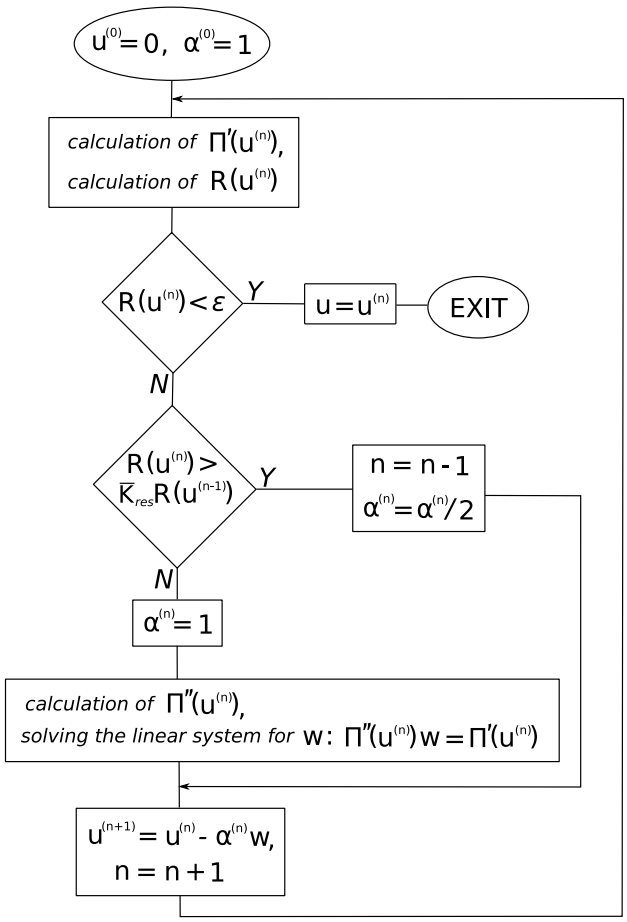

Figure 6.1: Flowchart for the nonlinear Newton-Raphson iterative scheme with adaptive determination of the relaxation factor $\alpha^{(n)}$.

The vector $u^{(n)}$ is then the final approximation of u_{ex}. In our computations, we used the value $\varepsilon = 10^{-15}$.

We now discuss how the relaxation factor $\alpha^{(n)}$ is determined. We start every iteration step with $\alpha^{(n)} = 1$. Because of the strong nonlinearity of the problem, an iteration may slip out occasionally so that the whole process gets out of control. To prevent this, every time the residual increases such that

$$R(u^{(n+1)}) > \overline{K}_{res} R(u^{(n)})$$

for a constant $\overline{K}_{res}$, the iteration step is repeated with a new relaxation factor $\alpha^{(n)} = \alpha^{(n)}/2$. Our experience shows that a reasonable value of $\overline{K}_{res}$ ranges from 2 to 10. The flowchart for the iterative scheme is illustrated in Fig. 6.1.

However, sometimes it is harmful to apply this adaptivity from the first iteration step because the iteration process may need to settle down. Hence, the adaptivity is omitted in first N_f steps and in these steps we use a fixed value of $\alpha^{(n)} = \alpha_f$. Again, our experience suggests the value of $\alpha_f = 0.1 - 0.5$.

6.2.3 Application of the iterative scheme

At the n-th step of the Newton-Raphson iterative scheme, $\Pi_h'(u^{(n)})$ and $\Pi_h''(u^{(n)})$ have to be calculated. We have the following formulas, cf. also (5.21) and (5.26):

$$\left[\Pi_h'(u^{(n)})\right]_k = \Pi'(\tilde{u}^{(n)};\psi_k) = \int_\Omega \mathcal{G}(\operatorname{curl}(\tilde{u}^{(n)}+\overline{u}_h))\operatorname{curl}\psi_k \mathrm{d}x - \int_\Omega j\psi_k \mathrm{d}x, \tag{6.15}$$

$$\left[\Pi_h''(u^{(n)})\right]_{k,l} = \Pi''(\tilde{u}^{(n)};\psi_k,\psi_l) = \int_\Omega (\operatorname{curl}\psi_k)^T \mathcal{G}'(\operatorname{curl}(\tilde{u}^{(n)}+\overline{u}_h))\operatorname{curl}\psi_l, \tag{6.16}$$

where $\tilde{u}^{(n)} = \sum_{k=1}^N u_k^{(n)}\psi_k$. The elements of the Jacobian matrix $\mathcal{G}'$ can be calculated for $x \in \Omega_1$ as

$$\partial_1 \mathcal{G}'_{f,1}(x;s,t) = \left[\mathcal{G}_{f,1}(s+\delta s,t) - \mathcal{G}_{f,1}(s,t)\right]/\delta s, \quad s,t \in \mathbb{R}^2, x \in \Omega_1 \tag{6.17}$$

with $\delta s = 10^{-10}$ etc.

Because (3.25) holds, the matrix $\mathcal{G}'$ is symmetric. We have

$$\begin{aligned}\left[\Pi_h''(u^{(n)})\right]_{l,k} &= \int_\Omega (\operatorname{curl}\psi_l)^T \mathcal{G}'(\operatorname{curl}(\tilde{u}^{(n)}+\overline{u}_h))\operatorname{curl}\psi_k \mathrm{d}x = \\ &= \int_\Omega (\operatorname{curl}\psi_k)^T \left[\mathcal{G}'(\operatorname{curl}(\tilde{u}^{(n)}+\overline{u}_h))\right]^T \operatorname{curl}\psi_l \mathrm{d}x = \left[\Pi_h''(u^{(n)})\right]_{k,l}.\end{aligned} \tag{6.18}$$

We see that the matrix $\left[\Pi_h''(u^{(n)})\right]$ is also symmetric. Because Π_h is uniformly convex on $\mathbb{R}^N$, the matrix is (uniformly) positive definite. Hence, it is nonsingular and the expression (6.14) makes sense.

The calculation of the Hessian matrix $\left[\Pi_h''(u^{(n)})\right]$ is the most time-consuming procedure in every iteration step and it is desirable to optimize its effectiveness. First, from (6.16) and (6.17) we see that it highly depends on the effectiveness of calculating the value of $\mathcal{G}(s,t)$ for given $(s,t) \in \mathbb{R}^2$. The second important factor is the actual choice of the finite element space for the computation. For instance, the piecewise linear approximation leads to just one calculation of the derivative $\mathcal{G}'$ per element, because

$$\operatorname{curl}(u^{(n)}+\overline{u}_h) = \text{const. on } K \quad \forall K \in \mathcal{T}_h,$$

thus our choice of X_h is very suitable for the computation.

As we have seen in Section 3.2.7, the function $\mathcal{G}$ for a full 2D model is not necessarily irrotational. Hence, its Jacobian matrix $\mathcal{G}'$ is not symmetric. In this case, the potential Π of the boundary value problem $\mathcal{Q}^A$ does not even exist. However, we can apply the Newton-Raphson iterative scheme even in this case regardless the nonexistence of the potential Π_h, since the right sides of the equations (6.15)–(6.16) are well defined even when $\mathcal{G}'$ is non-symmetric. Nevertheless, from (6.18) we see that the matrix for the linear system to solve in every iteration step is also non-symmetric in this case. This has a significant impact on the convergence rate of the iteration process.

6.3 Application of the nonlinear scheme in practical computations

The nonlinear iterative scheme was applied to a benchmark problem and to the computation of the magnetic field distribution in a three phase transformer core model. As a programming tool, we used the high level programming language FreeFEM++. All computations were performed twice – the solution of the first computation on the initial, non-adapted mesh served for the generation of the final, adapted mesh. For that purpose, we used FreeFEM++'s `adaptmesh(...)` primitive. The results of the computations are included in Appendix B.

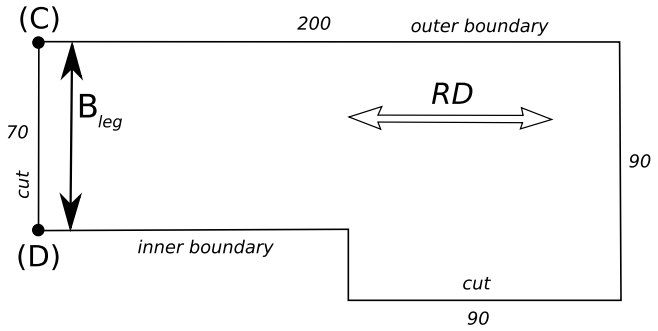

Figure 6.2: The benchmark problem for models of anisotropic steels. All dimensions are in mm.

6.3.1 A benchmark problem for anisotropic models

The following benchmark problem was proposed in [31] and serves as a demonstration problem that emphasizes the differences among various models of anisotropic steels. The problem models a one phase transformer core under load. When taking into account the symmetries of the problem, we can consider only one quarter of the core, cf. Fig. 6.2.

The input for the benchmark problem is the average flux density B_{leg} flowing through the upper yoke of the core. With regard to (4.29) we have

$$B_{leg} = \frac{\Phi_m}{|CD|} = \frac{\overline{u}(D) - \overline{u}(C)}{|CD|}.$$

Hence we obtain

$$\overline{u}(D) - \overline{u}(C) = |CD| B_{leg} = 0.07 \cdot B_{leg}.$$

If we assume no flux leakage through the boundary of the core, we may prescribe the Dirichlet boundary conditions on the inner and outer boundaries as

$$\begin{aligned} \hat{u}|_{inner} &= 0.07 \cdot B_{leg}, \\ \hat{u}|_{outer} &= 0. \end{aligned}$$

The symmetry considerations suggest us to define the homogeneous Neumann conditions on the cuts through the core.

Appendix B shows the results of the computations for the conventional and full 2D model of the AISI-M0H grain oriented silicon steel. For comparision, we included also the model of an isotropic steel defined in [24]. The suggested values of B^{leg} are 0.5 T and 1.7 T.

Fig. 6.3 shows the convergence rates of the iterative scheme at $B_{leg} = 1.7$ T for both models of the anisotropic steel. While a stable convergence was observed in case of the conventional model, when the full 2D model was used the convergence was more problematic. This was probably due to solving the linear systems with non-symmetric matrices.

6.3.2 The model of a three phase transformer core

Next to the benchmark problem, we have applied the iterative scheme to the model of a three phase, three limb transformer core under full load. The model was proposed

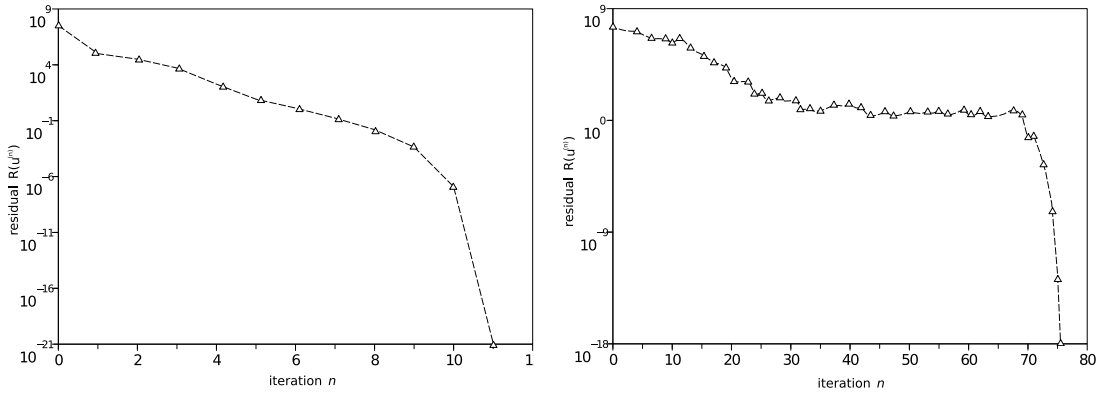

Figure 6.3: Convergence rate of the iterative scheme for the benchmark problem at $B_{leg} = 1.7\,\mathrm{T}$. Conventional (left) and full 2D model (right).

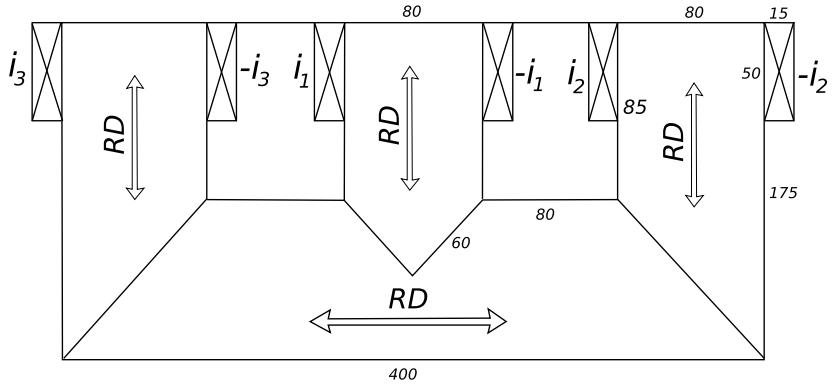

Figure 6.4: The model of a three phase, three limb transformer core. All dimensions are in mm.

in [13]. Again, the symmetry considerations allow us to limit the domain of interest to one half of the core, see. Fig. 6.4.

Phase-shifted alternating currents flow through the coils embracing the limbs with the amplitude $I_{max} = 1\,\mathrm{kA}$. The individual currents in the branches of the core are then

$$\begin{aligned} i_1(t) &= I_{max}\cos(\omega t), \\ i_2(t) &= I_{max}\cos(\omega t - 2/3\,\pi), \\ i_3(t) &= I_{max}\cos(\omega t + 2/3\,\pi). \end{aligned}$$

We applied the homogeneous Dirichlet boundary condition on the outer boundary and homogeneous Neumann condition on the horizontal cut through the core.

We performed the calculations at four different time phases, $\omega t = 0°$, $30°$, $60°$ and $90°$. Again, we used the material AISI-M0H as the reference material for both the conventional and full 2D models. The behaviour of the convergence was similar to that of the benchmark problem; while a stable convergence was achieved for the conventional model, the convergence was more problematic in case the full 2D model was used.

Chapter 7

Conclusion

We have covered in a comprehensive manner the current state of the stationary magnetic modelling including anisotropic ferromagnets. We made an advance in theoretical description of the problem, where we suggested a different mathematical representation of the material characteristics than it is usual. This representation allowed us to prove the existence and uniqueness theorems for the weak solutions of the boundary value problems under the unique assumption on the material to be anhysteretic. Further, we made some improvements to the current 2D models and we suggested an extension of the Bastos-Quichaud model for the laminated cores [2]. We also proved the convergence theorems for the discrete solutions.

Two models of the reference material AISI:M-0H were chosen for our computation, the conventional model that is widely used in practical computations and the full 2D model that is the most accurate one. Significant differencies were observed in the results of the benchmark problem mainly for the value of $B_{leg} = 1.7\,\mathrm{T}$. The model of a three phase transformer also showed some differencies in the obtained solutions, most notably at the time phase $\omega t = 90°$.

Our theory can probably be further developped to cover anhysteretic materials and it can be possibly extended to a full 3D case. These extensions of the current theory may be subjected to further research.

Appendix A

Figures of 2D model construction

These figures complement the text from Section 3.2.7.

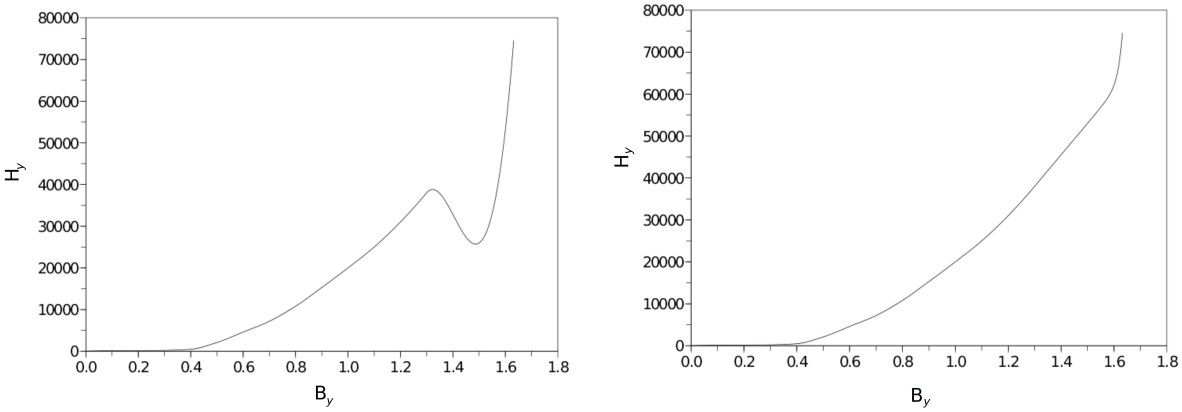

Figure A.1: The behavior of the function g_j when defined on $\mathcal{K}_j^t$ by a cubic interpolation (left) or a function from the class $e^{A\sigma+B}+C\sigma+D$ (right). For $\mathcal{G}_y$ at constant $B_x^j = 1.4\,\mathrm{T}$.

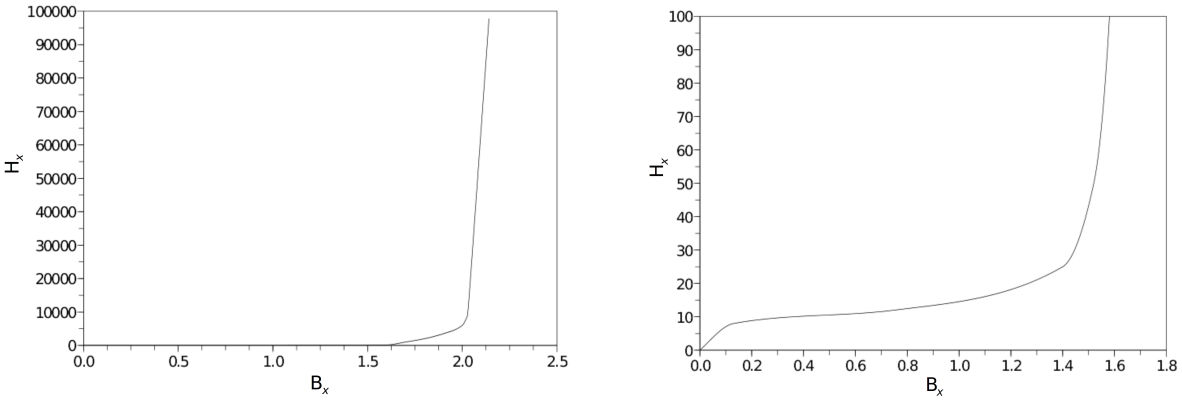

Figure A.2: The function g_j for $\mathcal{G}_x$ at constant $B_y^j = 0.2\,\mathrm{T}$. Big (left) and small (right) scale.

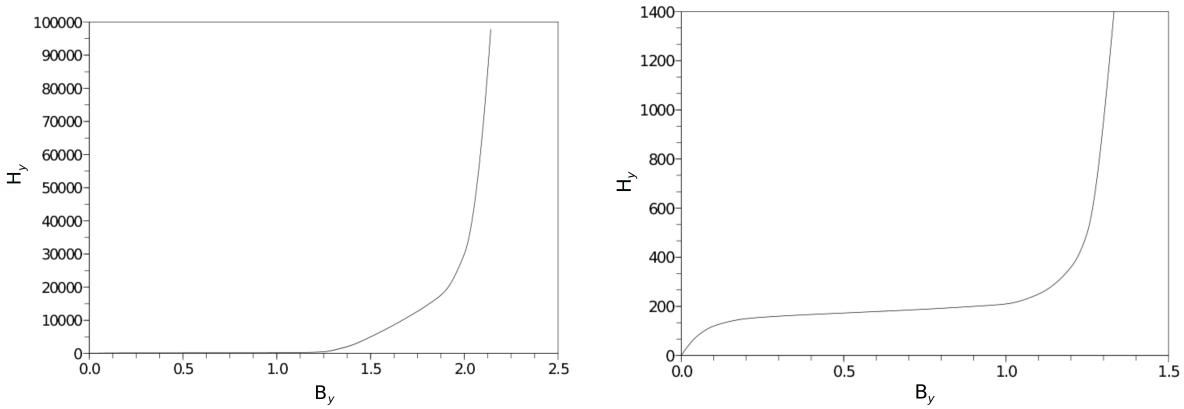

Figure A.3: The function g_j for $\mathcal{G}_y$ at constant $B_x^j = 0.2\,\mathrm{T}$. Big (left) and small (right) scale.

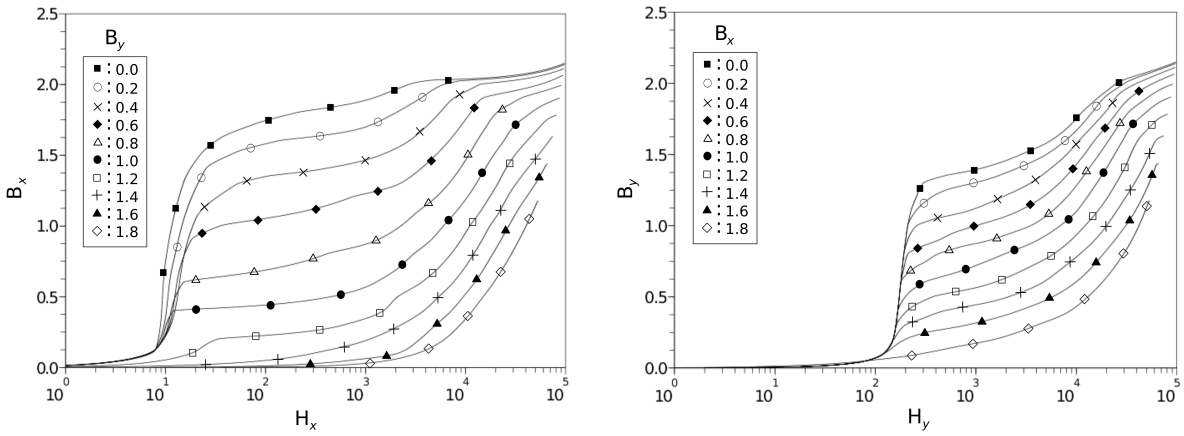

Figure A.4: All functions g_j for $\mathcal{G}_x$ (left) and $\mathcal{G}_y$ (right), logarithmic scale.

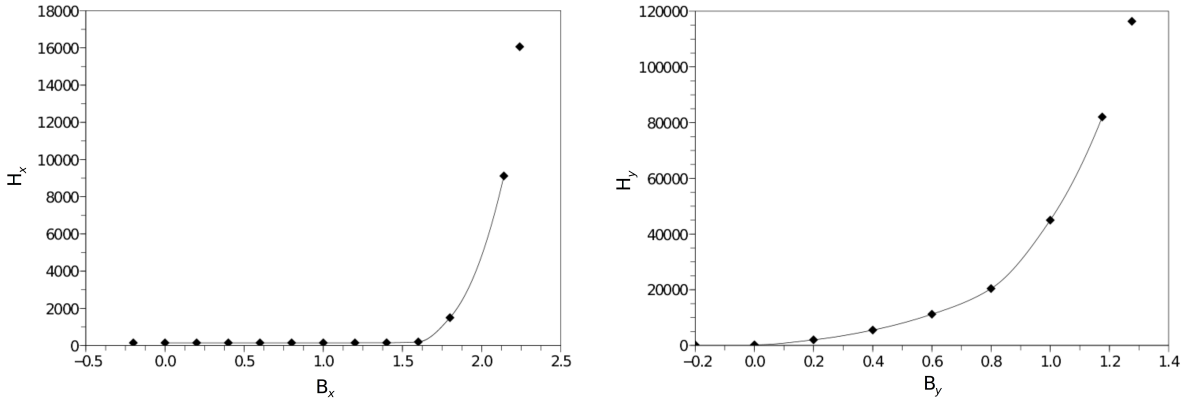

Figure A.5: The function h_k for $\mathcal{G}_x$ at constant $B_x^k = 0.2\,\mathrm{T}$ (left) and for $\mathcal{G}_y$ at constant $B_y^k = 1.8\,\mathrm{T}$ (right). The marks denote the interpolation nodes. The first and last nodes are defined from the derivatives of h_k at $\tau_1 = 0$ and $\tau_{M_k+1} = B_{y,k}^{sat}$.

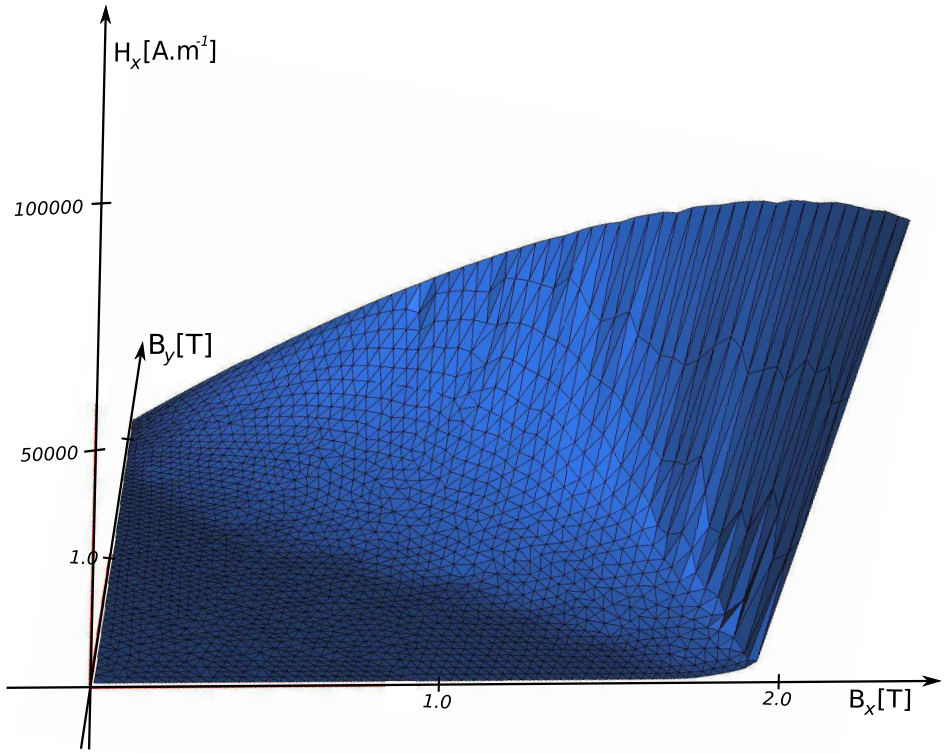

Figure A.6: The resulting full 2D model function $\mathcal{G}_x(B_x, B_y)$ for material AISI:M-0H

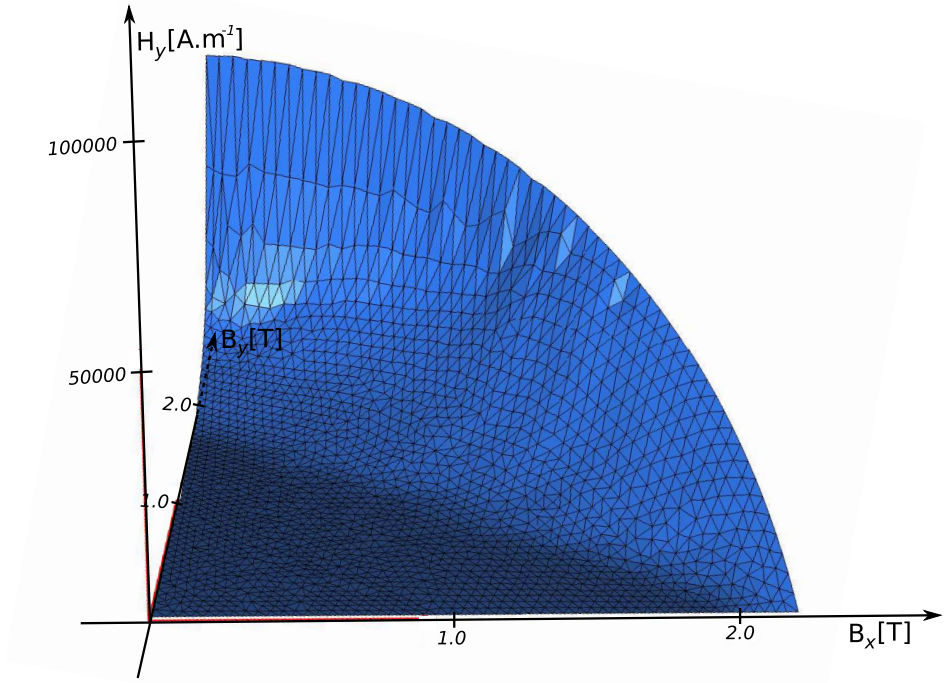

Figure A.7: The resulting full 2D model function $\mathcal{G}_y(B_x, B_y)$ for material AISI:M-0H

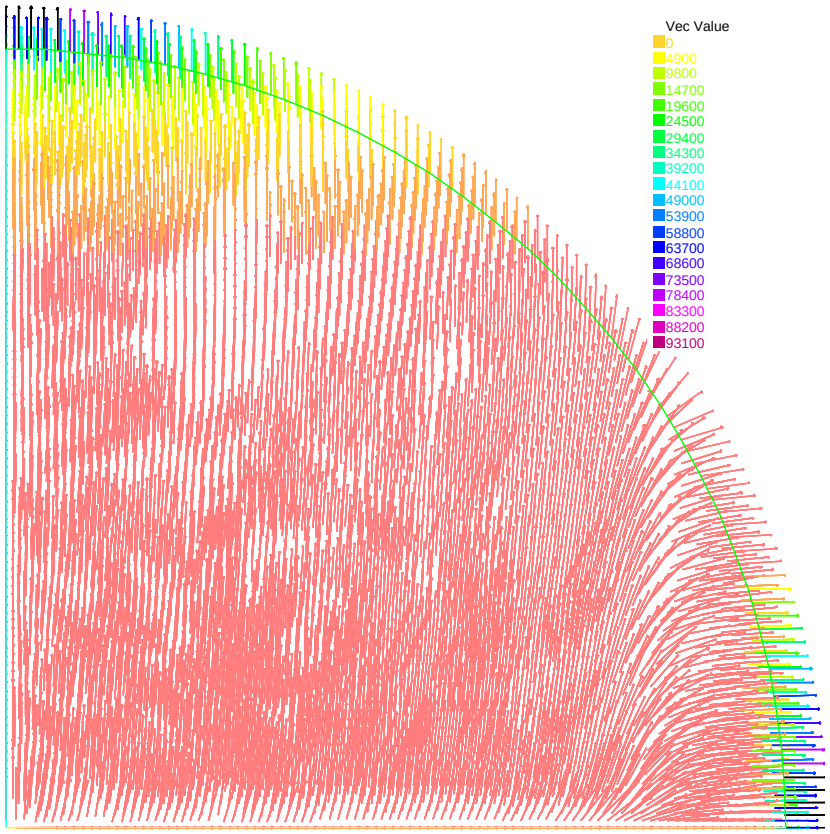

Figure A.8: Conventional model function $\mathcal{G}(B_x, B_y)$ for material AISI:M-0H

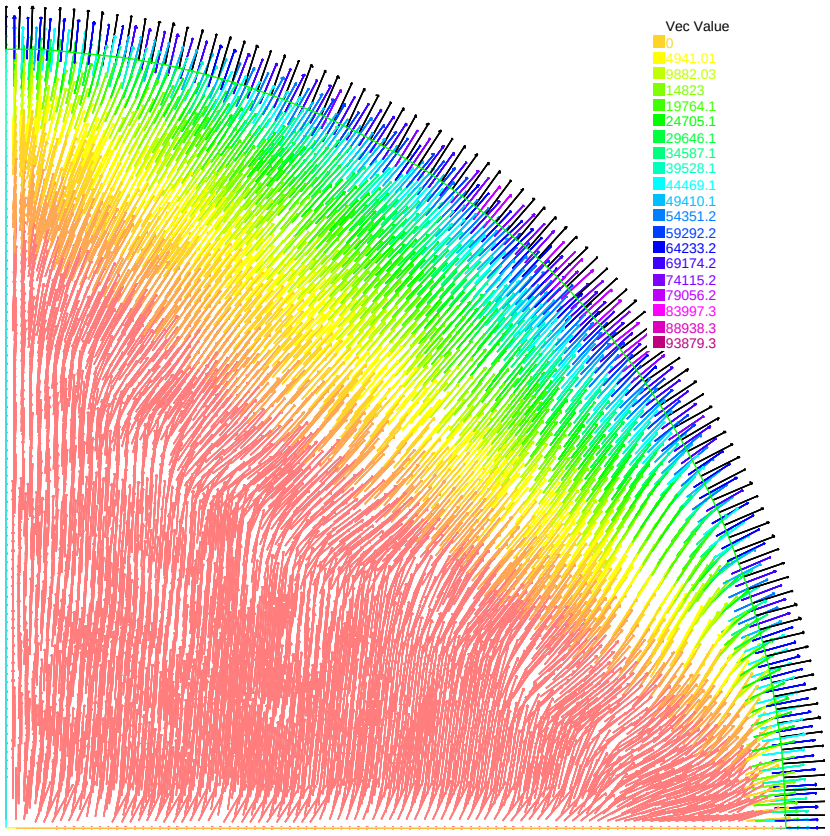

Figure A.9: Full 2D model function $\mathcal{G}(B_x, B_y)$ for the material AISI:M-0H

Appendix B

Results of the computations

The benchmark problem discovered the differences between the conventional and full 2D model, mainly at the value of $B_{leg} = 1.7\,\mathrm{T}$. The bending of flux lines in the corner of the core is unnatural and obviously erroneous when the conventional model is chosen, compare Fig. B.7 with Fig. B.8. The differences are also noticeable at $B_{leg} = 0.5\,\mathrm{T}$, compare Fig. B.4 with Fig. B.5.

Our results obtained for the model of a three phase transformer core under full load showed that, in case of the electric current amplitude of $I_{max} = 1\,\mathrm{kA}$, the average flux density through the magnetic circuit exceeds 1.9 T. The differences between the models were observed mainly at the time phase $\omega t = 90°$, where, in case of the convential model, the magnetic flux penetrates the center limb of the core much more than when the full 2D model is chosen, compare Fig. B.17 and Fig. B.18. Some minor differences are also observed for $\omega t = 30°$ and $60°$.

The results obtained by our computations are in good agreement with the ones previously published, see [13, 31].

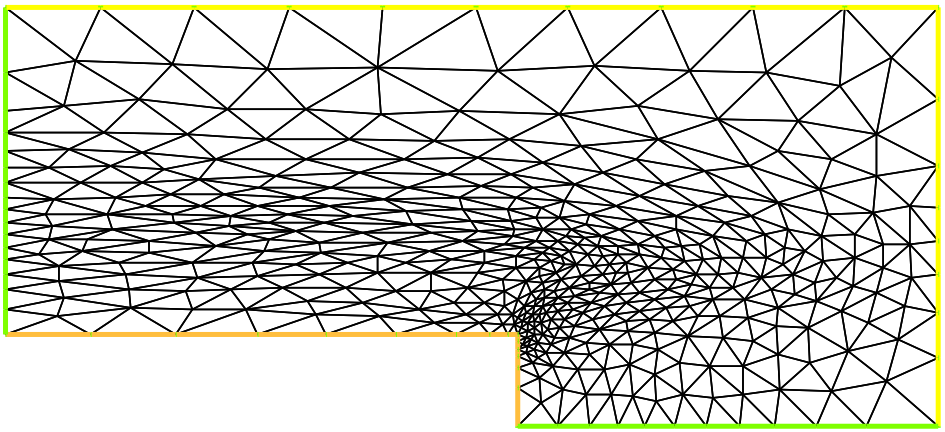

Figure B.1: Adapted mesh for the benchmark problem at $B_{leg} = 0.5\,\mathrm{T}$.

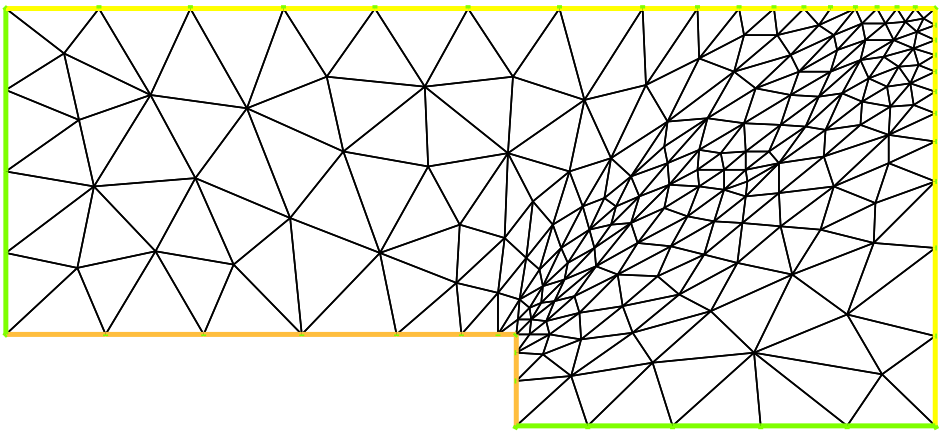

Figure B.2: Adapted mesh for the benchmark problem at $B_{leg} = 1.7\,\mathrm{T}$.

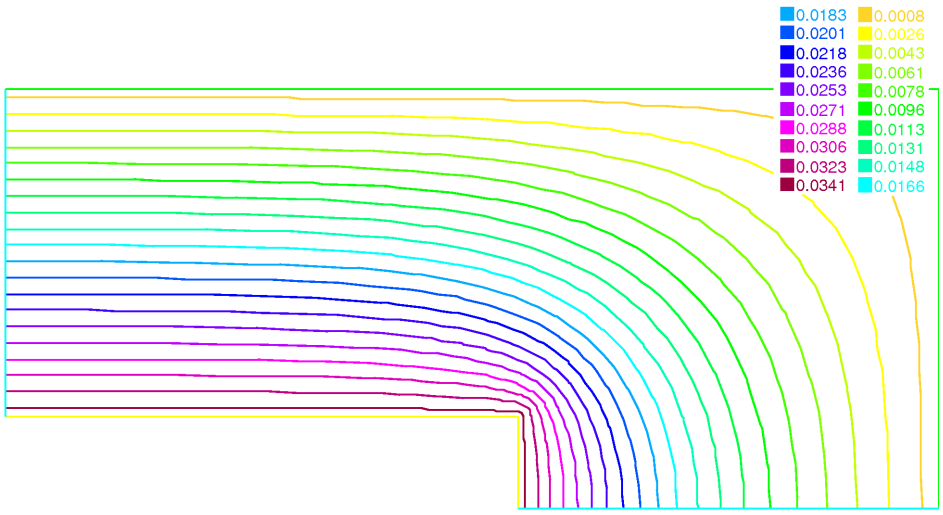

Figure B.3: Benchmark problem, isotropic material, $B_{leg} = 0.5\,\mathrm{T}$, AISI:M-0H.

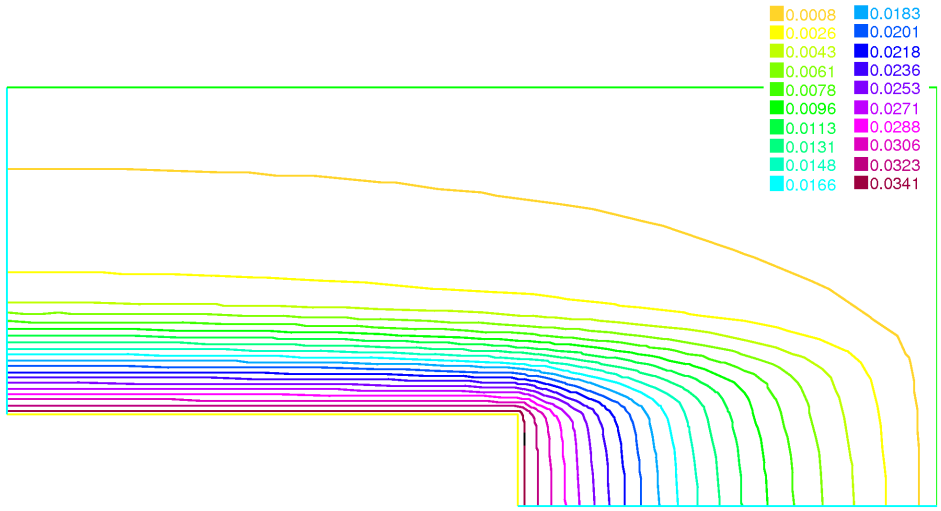

Figure B.4: Benchmark problem, conventional model, $B_{leg} = 0.5\,\mathrm{T}$, AISI:M-0H.

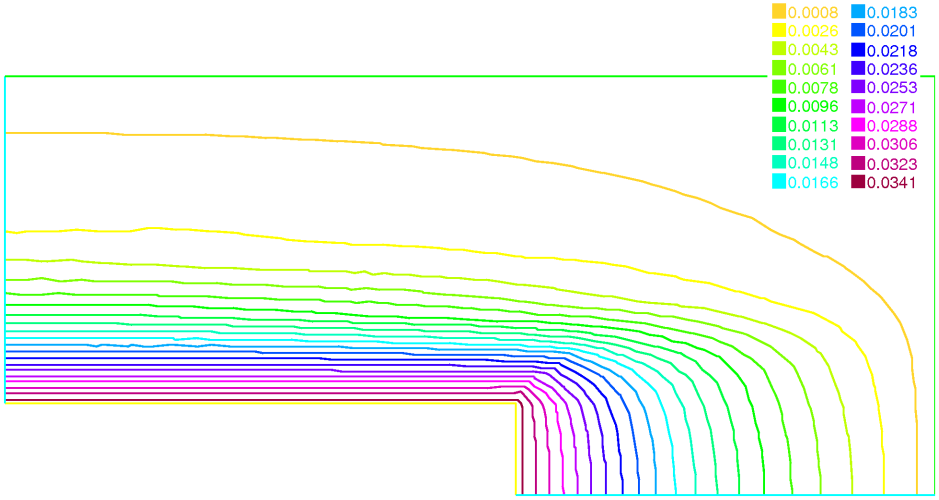

Figure B.5: Benchmark problem, full 2D model, $B_{leg} = 0.5\,\mathrm{T}$, AISI:M-0H.

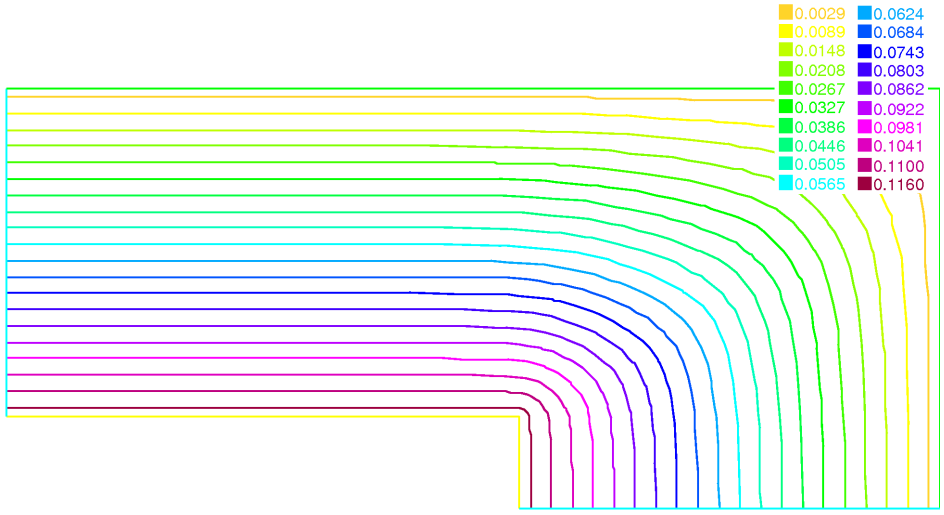

Figure B.6: Benchmark problem, isotropic material, $B_{leg} = 1.7\,\mathrm{T}$, AISI:M-0H.

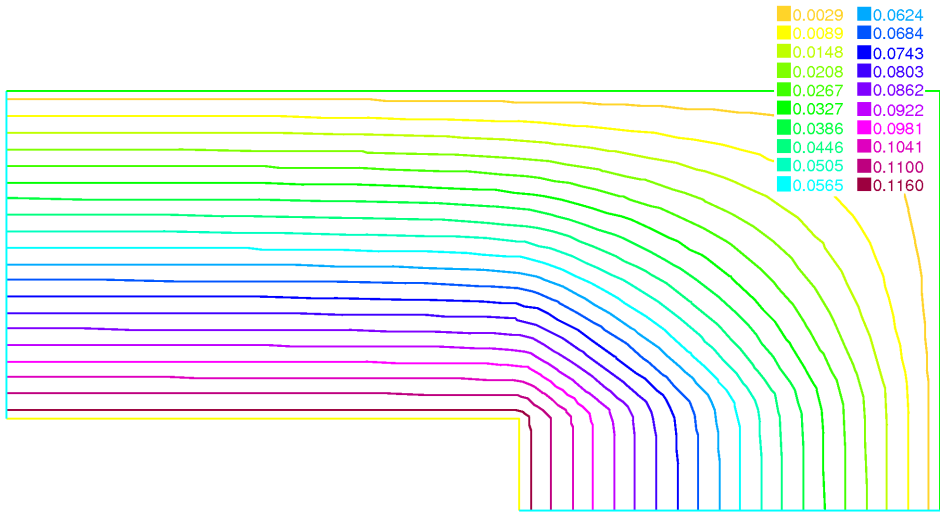

Figure B.7: Benchmark problem, conventional model, $B_{leg} = 1.7\,\mathrm{T}$, AISI:M-0H.

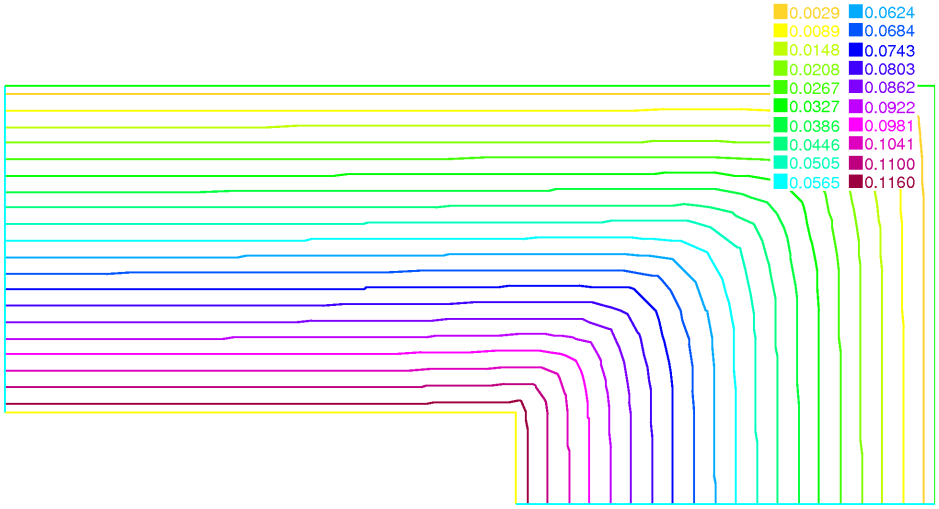

Figure B.8: Benchmark problem, full 2D model, $B_{leg} = 1.7\,\mathrm{T}$, AISI:M-0H.

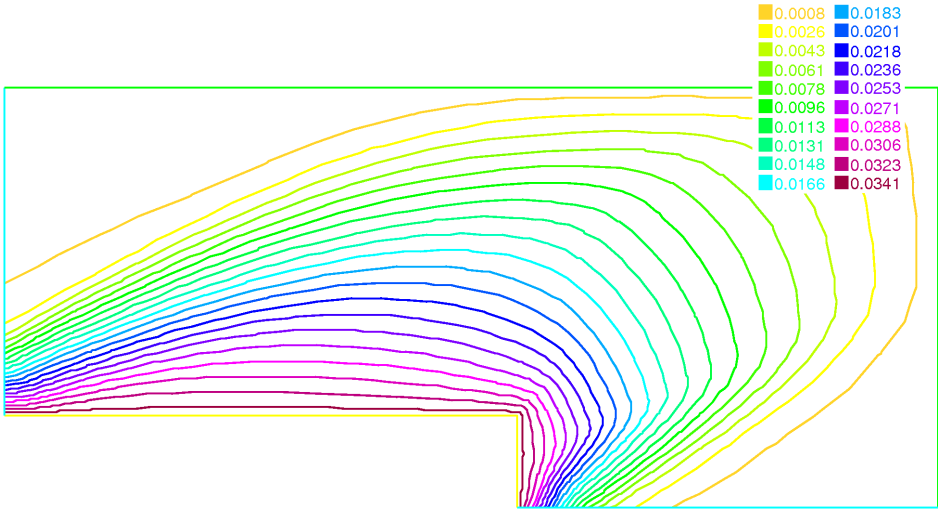

Figure B.9: Benchmark problem with deviated RD by 30° from the horizontal axis, conventional model, AISI:M-0H.

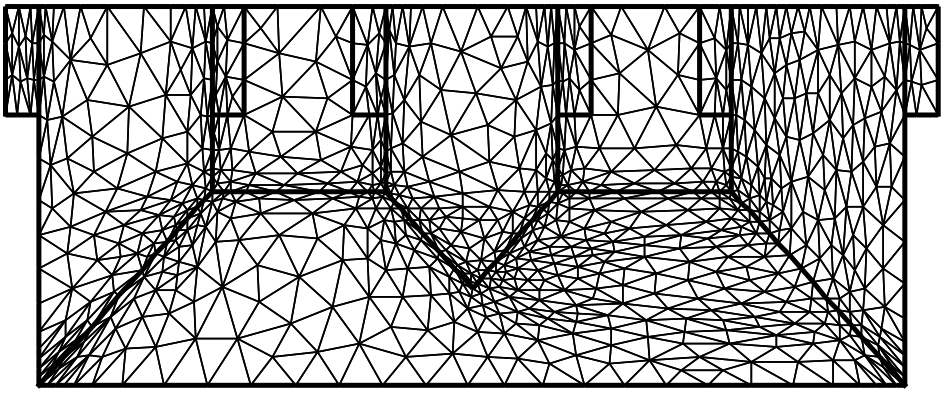

Figure B.10: Adapted mesh for the the transformer core problem at $\omega t = 30°$.

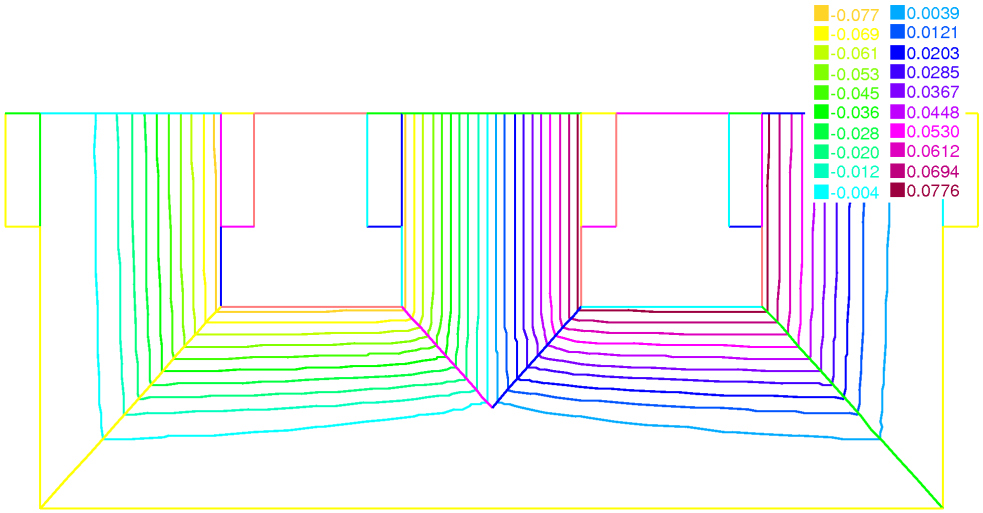

Figure B.11: Transformer core problem at $\omega t = 0°$, conventional model, AISI:M-0H.

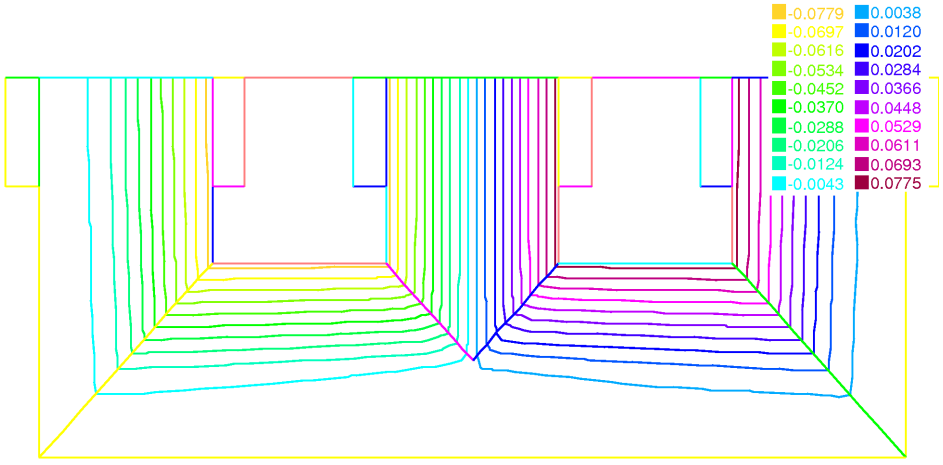

Figure B.12: Transformer core problem at $\omega t = 0°$, full 2D model, AISI:M-0H.

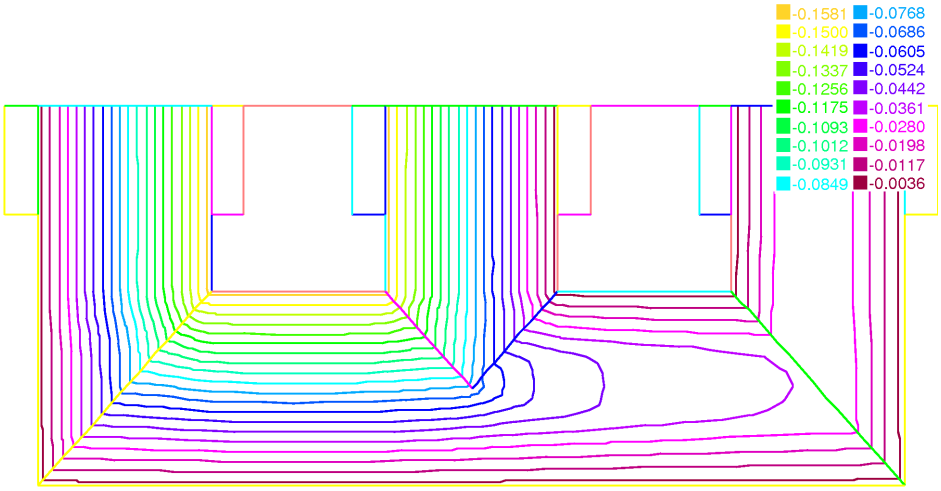

Figure B.13: Transformer core problem at $\omega t = 30°$, conventional model, AISI:M-0H.

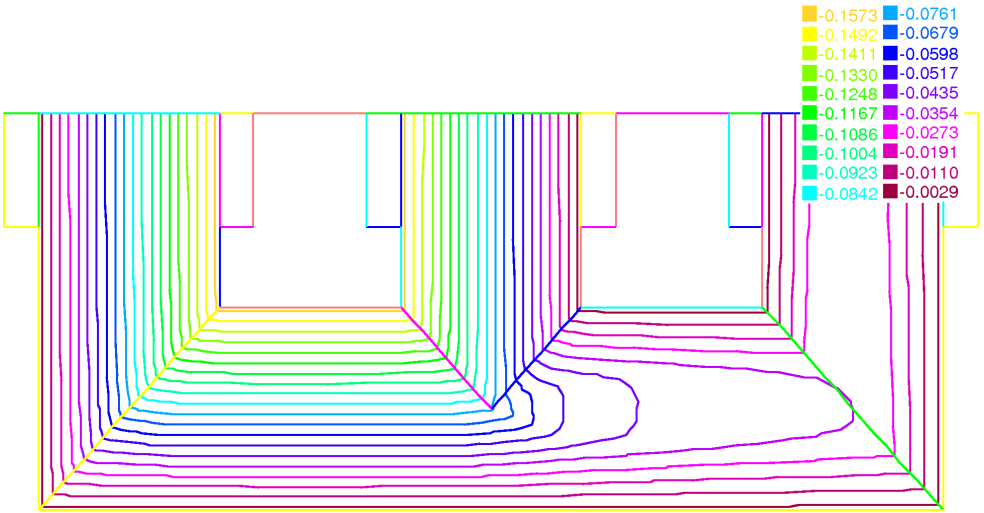

Figure B.14: Transformer core problem at $\omega t = 30°$, full 2D model, AISI:M-0H.

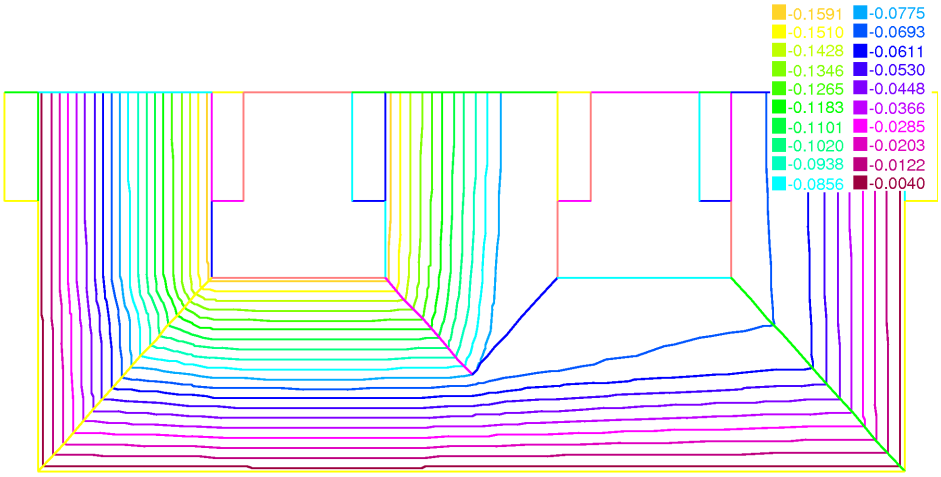

Figure B.15: Transformer core problem at $\omega t = 60°$, conventional model, AISI:M-0H.

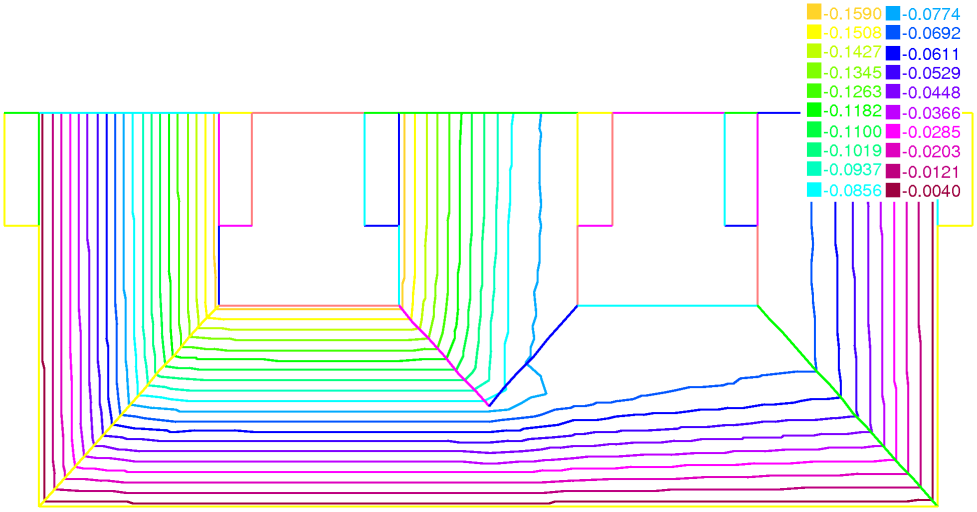

Figure B.16: Transformer core problem at $\omega t = 60°$, full 2D model, AISI:M-0H.

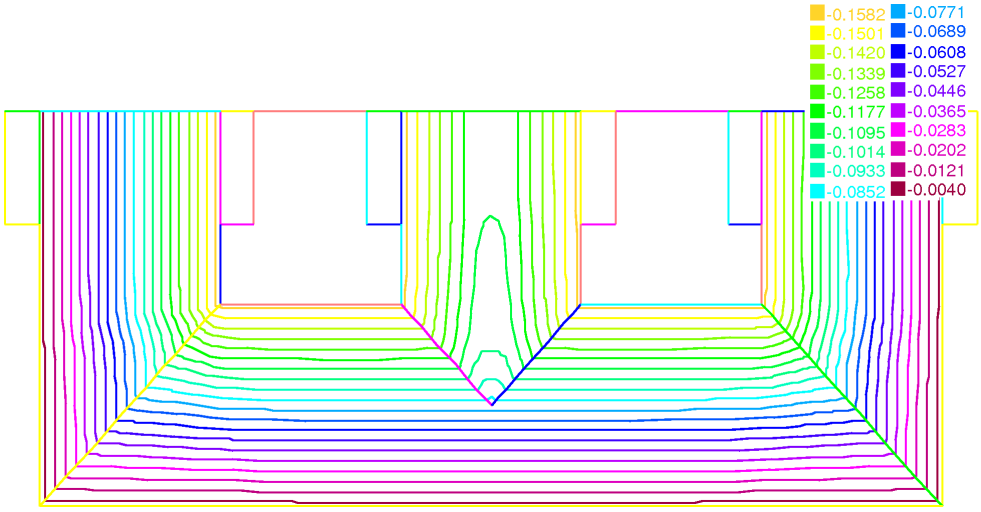

Figure B.17: Transformer core problem at $\omega t = 90°$, convential model, AISI:M-0H.

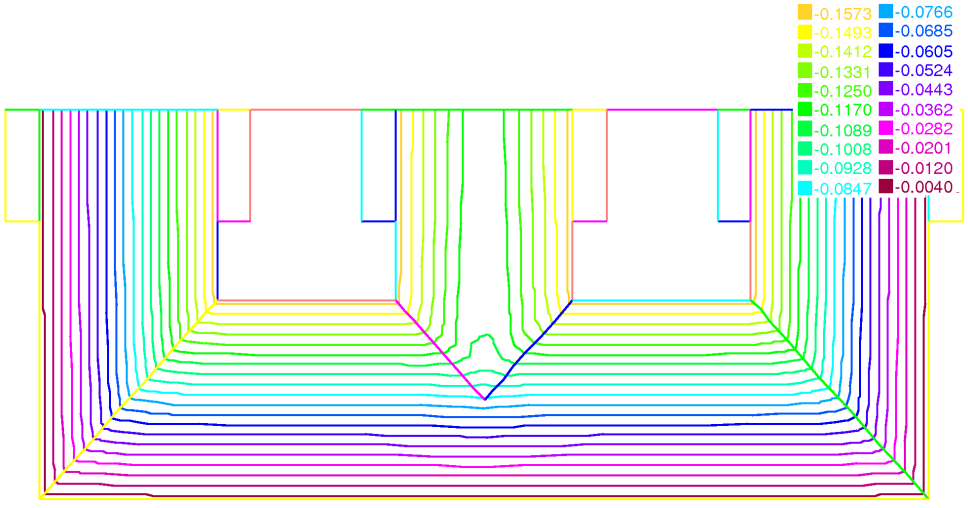

Figure B.18: Transformer core problem at $\omega t = 90°$, full 2D model, AISI:M-0H.

Bibliography

[1] Arfken, G. B.; Weber, H. J.: Mathematical Methods for Physicists, 6th edition, Elsevier, San Diego, 2005.

[2] Bastos, J. P. A.; Quichaud G.: 3D Modelling of a Non-linear Anisotropic Lamination, IEEE Transactions on Magnetics 21 (1985) 2366–2369.

[3] Bastos, J. P. A.; Sadowski, N.: Electromagnetic Modeling by Finite Element Methods, Marcel Dekker, New York, 2003.

[4] Brauer, J. R.: Simple Equations for the Magnetization and Reluctivity Curves of Steel, IEEE Transactions on Magnetics 11 (1975) 81–81.

[5] Brauer, J. R.: What Every Engineer Should Know about Finite Element Analysis, Marcel Dekker, New York, 1993.

[6] Céa, J.: Optimisation, théorie et algorithmes, Dunod, Paris, 1971.

[7] Chiampi, M.; Negro A. L.; Tartaglia M.: A Finite Element Method to Compute Three-Dimensional Magnetic Field Distribution in Transformer Cores, IEEE Transactions on Magnetics 16 (1980) 1413–1419.

[8] Ciarlet, P. G.; Lions, J. L.: Handbook of Numerical Analysis, Vol. II Finite Element Methods, North-Holland, Amsterdam, 1991.

[9] Costabel, M.; Dauge, M.: Singularities of Electromagnetic Fields in Polyhedral Domains, Archive for Rational Mechanics and Analysis 151 (2000) 221–276.

[10] Dautray, R.; Lions J.-L.: Mathematical analysis and numerical methods for science and technology, Springer, Berlin, 1990.

[11] Egorov, Y. V.; Shubin, M. A.: Foundations of the Classical Theory of Partial Differential Equations, Springer, Berlin, 1998.

[12] Enokizono, M.; Soda, N.: Finite Element Analysis of Transformer Model Core with Measured Reluctivity Tensor, IEEE Transactions on Magnetics 33 (1997) 4110–4112.

[13] Enokizono, M.; Yuki, K.; Kawano, S.: An Improved Magnetic Field Analysis in Oriented Steel Sheet by Finite Element Method considering Tensor Reluctivity, IEEE Transactions on Magnetics 31 (1995) 1797–1800.

[14] Fučík, S.; Kufner, A.: Nelineární Diferenciální Rovnice, SNTL, Praha, 1978.

[15] Fučík, S.; Nečas, J.; Souček, V.: Úvod do variačního počtu, SPN, Praha, 1972.

[16] Goldman, A.: Handbook of Modern Ferromagnetic Materials, Springer, Berlin, 1999.

[17] Haas, H.; Schmoellebeck, F.: Approximation of Nonlinear Anisotropic Magnetization Characteristics, IEEE Transactions on Magnetics 28 (1992) 1255–1258.

[18] Heathcote, M.: J&P Tarnsformer Book: A Practical Technology of the Power Transformer, Newnes, Oxford, 1998.

[19] Heise, B.: Analysis of a Fully Discrete Finite Element Method for a Nonlinear Magnetic Field Problem, SIAM J. Numer. Anal. 31 (1994) 745–759.

[20] Hoole, S. R. H.: Finite Elements, Electromagnetics and Design, Elsevier, San Diego, 1995.

[21] Jǎnicke, L.; Kost, A.; Merte R.; Nakata, T.; Takahashi, N.; Fujiwara, N.; Muramatsu, K.: Numerical Modeling for Anisotropic Magnetic Media Including Saturation Effects, IEEE Transactions on Magnetics 33 (1995) 1788–1791.

[22] Jiles, D.: Introduction to Magnetism and Magnetic Materials, CRC Press, Boca Raton, 1998.

[23] Kennedy, B. W.: Energy Efficient Transformers, McGraw-Hill Professional, New York, 1997.

[24] Křížek, M.; Segeth, K.: Numerické Modelování Problémů Elektrotechniky, Karolinum, Praha, 2001.

[25] Lin, D.; Zhou, P.; Badics Z.; Fu, W. N.; Chen, Q. M.; Cendes, Z. J.: A New Nonlinear Anisotropic Model for Soft Magnetic Materials, IEEE Transactions on Magnetics 42 (2006) 963–966.

[26] Liu, J.; Shirkoohi, G. H.: Anisotropic Magnetic Material Modelling Using Finite Element Method, IEEE Transactions on Magnetics 30 (1993) 1078–1080.

[27] Lukeš, J.; Malý, J.: Míra a Integrál, Karolinum, Praha, 2002.

[28] Nakano, M.; Nishimoto, H.; Fujiwara, K.; Takahashi, N.: Improvements of Single Sheet Testers for Measurements of 2-D Magnetic Properties Up to High Flux Density, IEEE Transactions on Magnetics 35 (1999) 3965–3967.

[29] Nakata, T.; Takahashi, H.; Kawase, Y.; Nakano, M.; Miura, M.; Sievert, J.D.: Numerical Analysis and Experimental Study of the Error of Magnetic Field Strength Measurements with Single Sheet Testers, IEEE Transactions on Magnetics 22 (1986) 400–402.

[30] Nakata, T.; Takahashi, H.; Fujiwara, N.; Nakano, M.: Measurement of Magnetic Characteristics along Arbitrary Directions of Grain-Oriented Silicon Steel up to High Flux Densities, IEEE Transactions on Magnetics 29 (1993) 3544–3546.

[31] Nakata, T.; Fujiwara, K.; Takahashi, N.; Nakano, M.; Okamoto, N.: An Improved Numerical Analysis of Flux Distributions in Anisotropic Materials, IEEE Transactions on Magnetics 30 (1994) 3395–3398.

[32] Napoli, A.; Paggi, R.: A Model of Anisotropic Grain-Oriented Steel, IEEE Transactions on Magnetics 19 (1983) 1557–1561.

[33] Péra, T.; Ossart, F.; Waeckerle, T.: Field Computation in Non Linear Anisotropic Sheets Using the Coenergy Model, IEEE Transactions on Magnetics 29 (1993) 2425–2427.

[34] Sande, H. V.; Henrotte, F.; Froyen, L.; Hameyer, K.: A Hybrid Method for Determining the Reluctivity Tensor Components of Goss Textured Ferromagnetic Materials, IEEE Transactions on Magnetics 30 (2004) 1078–1080.

[35] Sedlák, B.; Štoll, I.: Elektřina a Magnetismus, Academia, Praha, 2002.

[36] Shirkoohi, G. H.; Arikat M. A. M.: Anisotropic Properties of High Permeability Grain-oriented 3.25% Si-Fe Electrical Steel, IEEE Transactions on Magnetics 30 (1994) 928–930.

[37] Shirkoohi, G. H.; Liu, J.: A Finite Element Method for Modelling of Anisotropic Grain-Oriented Steels, IEEE Transactions on Magnetics 30 (1994) 1078–1080.

[38] Sievert, J. D.: Determination of AC Magnetic Power Losses of Electrical Steel Sheet: Present Status and Trends, IEEE Transactions on Magnetics 30 (1984) 1078–1080.

[39] Silvester, P. P.; Gupta R. P.: Effective Computational Models for Anisotropic Soft B–H Curves, IEEE Transactions on Magnetics 27 (1991) 3804–3807.

[40] Tomida, T.; Uenoya, S.; Sano, N.: Doubly oriented magnetic steel sheet and a method for manufacturing the same, US Patent No. 5948180, 1999.

[41] Vorst, A. V.; Rosen, A.; Kotsuka, Y.: RF/Microwave Interaction with Biological Tissues, Wiley, New Jersey, 2006.

[42] Ženíšek, A.: Sobolev Spaces and Their Applications in the Finite Element Method, Vutium Press, Brno, 2005.